Loss of Inhibitory CD33 Signaling Results in Increased Microglial Activation

Dissertation

zur

Erlangung des Doktorgrades (Dr. rer. nat.)

der

Mathematisch-Naturwissenschaftlichen Fakultät

der

Rheinischen Friedrich-Wilhelms-Universität Bonn

vorgelegt von

Jannis Wißfeld

aus

Koblenz, Deutschland

Bonn, Januar 2021

Angefertigt mit Genehmigung der Mathematisch-Naturwissenschaftlichen Fakultät der Rheinischen Friedrich-Wilhelms-Universität Bonn am Institut für Rekonstruktive Neurobiologie.

1. Gutachter: Prof. Dr. Harald Neumann
2. Gutachter: Prof. Dr. Walter Witke

Tag der Promotion: 04.06.2021
Erscheinungsjahr: 2021

Table of Contents

List of Figures, Tables and Equations

Figures

Tables

Equations

List of Abbreviations

AD	Alzheimer's disease
ADAM	disintegrin and metalloproteinase domain-containing protein 10
AIF	allograft inflammatory factor
AML	acute myeloid leukemia
ANOVA	analysis of variance
APC	allophycocyanin
APOE	apolipoprotein E
APP	amyloid precursor protein
ASC	apoptosis-associated speck-like protein containing a CARD
ATP	adenosine triphosphate
AUC	area under curve
BACE	beta-site APP-cleaving enzyme
BATF	basic leucine zipper ATF-like transcription factor
BDNF	brain-derived neurotrophic factor
BSA	bovine serum albumin
CARD	caspase activation and recruitment domain
Cas	CRISPR-associated protein
CD	cluster of differentiation
CMAH	cytidine monophospho-N-acetylneuraminic acid hydroxylase
CMP	cytidine monophosphate
CMV	cytomegalovirus
CNS	central nervous system
CRISPR	clustered regularly interspaced short palindromic repeats
CSF	cerebrospinal fluid
CSF1R	colony stimulating factor 1 receptor
CXCL	C-X-C motif chemokine ligand
DAG	diacylglycerol
DAMP	danger-associated molecular patterns
DAP	DNAX-activation protein
DAPI	4′,6-diamidino-2-phenylindole
DE	differentially expressed
DHE	dihydroethidium
DMSO	dimethyl sulfoxide
DNA	deoxyribonucleic acid
DTT	dithiothreitol
EB	embryoid body
EDTA	ethylenediaminetetraacetic acid
EEF	eukaryotic elongation factor
ER	endoplasmic reticulum
EV	empty vector
FACS	fluorescence-activated cell sorting
FBS	fetal bovine serum
FC	fold change
FCGR	Fc fragment of IgG receptor
FDR	false discovery rate
FITC	fluorescein isothiocyanate
FRT	Flippase recognition target
Fwd	forward
GAS	growth arrest-specific
GCR	genetic compensation response
GDNF	glial cell-derived neurotrophic factor
GEO	gene expression omnibus
GFP	green fluorescent protein
GO	gemtuzumab ozogamcin
GPR	G protein-coupled receptor

GWAS	genome-wide association study
HBSS	Hank's balanced salt solution
HEK	human embryonic kidney
HEPES	4-(2-hydroxyethyl)-1-piperazineethanesulfonic acid
HEXB	hexosaminidase subunit beta
IBA	ionized calcium-binding adapter molecule
IFN	interferon
IgG	immunoglobulin G
IL	interleukin
iMGL	iPSC-derived microglia-like cells
INPP5D	inositol polyphosphate-5-phosphatase D
iPSC	induced pluripotent stem cells
iPSdMiG	iPSC-derived microglia
IRES	internal ribosome entry site
IRF	interferon regulatory factor
ITAM	immunoreceptor tyrosine-based activatory motif
ITGAM	integrin subunit alpha M
ITIM	immunoreceptor tyrosine-based inhibitory motif
LB	lysogeny broth
LPS	lipopolysaccharide
LTA	lipoteichoic acid
ManNAc-6-P	N-acetyl-d-mannose-6-phosphate
MAP	microtubule-associated protein
MAPK	mitogen-activated protein kinase
MEM	minimal essential medium
MERTK	MER proto-oncogene, tyrosine kinase
MFI	(geometric) mean fluorescence intensity
MHC	major histocompatibility complex
MS	multiple sclerosis
NADPH	reduced nicotinamide adenine dinucleotide phosphate
NANOG	nanog homeobox
NCBI	National Center for Biotechnology Information
NEAA	non-essential amino acids
NEFL	neurofilament light
Neu5Ac	N-acetylneuraminic acid
Neu5Gc	N-glycolylneuraminic acid
NFT	neurofibrillary tangle
NGS	next generation sequencing
NIH	National Institute of Health
NK	natural killer
NLRP	NLR family pyrin domain-containing
NO	nitric oxide
NOD	nucleotide-binding oligomerization domain-containing
NOX	NADPH oxidase
NTP	nucleotide triphosphate
OCT	octamer-binding transcription factor
OLFML	olfactomedin-like
ORF	open reading frame
PAMP	pathogen-associated molecular pattern
PBS	phosphate-buffered saline
PC	principal component
PCA	principal component analysis
PCR	polymerase chain reaction
PD	Parkinson's disease
PE	phycoerythrin
PEP	phosphoenolpyruvate
PET	positron emission tomography

PFA	paraformaldehyde
PIP	phosphatidylinositol phosphate
PKB	protein kinase B
PLC	phospholipase C
PLL	poly-L-lysine
PLO	poly-L-ornithine
PODXL	podocalyxin-like
POU5F1	POU class 5 homeobox 1
PROS	protein S
PRR	pattern recognition receptor
PS1	presenilin 1
PSEN	presenilin
PTBP	polypyrimidine tract binding protein
PTPN	protein tyrosine phosphatase, non-receptor type
PTPRC	protein tyrosine phosphatase, receptor type
qRT-PCR	(semi-) quantitative real-time PCR
Rev	reverse
RNA	ribonucleic acid
ROCK	Rho-associated coiled-coil containing protein kinase
ROS	reactive oxygen species
RT	room temperature
RUNX	runt-related transcription factor
SALL	spalt like transcription factor
SAMP	self-associated molecular pattern
SEM	standard error of the mean
SH2	Src homology region 2
SHIP	SH2 domain-containing inositol polyphosphate 5-phosphatase
SHP	SH2 domain-containing phosphatase
SIGLEC	sialic acid-binding immunoglobulin-like lectin
SIRP	signal regulatory protein
SLC12A5	solute carrier family 12 member 5
SNAP	synaptosome-associated protein
SNP	single nucleotide protein
SOX	SRY-box transcription factor
SPI1	Spi-1 proto oncogene
SRC	SRC proto-oncogene, non-receptor tyrosine kinase
SRSF	serine and arginine rich splicing factor
SYK	spleen-associated tyrosine kinase
SYT	synaptotagmin
TGF	transforming growth factor
TGFBR	transforming growth factor beta receptor
TLR	toll-like receptor
TMEM	transmembrane protein
TNF	tumor necrosis factor
TREM	triggering receptor expressed on myeloid cells
TYROBP	transmembrane immune signaling adaptor TYROB
UT	untreated
WB	Western blot
WGCNA	weighted gene correlation network analyses
WHO	World Health Organization
WT	wild type

1 Introduction

1.1 Microglia – key players of brain immunity

The human brain mainly consists of neurons, glial cells, blood vessels, and neural stem cells. The exact amounts and ratios of the cells making up the human brain are still a matter of debate. Previously, it was thought that glial cells outnumber neuronal cells by at least 10:1, however, a recent study claims equal ratios of neuronal and non-neuronal cells of around 8.5×10^{10} cells each (Azevedo *et al*., 2009; Herculano-Houzel, 2014). Glial cells are further divided into macroglia and microglia. Macroglia represents a generic term for astrocytes, oligodendrocytes, ependymal cells, and radial glia, which are derived from ectodermal tissue. They fulfill numerous tasks to maintain central nervous system (CNS) development and homeostasis (reviewed in Allen & Lyons, 2018; Jäkel & Dimou, 2017). Microglia are the only resident innate immune cells of the CNS. The term “microglia” was first introduced by Pío del Río Hortega in 1919 (Río-Hortega, 1919; Sierra *et al*., 2016). Microglia make up around 10 % of brain cells highly depending on the brain region (Alliot *et al*., 1999; Lawson *et al*., 1990, 1992). They originate from primitive myeloid progenitors during the primitive hematopoiesis in the embryonic yolk sac, which occurs as early as embryonic day 8 in mice. After microglial progenitors migrated into the CNS region the blood-brain-barrier forms, which leads to isolation of the microglial progenitors within the CNS (Alliot *et al*., 1999; Ginhoux *et al*., 2010; Kierdorf *et al*., 2013). The microglial progenitors mature among neurons and other glial cells – a fundamental step to gain their cellular identity (Bennett *et al*., 2018; Butovsky *et al*., 2014; Gautier *et al*., 2012). Development of peripheral immune cells – excluding tissue macrophages – takes place within the definitive hematopoiesis, which separates microglia spatiotemporally from their peripheral counterparts (Ginhoux *et al*., 2010).

Although microglia and peripheral macrophages have a different origin, they express a similar pattern of receptors and fulfill similar functions (reviewed in Guillemin & Brew, 2016). However, the environmental influence and the direct contact with neurons and other glial cells seems to be of high importance as *ex vivo* microglia quickly downregulate the expression of numerous cell-specific receptors (Bennett *et al*., 2018). Microglial functions include homeostatic surveillance of the CNS, detection and elimination of invading pathogens, and synaptic pruning. During brain development

microglia trim excess synapses and axons in a complement-dependent way to fine tune CNS connectivity – a process known as synaptic pruning (Paolicelli *et al*., 2011; Squarzoni *et al*., 2014; Stevens *et al*., 2007). Throughout life, microglia clear debris, protein aggregates, and dead cells to keep CNS homeostasis (Davalos *et al*., 2005; Nimmerjahn *et al*., 2005). As the only resident innate immune cells of the CNS microglia are also the first responders to invading pathogens and fight infectious diseases (Klein *et al*., 2008).

Microglia constantly surveil their environment using their highly motile processes to fulfill their tasks. These processes are equipped with a broad range of pattern recognition receptors (PRRs). PRRs are a receptor family that is able to sense molecular cues derived from pathogens or dying cells. These molecular cues are known as either pathogen-associated molecular patterns (PAMPs) or danger-associated molecular patterns (DAMPs). Recent discoveries also highlighted the importance of self-associated molecular patterns (SAMPs) as molecular cues (A. Varki, 2011b, 2020). Toll-like receptors (TLRs) are a major group of PAMP-recognizing PRRs. They bind to components of the bacterial cell wall, such as lipopolysaccharide (LPS) and lipoteichoic acid (LTA), or to bacterial and viral RNA/DNA. PAMP recognition by TLRs results in pro-inflammatory microglial activation including cytokine and chemokine secretion, reactive oxygen species (ROS) production, and activation of the phagocytic machinery (Klein *et al*., 2008; Park *et al*., 2015). Recognition of DAMPs, such as extracellular nucleotides by P2X and P2Y receptors (Beamer *et al*., 2016; Shieh *et al*., 2014), heat shock proteins, or peroxiredoxins by TLRs (Asea *et al*., 2002; Shichita *et al*., 2012), or phosphatidylserine on apoptotic cells by, e.g., triggering receptor expressed on myeloid cells (TREM) 2 (Takahashi *et al*., 2005), also results in microglial activation to clear the dying cell. The molecular cues polarize microglia towards an either pro- (M1) or anti-inflammatory (M2) phenotype. However, these two microglial phenotypes are not as static as they seem to be and the nomenclature M1 and M2 microglia is partially considered deprecated. In reality, there is a fluid transition between these two phenotypes with innumerous intermediate stages depending on the molecular cues microglia encounter (Figure 1) (Lawson *et al*., 1990; Morrison & Filosa, 2013; Stout *et al*., 2005; W J Streit *et al*., 1988).

Pro-inflammatory microglia – often associated with activation by LPS or interferon (IFN) γ – secrete cytokines, such as tumor necrosis factor (TNF) α and interleukin (IL) 1β, as well as radicals, such as reactive oxygen species (ROS) and nitric oxide

(NO), to fight invading pathogens. Pro-inflammatory-primed microglia are often considered cytotoxic and supportive of neurodegeneration as they can cause collateral damage to neurons. On the other hand, anti-inflammatory microglia, which are polarized by IL-4, IL-10, IL-13, or macrophage colony stimulating factor 1 (M-CSF) secrete brain-derived neurotrophic factor (BDNF), glial cell-derived neurotrophic factor

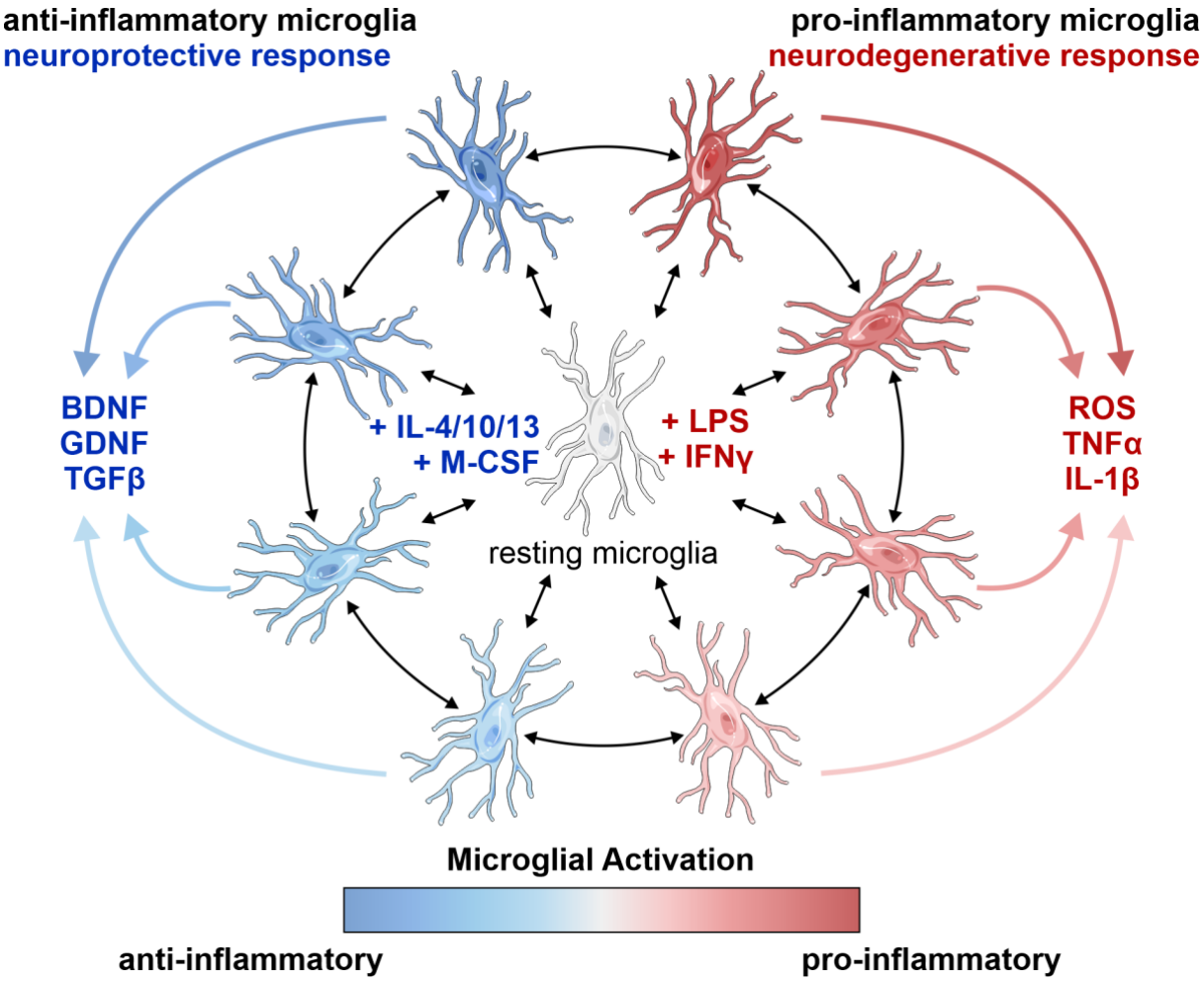

Figure 1: Differential microglial activation patterns.
Microglial activation is dependent on the environmental stimulation they experience. Resting microglia, which are activated by IL-4, -10, -13, or M-CSF are polarized towards an anti-inflammatory phenotype. Anti-inflammatory-polarized microglia secrete BDNF, GDNF and TGFβ among others as anti-inflammatory factors. They fulfill neuroprotective and neuroregenerative functions (left). Activation of microglia by stimuli such as LPS or IFNγ results in polarization towards a pro-inflammatory microglial phenotype. Pro-inflammatory microglia secrete ROS and pro-inflammatory cytokines, including TNFα and IL-1β, and are associated with pathogen clearance and neurodegenerative properties (right). The exact composition of stimuli, their amount and the time interval microglia are exposed to them results in specific activation patterns with innumerous intermediate steps. Transition between these steps is rather fluid than static and microglia can adapt quickly to new stimuli they encounter and switch their phenotype. BDNF = brain-derived neurotrophic factor; GDNF = glial cell-derived neurotrophic factor; IFNγ = interferon γ; IL = interleukin; LPS = lipopolysaccharide; M-CSF = macrophage colony stimulating factor 1; ROS = reactive oxygen species; TGFβ = transforming growth factor β; TNFα = tumor necrosis factor α. Microglia illustration adapted or modified from Servier Medical Art.

(GDNF) and transforming growth factor (TGF) β. Anti-inflammatory-primed microglia resolve inflammation and support tissue repair as well as regeneration. Therefore, they are considered to have a neuroprotective function (Durafourt *et al*., 2012; Martinez & Gordon, 2014; Michelucci *et al*., 2009). Using the specific responses to different molecular cues, microglia can communicate and activate other cells as well as attract peripheral immune cells to the CNS. During brain infections or diseases microglia upregulate major histocompatibility complexes (MHC) I and II and function as antigen-presenting cells in order to orchestrate the adaptive immune response of, e.g., infiltrating T cells (Olson *et al*., 2001; Schetters *et al*., 2018).

Microglia enjoy a unique role as the only resident immune cells of the CNS. However, malfunctioning of microglia is often associated with severe neurodegenerative diseases, such as Alzheimer's disease (AD), Parkinson's disease (PD) and multiple sclerosis (MS) (reviewed in Hickman *et al*., 2018).

1.2 Neuroinflammation in Alzheimer's disease

Alzheimer's disease (AD) is the most common form of dementia accounting for up to 60-70 % of dementia cases worldwide with growing prevalence (WHO, 2020). It was first described by and named after the German psychiatrist Alois Alzheimer in 1906/07 (Alzheimer, 1907). AD – as typical for neurodegenerative diseases – starts slowly with a gradually increasing disease burden and symptoms over time. In the late stage, patients suffer from progressive aphasia, memory loss, disorientation, mood swings, and other behavioral issues, which finally results in death of the patient (Alzheimer, 1907; Merriam *et al*., 1988; Toyota *et al*., 2007). On molecular level, the disease is characterized by cortical atrophy, extracellular amyloid β (Aβ) protein aggregates (Aβ plaques), intraneuronal hyperphosphorylated microtubule-associated TAU protein aggregates, and reactive microglia (Figure 2). These TAU aggregates are also known as neurofibrillary tangles (NFTs). Aβ plaques consist of accumulated processed amyloid precursor protein (APP). APP can be cleaved in a first step by either α-secretases, such as disintegrin and metalloproteinase domain-containing protein 10 (ADAM10) or β-secretases, such as beta-secretase 1 (BACE1) (Cai *et al*., 2001; Kuhn *et al*., 2010). Thereby, ADAM10 cleaves APP within the Aβ region, which results in secretion of soluble APPα and a rather short membrane-bound C-terminal fragment. Subsequently, γ-secretase cleavage leads to release of the p3 peptide. BACE1, however, cleaves APP together with the γ-secretase to release Aβ into the extracellular

space. Both, increased β-secretase activity as well as dysfunctional Aβ clearance by microglia can contribute to the generation of insoluble Aβ plaques (reviewed in Nunan & Small, 2000). These Aβ plaques are known to be on one hand neurotoxic itself (Cirrito *et al*., 2005; Walsh *et al*., 2002) and on the other hand able to induce TAU hyperphosphorylation and thus the generation of NFTs (Götz *et al*., 2001; Lewis *et al*., 2001). However, there are reported cases of dementia-free individuals with excessive Aβ plaque load (Aizenstein *et al*., 2008; Esparza *et al*., 2013; Rentz *et al*., 2010). While Aβ plaques are very characteristic for AD, NFTs are not solely restricted to AD. Instead, they can be found in many diseases summarized as tauopathies (reviewed in Götz *et al*., 2019). Physiologically, TAU stabilizes microtubules in axons of neurons (Cleveland *et al*., 1977). However, when it becomes hyperphosphorylated it dissociates from microtubules and forms insoluble aggregates. The lack of TAU on microtubules disrupts their dynamics and hyperphosphorylated TAU might contribute in several ways to neurotoxicity, including microtubule disintegration, sequestration of

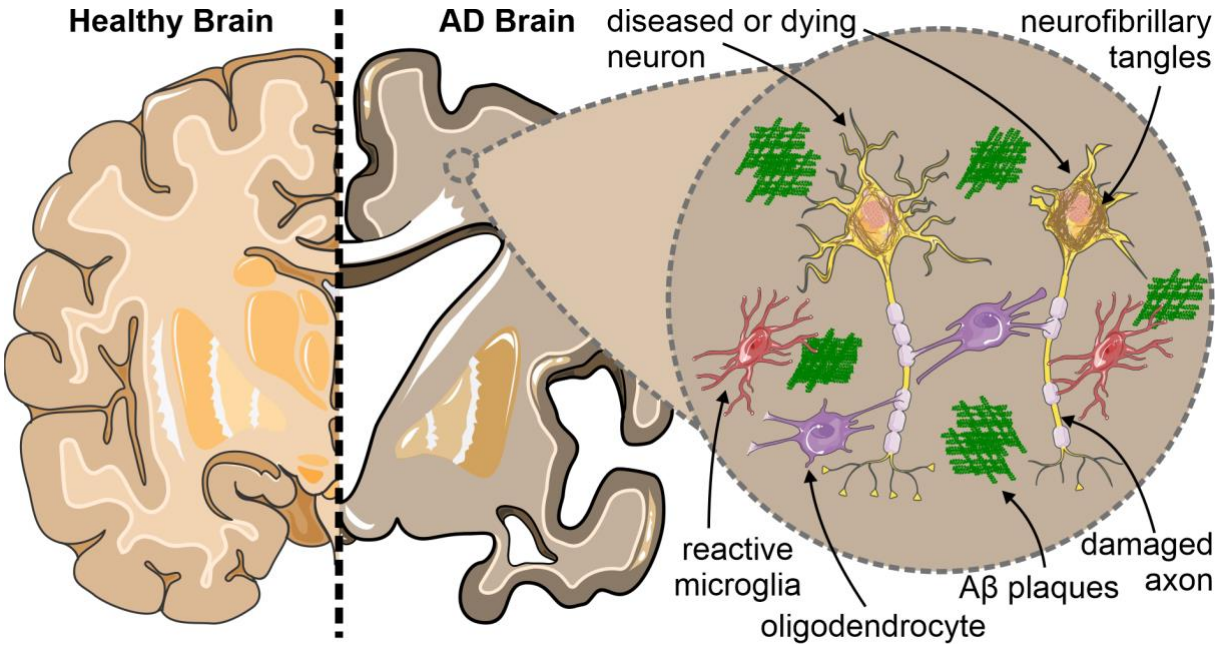

Figure 2: Molecular pathology of Alzheimer's disease.
AD brains show significant lower brain volume and convolution due to neurodegeneration. On molecular level, neurodegeneration is caused by extracellular Aβ plaques, intraneuronal neurofibrillary tangles (NFTs) and reactive microglia. Aβ plaques are dense Aβ protein aggregates with neurotoxic properties. Formation of NFTs due to aggregation of aberrantly hyperphosphorylated microtubule-associated protein TAU results in destabilization of microtubules, impaired microtubule transport and subsequently neuronal death. Reactive microglia exhibit a pro-inflammatory neurodegenerative phenotype. In addition, they also show an impaired phagocytosis of Aβ plaques. All three pathological features finally contribute to the neurodegeneration in AD. Aβ = amyloid β; AD = Alzheimer's disease. Illustrations modified from Servier Medical Art.

microtubule-associated proteins, blockage of intracellular trafficking, and promotion of cell cycle entry (reviewed in J. Z. Wang & Liu, 2008). Accumulated loss of neurons finally results in disease manifestation.

In general, two forms of AD are distinguished – the early-onset or familial form and the late-onset or sporadic form of AD. Early-onset AD is inheritable and caused by mutations in APP or the γ-secretase catalytic subunits presenilin 1 or 2 (PSEN1/2) (Shea *et al*., 2016). Patients are usually younger than those suffering from the sporadic form of AD, which is normally diagnosed at the age of 65 and above (Koedam *et al*., 2010; Shea *et al*., 2016). However, the nomenclature familial and sporadic AD is rather misleading as recent studies discovered many genetic risk factors for developing the late-onset form of AD (Hollingworth *et al*., 2011; Lambert *et al*., 2013; Naj *et al*., 2011). In the earlier days of AD research two main hypotheses for the disease cause were developed: the amyloid cascade and the TAU hypothesis – each focusing at one of the two main pathological features as major driver of the disease (Kametani & Hasegawa, 2018). Today's AD research assumes that both pathological features might have an underlying link, which eventually causes the disease (Heneka *et al*., 2015). Genome-wide association studies (GWAS) identified several genetic polymorphisms, which increase the risk to develop AD. Interestingly, most of the newly discovered genes were not of neuronal but microglial origin (Hollingworth *et al*., 2011; Lambert *et al*., 2013; Naj *et al*., 2011), which gave rise to a new hypothesis – the neuroinflammatory hypothesis of AD. To date, microglial contribution to AD is widely undisputed. However, it is still a matter of debate whether microglial contribution is causal or consequential of the disease. In several studies, polymorphisms in *TREM2*, *transmembrane immune signaling adaptor TYROBP* (*TYROBP*), *inositol polyphosphate-5-phosphatase D* (*INPP5D*), and *cluster of differentiation* (*CD*) *33* were found to be associated with AD (Chan *et al*., 2015; Guerreiro *et al*., 2013; Hollingworth *et al*., 2011; Jonsson *et al*., 2013; Lambert *et al*., 2013; Naj *et al*., 2011). Microglia appear to play an ambivalent role in AD. Their activation is required to clear extracellular Aβ before it accumulates and forms Aβ plaques but on the other hand excessive microglial activation is known to exacerbate AD pathology (Edison *et al*., 2008). Interestingly, many of the genetic polymorphisms linked to AD hint towards an impaired microglial response (Griciuc *et al*., 2013; Kober *et al*., 2016). Aβ plaque deposition starts decades before clinical disease diagnosis suggesting improper clearance by microglia (Rajan *et al*., 2015). Indeed, polymorphisms of CD33 and TREM2 result in decreased Aβ uptake, which

over time might lead to the formation of Aβ plaques, neuronal loss and consequently to AD (Bradshaw *et al*., 2013; Griciuc *et al*., 2013; Yeh *et al*., 2016). Recent discoveries further suggest that once Aβ plaques have formed microglia migrate towards these and become aberrantly activated, which is also referred to as reactive microglia (reviewed in Solito & Sastre, 2012).

In general, Aβ uptake by microglia is mediated by interaction with CD14, TLR2, TLR4 or TREM2 (Fujikura *et al*., 2019; Reed-Geaghan *et al*., 2009; Y. Zhao *et al*., 2018). Reactive microglia are unable to properly phagocytose the Aβ plaques but produce cytokines and ROS, such as superoxide (Heneka *et al*., 2015). ROS are cytotoxic agents, and in addition, found to induce TAU hyperphosphorylation in neurons (Lovell *et al*., 2004; Su *et al*., 2010). Compared to healthy controls, increased radical damage was observed in the brains of AD patients post mortem (Ansari & Scheff, 2010; Scheff *et al*., 2016). Microglial ablation by colony stimulating factor 1 receptor (CSF1R) inhibitors decreased the number of Aβ plaques as well as dystrophic neurites and improved cognitive behavior in 5xFAD mice, a mouse model of Alzheimer's disease (Sosna *et al*., 2018; Spangenberg *et al*., 2019). Further, apoptosis-associated speck-like protein containing a CARD (ASC)-Aβ composites, which are taken up by microglia result in NOD-like receptor protein (NLRP) 3 inflammasome activation. The NLRP3 inflammasome amplifies microglial pro-inflammatory response eventually resulting in pyroptotic cell death and release of ASC-Aβ composites. In a feedforward loop ASC-Aβ composites are able to exacerbate the inflammatory AD pathology (Friker *et al*., 2020). Thus, neuroinflammation induced by microglia is a concomitant event if not a major driver of AD. Current therapeutic interventions in AD are mostly focus on clearance of Aβ plaques. Therefore, Aβ plaque-targeting antibodies were designed, which facilitate antibody-mediated uptake by microglia. However, this strategy has major limitations. First, the bioavailability of systemically-injected antibodies is very low in the brain (St-Amour *et al*., 2013). Further, antibody-dependent cell-mediated cytotoxicity by Fc-binding receptors could activate microglia to produce ROS, which eventually could lead to collateral damage and thus death of neurons (Ulvestad *et al*., 1994). Many clinical trials using Aβ plaque-targeting antibodies failed because they lacked efficacy (summarized in Mullard, 2019). Therefore, current research focuses on alteration of microglial response by investigating AD-associated microglial risk genes, such as CD33 – a member of the sialic acid-binding immunoglobulin-like lectins.

1.3 Sialic acid-binding immunoglobulin-like lectins

Sialic acid-binding immunoglobulin-like lectins (SIGLECs) are a subgroup of the immunoglobulin superfamily (IgSF) and developed around 180 million years ago (Cao & Crocker, 2011). Their expression is mostly restricted to cells of the hematopoietic lineage – excluding SIGLEC4 and SIGLEC6. As their name suggests the ligands of this receptor family are sialic acids. Sialoadhesin (SIGLEC1) and CD22 (SIGLEC2) belong to the first discovered SIGLECs, which are expressed on macrophages and B cells, respectively. Upon sialidase treatment the cell-cell interactions mediated by these receptors were lost suggesting sialic acids on the cell surfaces as the ligands of these receptors (Crocker & Gordon, 1986, 1989; Stamenkovic & Seed, 1990). SIGLECs are categorized into two groups: the evolutionary-conserved SIGLECs and the quickly-evolved CD33-related SIGLECs. SIGLECs 1, 2, 4, and 15 belong to the evolutionary-conserved SIGLECs, which have orthologs in other SIGLEC-expressing animals. These SIGLECs have a comparable low sequence identity (25-30 %). CD33-related SIGLECs, however, show a higher sequence identity (50-99 %) possibly an effect of their quick evolution (Bornhöfft *et al*., 2018). Hence, not all these SIGLECs have direct orthologs in other SIGLEC-expressing animals and thus are considered to be mostly species-specific. The group of CD33-related SIGLECs consists of CD33 (SIGLEC3), SIGLECs 5-12, 14, and 16 in humans and CD33, Siglec-E, -F, -G, and -H in mice (Angata *et al*., 2004; Crocker *et al*., 2007).

In general, all SIGLECs are composed of a single N-terminal variable (V-set) immunoglobulin-like domain followed by a varying number of constant (C2-set) immunoglobulin-like domains and a single-pass transmembrane domain. The V-set domain is considered to be responsible for ligand binding. Most SIGLECs (i.e., SIGLECs 2, 3 and 5-12) have immunoreceptor tyrosine-based inhibitory motif (ITIM) and ITIM-like domains in their intracellular domains. SIGLECs 14-16 bear a positive charged residue, which is associated with immunoreceptor tyrosine-based activatory motif (ITAM) signaling. Only SIGLEC1 and 4 are not associated with classical ITIM or ITAM signaling (Angata *et al*., 2004; Cao & Crocker, 2011; Linnartz *et al*., 2010). SIGLECs can bind ligands in *cis* (on the same cell) or in *trans* (on another cell) to induce signaling. Their main purpose is to modulate leukocyte activation by counteracting ITAM signaling and initiation of anti-inflammatory responses by binding their specific sialic acid ligands (Avril *et al*., 2004; Paul *et al*., 2000).

1.4 Sialic acids and sialic acid recognition by leukocytes

The glycocalyx is a dense layer of different sugars covering nearly all types of cells. These sugars – generally referred to as glycans – are covalently attached to plasma membrane proteins as well as lipids and are important for cell-cell interactions and recognition (Hart & Copeland, 2010; Kageshita *et al*., 1995; A. Varki, 2011a). Glycoproteins and glycolipids are glycosylated intracellularly by glycosyltransferases, which attach oligosaccharides to amino acid side chains or the polar head group of lipids (Patt & Grimes, 1974). Glycans are very variable in their length and composition. However, in most vertebrates, the outermost sugar of these glycans are sialic acids suggesting a substantial role in cell-cell interactions and host cell recognition (Angata & Varki, 2002). In humans, single mutations in genes belonging to the sialic acids synthesis pathway result in severe diseases (Hinderlich *et al*., 2015), and knockout of critical enzymes within these pathways are embryonically lethal in mice (Schwarzkopf *et al*., 2002). Sialic acids are nine-carbon alpha-keto aldonic acids (X. Chen & Varki, 2010) for which more than 50 additional modifications or linkages were identified to date (Angata & Varki, 2002; Schauer, 1982). The nine-carbon backbone is generated by enzyme-catalyzed condensation of a phosphoenolpyruvate (PEP) with N-acetyl-d-mannose-6-phosphate (ManNAc-6-P), which is afterwards dephosphorylated to produce N-acetylneuraminic acid (Neu5Ac). Cytidine triphosphate is then hydrolyzed to the newly synthesized sialic acid (CMP-Neu5Ac) in order to enable multimerization and transfer onto oligosaccharides in different kinds of linkages, including α-2,3, α-2,6, and α-2,8 by sialyltransferases in the Golgi apparatus (Warren & Felsenfeld, 1962). In a final step, glycans are attached to glycolipids and glycoproteins.

Neu5Ac is the most abundant and important sialic acid in humans. An Alu-mediated 92 base pair deletion in the *cytidine monophospho-N-acetylneuraminic acid hydroxylase* (*CMAH*) gene, which occurred around 2.2 million years ago in human ancestors, rendered the enzyme for the most common mammalian Neu5Ac modification unfunctional (Chou *et al*., 2002; Irie *et al*., 1998). In other mammals – including higher primates – CMAH converts Neu5Ac to N-glycolylneuraminic acid (Neu5Gc) by hydroxylation of the acetyl group to result in a glycolyl group (Chou *et al*., 2002; Irie *et al*., 1998). Thus, modern humans have a clearly diverging sialic acid profile to other mammals, which might have led to evolutionary pressure on SIGLECs. This

could be the reason for the quickly evolved CD33-related human SIGLECs of which some do not have orthologs in other mammals (Padler-Karavani *et al*., 2014).

Sialic acids serve as SAMPs and can be recognized by different SIGLECs depending on their linkage and degree of polymerization. Most SIGLECs induce a very specific immunomodulatory ITIM-mediated response, which dampens leukocyte activation upon encountering host cells (Doody *et al*., 1995; Liu *et al*., 2010; Shahraz *et al*., 2015; Y. Wang & Neumann, 2010). On the other hand, ITAM-associated SIGLECs are thought to be a tool to effectively clear sialylated pathogens. These pathogens produce sialidases to cleave off host cell sialic acids and subsequently incorporate these. Using the host sialic acid to cover their own glycocalyx they are also able to bind to ITIM-associated SIGLECs to limit potent leukocyte activation and thus evade the host immune system (Schoenhofen *et al*., 2006; A. Varki & Gagneux, 2012; N. M. Varki & Varki, 2007).

Interestingly, the brain is the organ with the highest sialic acid content. Here, sialic acids were found to play a role in brain development (Svennerholm, 1980; B. Wang & Brand-Miller, 2003). Further, ITIM-mediating SIGLECs, such as CD33 and SIGLEC11, were recently linked to AD together with molecules triggering ITAM-mediated responses including TREM2 and TYROBP (Bellenguez *et al*., 2020; Hollingworth *et al*., 2011; Lambert *et al*., 2013; Naj *et al*., 2011). Thus, the ITIM/ITAM signaling axis seems to have a considerable impact on AD development.

1.5 The immunoreceptor tyrosine-based activatory and inhibitory motif signaling axis

The ITIM/ITAM signaling axis is a well-balanced immunomodulatory system. Activatory signaling arising from ITAM receptors, such as TREM2, complement receptor (CR) 3, or Fc fragment of IgG receptor I (FcγRI), can be antagonized by inhibitory signaling arising from ITIM receptors including CD33, signal regulatory protein alpha (SIRPα) and other SIGLECs (Figure 3). Activation of, e.g., TREM2 results in recruitment and phosphorylation of ITAM-containing adapter molecules such as TYROBP by SRC proto-oncogene, non-receptor tyrosine kinase (SRC). Activated, i.e., phosphorylated TYROBP recruits spleen-associated tyrosine kinase (SYK), which in turn causes upregulation of cytokine production, phagocytosis, and ROS production as well as increased proliferation and survival (Linnartz & Neumann, 2013; Mocsai *et al*., 2006; Wakselman *et al*., 2008). Simultaneous activation of ITIM-bearing receptors such as

CD33 results in phosphorylation of the ITIM domains also by SRC family kinases, which leads to recruitment of phosphatases such as protein tyrosine phosphatase, non-receptor type (PTPN) 6 and 11 (also known as Src homology region 2 (SH2) domain-containing phosphatases (SHP) 1 and 2), or inositol polyphosphate-5-phosphatase D (INPP5D; also called SH2 domain-containing inositol polyphosphate 5-phosphatase (SHIP) 1). Activation of these phosphatases counteracts ITAM signaling by dephosphorylation of the ITAM domains, ITAM-associated kinases, such as SYK, or other downstream targets (Huang *et al*., 2003; Osborne *et al*., 1996).

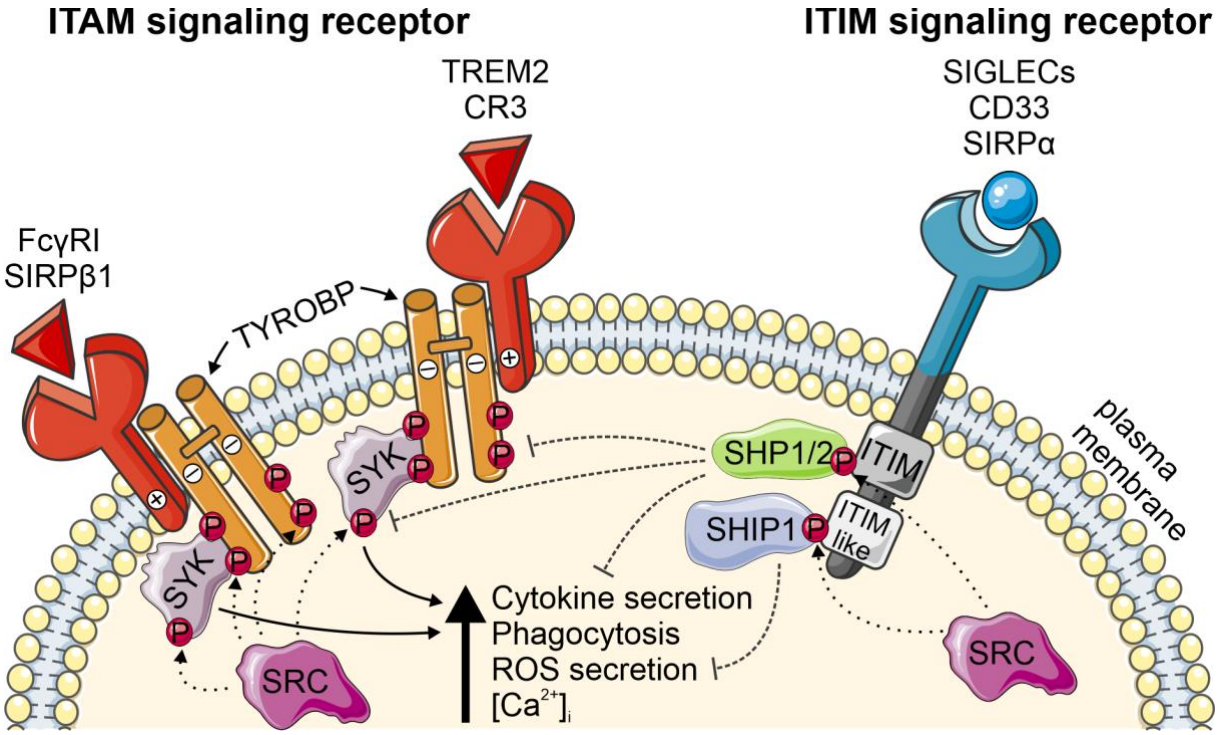

Figure 3: The ITIM/ITAM signaling axis in microglia.
Activation of ITAM signaling receptors, such as TREM2, CR3, FcγRI, or SIRPβ1, results in recruitment of TYROBP and its phosphorylation by SRC family kinases. Activated, i.e., phosphorylated TYROBP recruits and activates SYK which eventually leads to cellular activation including increased cytokine and ROS secretion, phagocytosis, and intracellular calcium levels. Simultaneous activation of ITIM signaling receptors, such as SIRPα, CD33, or other SIGLECs, results in phosphorylation of the ITIM and ITIM-like domains by SRC family kinases and recruitment as well as activation of protein tyrosine phosphatases, such as SHP1/2 and SHIP1. These phosphatases then dephosphorylate key molecules of the ITAM pathway, such as TYROBP, SYK, or PIP_3, thereby dampening the ITAM response. $[Ca^{2+}]_i$ = intracellular calcium; CR3 = complement receptor 3; FcγRI = Fc fragment of IgG receptor Ia; ITAM = immunoreceptor tyrosine-based activatory motif; ITIM = immunoreceptor tyrosine-based inhibitory motif; PIP_3 = phosphatidylinositol-trisphosphate; ROS = reactive oxygen species; SHIP1 = Src homology region 2 domain-containing inositol polyphosphate 5-phosphatase; SHP = Src homology region 2 domain-containing phosphatase; SIGLECs = sialic acid-binding immunoglobulin-like lectins; SIRP = signal regulatory protein; SRC = SRC proto-oncogene, non-receptor tyrosine kinase; SYK = spleen-associated tyrosine kinase; TREM2 = triggering receptor expressed on myeloid cells 2; TYROBP = transmembrane immune signaling adaptor TYROBP. Illustrations partly adapted or modified from Servier Medical Art.

Further, INPP5D is known to hydrolyze the 5' phosphate from phosphatidylinositol-(3,4,5)-trisphosphate ($PI(3,4,5)P_3$), which is known to activate cell growth and survival via protein kinase B (PKB)/AKT signaling (An *et al*., 2005; Osaki *et al*., 2004). In murine microglia it was shown that Siglec-E is able to dampen phagocytosis, *TNF* and *IL1B* gene transcription, and acts neuroprotective (Claude *et al*., 2013). In addition, activation of SIGLEC11 was proven to counteract LPS-induced inflammation in a human macrophage cell line (Shahraz *et al*., 2015; Y. Wang & Neumann, 2010). Thus, the ITIM/ITAM signaling axis plays a critical role for maintaining leukocyte homeostasis. Further, SIGLECs, which are able to recognize SAMPs limit leukocyte activation upon encountering of a host cell. Imbalances in the ITIM/ITAM signaling axis can lead to severe diseases and polymorphism in TREM2, TYROBP, INPP5D and CD33, which affect their signaling capacity were recently linked to AD (Chan *et al*., 2015; Guerreiro *et al*., 2013; Hollingworth *et al*., 2011; Jonsson *et al*., 2013; Lambert *et al*., 2013; Naj *et al*., 2011).

1.6 CD33 in health and disease

CD33 (SIGLEC3) belongs to the CD33-related SIGLECs and consists of an extracellular V-set immunoglobulin-like domain and a single C2-set immunoglobulin-like domain followed by a single-pass transmembrane domain and an ITIM as well as an ITIM-like domain intracellularly (Paul *et al*., 2000). Its ortholog in mice lacks the characteristic ITIM domain, only bearing an ITIM-like domain in the intracellular part. Further, it has an positive residue within the transmembrane domain, which was shown to enable interaction with ITAM-associated TYROBP and thus clearly differs from human CD33 (Bhattacherjee *et al*., 2019). CD33 is mainly expressed on myeloid cells including macrophages and microglia. CD33 preferentially binds α-2,6 followed by α-2,3 and α-2,8-linked sialylated glycans present on lipids or proteins. However, α-2,8-linked sialylated glycans are bound with much lower affinity (Brinkman-Van Der Linden & Varki, 2000; Freeman *et al*., 1995). Activation of CD33 results in inhibitory ITIM signaling mediated by SH2 domain-containing phosphatases such as SHP1, SHP2, or SHIP1, and receptor endocytosis (Paul *et al*., 2000; Taylor *et al*., 1999). Thereby, tyrosine phosphorylation of the intracellular domains seems to be crucial for endocytosis of CD33 (Walter *et al*., 2008). CD33-related SIGLECs are described to clear off sialylated antigens via receptor endocytosis (Lock *et al*., 2004; Walter *et al*., 2005) but are also known to bind to sialylated pathogens, including *Neisseria*

meningitides, Group B *Streptococci*, and *Campylobacter jejuni*, suggesting a role in host defense and pathogenicity (Avril *et al*., 2006; Carlin *et al*., 2007; Jones *et al*., 2003; Walter *et al*., 2008). However, the exact role of CD33 and in particular CD33 signaling in tissue macrophages, including microglia, remains elusive.

CD33 is linked to several diseases. It is highly abundant in a range of acute myeloid leukemia (AML) cells. Here, the endocytic capacity of CD33 was taken advantage to deliver a cytotoxic drug coupled to an antibody against CD33 (gemtuzumab ozogamicin (GO, brand name: Mylotarg)). GO binds to CD33 and initiates antibody-mediated receptor endocytosis, which finally leads to apoptosis of the cell via calicheamicin-γ1 derivative-caused DNA strand scissions (Damle & Frost, 2003; Giles *et al*., 2003; Linenberger, 2005).

Moreover, several recent genome-wide association studies (GWAS) linked genetic polymorphism of many microglial proteins, including CD33, to AD (Hollingworth *et al*., 2011; Naj *et al*., 2011). Due to these GWAS a new perspective of AD research emerged, now targeting microglia rather than Aβ plaque and NFT formation directly. Two isoforms of CD33 are mainly expressed in humans. The full-length form of CD33 (CD33M) is the more common isoform in the Caucasian population compared to the exon 2-deleted isoform of CD33 (CD33m or $CD33^{\Delta E2}$). Exon 2 of CD33 encodes for the major part of the V-set immunoglobulin sialic acid-binding domain suggesting that $CD33^{\Delta E2}$ cannot be activated by sialylated ligands (Hernández-Caselles *et al*., 2006). Expression of $CD33^{\Delta E2}$ is favored by the two co-inherited single nucleotide polymorphisms rs3865444(A/A) and rs12459419(T/T) and is associated with expression in peroxisomes rather than on the cell surface (Malik *et al*., 2013; Siddiqui *et al*., 2017). Further, carriers of rs3865444(A/A) have a reduced risk for developing AD with an overall odds ratio of 0.89 (Hollingworth *et al*., 2011; Lambert *et al*., 2013; Naj *et al*., 2011). The proportion of CD33-positive microglia and the amount of CD33 surface expression on microglia were found to positively correlate with the amount of Aβ plaques in the brains of AD patients and disease progression (Bradshaw *et al*., 2013; Griciuc *et al*., 2013). Furthermore, expression of human full-length CD33M on phagocytes was shown to decrease cargo uptake opposed to expression of human $CD33^{\Delta E2}$ or murine CD33 (Bhattacherjee *et al*., 2019; Siddiqui *et al*., 2017).

Thus, CD33 polymorphisms impact AD development and progression but only little is known about the CD33 signaling in respect to AD. However, increasing evidence suggests a beneficial outcome of modulation of CD33 signaling events in AD.

1.7 Aims and objectives of the thesis

Recent studies linked polymorphisms in the CD33 gene to Alzheimer's disease. However, the exact role of CD33 in microglia and Alzheimer's disease is still inconclusive. The aim of this project was to understand the role of CD33 signaling in human microglia in respect to Alzheimer's disease. To realize this, a good model system is necessary. Therefore, in a first step, human induced pluripotent stem cell-derived microglia (iPSdMiG) were analyzed as a microglia model system and compared to human primary microglia by *in silico* RNA sequencing analysis. Further, a CD33 reporter cell line was generated to study possible CD33 ligands and agonistic antibodies since potent modulators of CD33 signaling are unknown. For this purpose, a fusion protein construct consisting of CD33 and DAP12 was stably transfected together with a calcium-sensitive GFP reporter system into Flp-In-293 cells. On this basis, different CD33 antibodies were tested for their ability to induce CD33 signaling. Lastly, *CD33* knockout and AD-protective $CD33^{\Delta E2}$-expressing iPSdMiG were compared to isogenic wild type control iPSdMiG with regards to cellular activation, including cytokine production, phagocytosis, and ROS production.

2 Materials and Methods

2.1 Materials

2.1.1 Technical equipment

Instrument	Company
-20 °C freezer	Liebherr, Switzerland
+4 °C fridge	Liebherr, Switzerland
Acculab Scale	Sartorius AG, Germany
Axiovert200M	Carl Zeiss AG, Germany
BD Accuri C6 Plus	BD Bioscience, Germany
BD FACSCalibur	BD Bioscience, Germany
Biofuge Fresco (Centrifuge)	Heraeus Holding GmbH, Germany
EnVision 2104	PerkinElmer GmbH, Germany
Cell MateII (Pipette Boy)	Thermo Fisher Scientific Inc., USA
CoolCell LX	Corning Inc., USA
Gel Doc 2000	Bio-Rad Laboratories GmbH, Germany
HBO 50/AC	Carl Zeiss AG, Germany
Hera Cell 150 (Incubator)	Heraeus Holding GmbH, Germany
Hera Freeze (- 80°C Freezer)	Heraeus Holding GmbH, Germany
Hera Safe (Laminar-air Flow Workbench)	Kendro Laboratory Products GmbH, Germany
ImagerZ1	Carl Zeiss AG, Germany
IN Cell Analyzer 2200	GE Healthcare Life Sciences, UK
Laboclav	SHP Steriltechnik AG, Germany
Mastercycler ep gradient S	Eppendorf AG, Germany
Megafuge 1.0R	Heraeus Holding GmbH, Germany
Microwave Oven	Severin Elektrogeräte GmbH, Germany
NanoDrop 1000 Spectrophotometer	Thermo Fisher Scientific Inc., USA
Olympus IX81	Olympus K.K., Japan
PerfectBlue Gelsystem Mini M	VWR International GmbH, Germany
Pipettes (10 µl, 100 µl, 1000 µl)	Eppendorf AG, Germany
pH Meter	Mettler-Toledo GmbH, Germany
PowerPac Basic Power Supply	Bio-Rad Laboratories GmbH, Germany

Instrument	Company
Rocking Platform Shaker, Single	VWR International GmbH, Germany
Rotilabo-mini-centrifuge	Carl Roth GmbH & Co KG, Germany
Sorvall RC6 Plus	Thermo Fisher Scientific Inc., USA
T3 Thermocycler	Biometra GmbH, Germany
Thermomixer Compact	Eppendorf AG, Germany
Unimax 1010 (Bacterial shaker)	Heidolph Instruments GmbH & Co. KG, Germany
Vortex	VELP Scientifica Srl, Italy
VacuuHandControl	Vacuubrand GmbH & Co. KG, Germany
Water Bath WB/OB7-45	Memmert GmbH & Co KG, Germany

2.1.2 Chemicals and reagents

The chemicals used for this thesis were highly purified and accurately weighed using a digital scale. If necessary, the pH was adjusted by adding 1 M HCl or 1 M NaOH and measured using a calibrated pH meter. For the use in cell culture, the solutions were autoclaved or sterile filtered in addition.

Chemical	Company
100 bp DNA Ladder	Thermo Fisher Scientific Inc., USA
1 kb Plus DNA Ladder	Thermo Fisher Scientific Inc., USA
Accutase	Thermo Fisher Scientific Inc., USA
Agarose	Peqlab Biotechnologie GmbH, Germany
Albumin, human, liquid	Albunorm, Germany
Ampicillin	Sigma Aldrich Chemie GmbH, Germany
Ampuwa ddH_2O	Fresenius Kabi AG, Germany
Aqua-Poly/Mount	Polysciences Inc., USA
BamHI-HF	New England Biolabs GmbH, Germany
Biotinylated amyloid β_{1-42}	Bachem Holding AG, Germany
Boric acid	Carl Roth GmbH & Co KG, Germany
Bovine serum albumin	Sigma Aldrich Chemie GmbH, Germany
Calcium chloride ($CaCl_2$)	Sigma Aldrich Chemie GmbH, Germany
Chloroform	Carl Roth GmbH & Co KG, Germany

Chemical	Company
Cholesterol, plant derived	Sigma Aldrich Chemie GmbH, Germany
Collagenase, type IV	Thermo Fisher Scientific Inc., USA
CTS GlutaMAX-I Supplement	Thermo Fisher Scientific Inc., USA
dATP	Thermo Fisher Scientific Inc., USA
ddH_2O	Filtered and autoclaved in-house
DEPC-treated water	Thermo Fisher Scientific Inc., USA
Dihydroethidium (DHE)	Thermo Fisher Scientific Inc., USA
Dimethyl sulfoxide (DMSO)	Carl Roth GmbH & Co KG, Germany
DMEM, high glucose	Thermo Fisher Scientific Inc., USA
DMEM/F-12 with L-glutamine and HEPES	Thermo Fisher Scientific Inc., USA
dNTPs	Peqlab, Germany
EcoRI-HF	New England Biolabs GmbH, Germany
EDTA	Sigma Aldrich Chemie GmbH, Germany
Ethanol	Carl Roth GmbH & Co KG, Germany
Ethidium bromide	Sigma Aldrich Chemie GmbH, Germany
Fetal bovine serum	Thermo Fisher Scientific Inc., USA
Fibronectin from human plasma	Sigma Aldrich Chemie GmbH, Germany
GelStar nucleic acid gel stain	Lonza Cologne GmbH, Germany
Geltrex	Thermo Fisher Scientific Inc., USA
Glacial acetic acid	Carl Roth GmbH & Co KG, Germany
Glucose	Carl Roth GmbH & Co KG, Germany
Glutaraldehyde	Sigma Aldrich Chemie GmbH, Germany
Glycerol	Sigma Aldrich Chemie GmbH, Germany
HBSS	Thermo Fisher Scientific Inc., USA
HEPES	Carl Roth GmbH & Co KG, Germany
Hexanucleotide mix	Roche Holding GmbH, Germany
Hydrochloride acid (HCl)	Sigma Aldrich Chemie GmbH, Germany
Hygromycin B	Thermo Fisher Scientific Inc., USA
Insulin-Transferrin-Selenium-Ethanolamine	Thermo Fisher Scientific Inc., USA
In-Fusion HD Enzyme Premix	Takara Bio Inc., Japan
Isopropanol	Carl Roth GmbH & Co KG, Germany
Knockout Serum Replacement, XenoFree	Thermo Fisher Scientific Inc., USA

Chemical	Company
L-Ascorbic acid 2-phosphate	Sigma Aldrich Chemie GmbH, Germany
L-Glutamine	Thermo Fisher Scientific Inc., USA
Linoleic acid	Sigma Aldrich Chemie GmbH, Germany
Linolenic acid	Sigma Aldrich Chemie GmbH, Germany
Lipofectamin2000	Thermo Fisher Scientific Inc., USA
Lipopolysaccharide	Invivogen, USA
Loading dye	New England Biolabs GmbH, Germany
Lysogeny broth (LB)	Sigma Aldrich Chemie GmbH, Germany
LB agar	Sigma Aldrich Chemie GmbH, Germany
Magnesium chloride ($MgCl_2$)	Carl Roth GmbH & Co KG, Germany
Magnesium sulfate ($MgSO_4$)	Carl Roth GmbH & Co KG, Germany
MluI-HF	New England Biolabs GmbH, Germany
Mono-thioglycerol	Sigma Aldrich Chemie GmbH, Germany
N2 supplement	Thermo Fisher Scientific Inc., USA
N-acetylcysteine	Sigma Aldrich Chemie GmbH, Germany
NheI-HF	New England Biolabs GmbH, Germany
Non-essential amino acids (NEAA)	Thermo Fisher Scientific Inc., USA
Normal goat serum	Sigma Aldrich Chemie GmbH, Germany
OptiMEM	Thermo Fisher Scientific Inc., USA
Paraformaldehyde	Merck Millipore, Germany
PBS	Thermo Fisher Scientific Inc., USA
pHrodo Red *S. aureus* BioParticles	Thermo Fisher Scientific Inc., USA
Poly-L-lysine hydrobromide (PLL)	Sigma Aldrich Chemie GmbH, Germany
Poly-L-ornithine hydrobromide (PLO)	Sigma Aldrich Chemie GmbH, Germany
Polyvinyl alcohol	Sigma Aldrich Chemie GmbH, Germany
Potassium chloride (KCl)	Sigma Aldrich Chemie GmbH, Germany
Potassium phosphate dibasic (K_2HPO_4)	Carl Roth GmbH & Co KG, Germany
QIAzol lysis reagent	Qiagen GmbH, Germany
Random hexamer primer	Roche Holding GmbH, Germany
RNase-free DNase	Qiagen GmbH, Germany
ROCK inhibitor Y-27632	Merck Millipore, Germany
SOC medium	Takara Bio Inc., USA

Chemical	Company
Sodium chloride (NaCl)	Carl Roth GmbH & Co KG, Germany
Sodium dihydrogen phosphate monohydrate ($NaH_2PO_4 \cdot H_2O$)	Carl Roth GmbH & Co KG, Germany
Sodium hydroxide (NaOH)	Carl Roth GmbH & Co KG, Germany
Sodium phosphate dibasic heptahydrate ($Na_2HPO_4 \cdot 7H_2O$)	Carl Roth GmbH & Co KG, Germany
Sodium pyruvate	Thermo Fisher Scientific Inc., USA
S. aureus BioParticles, unlabeled	Thermo Fisher Scientific Inc., USA
STEMdiff APEL2	STEMCELL Technologies Inc., Kanada
Superoxide dismutase	Sigma Aldrich Chemie GmbH, Germany
SYBR Green	Thermo Fisher Scientific Inc., USA
TeSR-E8	STEMCELL Technologies Inc., Kanada
Trisaminomethane (TRIS)	Carl Roth GmbH & Co KG, Germany
Triton X-100	Sigma Aldrich Chemie GmbH, Germany
Trypan blue	Sigma Aldrich Chemie GmbH, Germany
Trypsin-EDTA (0.25%)	Thermo Fisher Scientific Inc., USA
Tween-20	Sigma Aldrich Chemie GmbH, Germany
XhoI	Roche Holding GmbH, Germany
Zeocin	Thermo Fisher Scientific Inc., USA

2.1.3 Consumable supplies

Implement	Company
6-well tissue culture plate	Cellstar, Greiner Bio One, Germany
12-well tissue culture plate	Cellstar, Greiner Bio One, Germany
96-well µ-plates	Ibidi, Germany
96-well flat bottom plates	Corning, Inc, USA
Cell strainer (40 µm)	Corning, Inc, USA
Cell lifter	Corning, Inc, USA
Cryovials (1.8 ml)	Sarstedt AG & Co KG, Germany
Falcon tubes (15 ml)	Cellstar, Greiner Bio One, Germany
Falcon tubes (50 ml)	Sarstedt AG & Co KG, Germany
Graduate pipette tips (10 µl, 100 µl, 1000 µl)	Starlab GmbH, Germany

Implement	Company
Inoculation loop	Sarstedt AG & Co KG, Germany
Nitrile gloves	Meditrade, Germany
Nunc Non-treated T75 Flasks	Thermo Fisher Scientific Inc., USA
Nylon Net Filter (47 mm, pore size 60 µm)	Merck KGaA, Germany
OptiPlate-384	PerkinElmer GmbH, Germany
Pasteur pipettes	Brand GmbH & Co KG, Germany
Petri dishes	Corning, Inc, USA
qPCR semi-skirted 96-well PCR plate	4titude Ltd., Germany
qPCR adhesive PCR plate seal	4titude Ltd., Germany
Stripettes (5 ml, 10 ml, 25 ml)	Sarstedt AG & Co KG, Germany
Safe-seal micro tubes (0.5 ml, 1.5 ml, 2 ml)	Sarstedt AG & Co KG, Germany
Syringes (5 ml, 10 ml, 20 ml)	Omnifix, Braun Meisungen AG, Germany
Tissue culture dishes (100 mm, 150 mm)	Sarstedt Inc., USA
Tissue culture flask (75 cm^3, 25 cm^3)	Sarstedt Inc., USA
Topseal-A adhesive film	PerkinElmer GmbH, Germany
TPP Filtermax, bottle top (500 ml)	TPP Techno Plastic Products AG, Switzerland

2.1.4 Buffers and solutions

Buffer/Solution	Composition/Company
Antibody staining solution	5 % BSA, 0.1% Triton X-100
Blocking solution	10 % BSA, 5 % normal goat serum, 0.1 % Triton X-100
Bovine serum albumin (BSA; 10 % w/v)	10 g BSA in 100 ml 1x PBS
EDTA (0.5 M)	52.025 g EDTA tetrasodium salt hydrate in 250 ml ddH_2O. Adjust pH to 8.5.
FACS staining buffer	1 % BSA, 2 mM EDTA and 0.1 % NaN_3 in PBS
Krebs-HEPES Buffer	135 mM NaCl, 5 mM KCl, 1 mM $MgSO_4$, 0.4 mM K_2HPO_4, 5.5 mM Glucose, 20 mM HEPES. Adjust the pH to 7.4.
LB agar	Roth; 15 g powder in 500 ml ddH_2O
LB broth	Roth; 10 g powder in 500 ml ddH_2O

Buffer/Solution	Composition/Company
Paraformaldehyde (4 %)	4 g Paraformaldehyde in 100 ml PBS; pH 7.4
Phosphate Buffered Saline (10X)	5.125 g $NaH_2PO_4 \cdot H_2O$, 175.25 g NaCl, 23.84 g $Na_2HPO_4 \cdot 7H_2O$ in 1 l ddH_2O. Adjust pH to 7.4
Poly-L-lysine (PLL; 5 µg/ml)	5 µg in 1 ml ddH_2O
Poly-L-ornithine (PLO; 10 µg/ml)	10 mg poly-L-ornithine, 9.2745 g H_3BO_3 in 1 l ddH_2O
Tris-Acetate-EDTA (TAE) Buffer (10x)	48.4 g Tris Base, 11.4 ml Glacial Acetic acid, 3.7 g EDTA in 1 l ddH_2O

2.1.5 Kits

Kit	Company
AlphaLISA SureFire Ultra p-SYK Assay Kit	Perkin Elmer GmbH, Germany
AlphaLISA SureFire Ultra Total SYK Assay Kit	Perkin Elmer GmbH, Germany
AccuPrime Pfx SuperMix	Thermo Fisher Scientific Inc., USA
In-Fusion HD Cloning Kit	Takara Bio Inc., USA
NucleoBond Xtra Maxi Kit	Macherey-Nagel GmbH & Co. KG, Germany
Maxima SYBR Green qPCR Master Mix	Thermo Fisher Scientific Inc., USA
QIAprep Spin Miniprep Kit	Qiagen GmbH, Germany
QIAquick Gel Extraction Kit	Qiagen GmbH, Germany
SuperScript III First-Strand Synthesis Kit	Thermo Fisher Scientific Inc., USA

2.1.6 Cell lines

Cell line	Origin
BIONi010-C (WT)	Reprogrammed iPSC line from fibroblasts of a healthy 15-19-year-old male Danish individual (Karyotype 46, XY). Kindly provided by Janssen Pharmaceutica. Commercially available at EBiSC (Rasmussen *et al*., 2014).
BIONi010-C-9 ($CD33^{-/-}$)	Isogenic cell line to BIONi010-C with a single alteration. One base in exon one as well as 578 bases downstream (including

Cell line	Origin
	whole exon 2) of *CD33* were deleted by CRISPR/Cas9. The base pair deletion led to a frame shift. Kindly provided by Janssen Pharmaceutica. Commercially available at EBiSC.
BIONi010-C-5 ($CD33^{\Delta E2}$)	Isogenic cell line to BIONi010-C with a single alteration. Exon 2 of *CD33* was excised by CRISPR/Cas9, which leads to expression of the CD33 isoform variant 2 also known as $CD33^{\Delta E2}$ or CD33m. Kindly provided by Janssen Pharmaceutica. Commercially available at EBiSC.
Flp-In-293	Cell line isolated from human embryonic kidneys transformed with the SV40 Large T-antigen and stably integrated FRT site. Kindly provided by Prof. Jochen Walter (University of Bonn). Commercially available at Thermo Fisher Scientific.

2.1.7 Media

Medium	Composition
293 medium	DMEM with L-Glutamine and 4.5 g/L D-glucose 10 % FBS 2 mM L-glutamine 1 mM sodium pyruvate 0.1 mM NEAA Antibiotics at indicated concentrations
APEL medium, homemade	DMEM/F-12 with L-glutamine and HEPES 0.5 % (w/v) human Albumin 0.05 % (w/v) Polyvinyl alcohol 100 ng/ml Linoleic acid 100 ng/ml Linolenic acid 2.1 µg/ml Cholesterol, plant derived 50 µg/ml 1-Thioglycerol 1 % (v/v) Insulin-Transferrin-Selenium-Ethanolamine 50 µg/ml L-Ascorbic acid 2-phosphate 2 mM CTS GlutaMAX-I Supplement
Freezing medium for 293 cells	90 % FBS 10 % DMSO

Medium	Composition
Freezing medium for stem cells	90 % Knockout serum replacement, XenoFree 10 % DMSO
iPSdMiG seeding medium	DMEM/F-12 with L-glutamine and HEPES 1 % N2 supplement 1 % CTS GlutaMAX-I Supplement
TeSR-E8	TeSR-E8 basic medium plus supplement

2.1.8 Antibodies

2.1.8.1 Primary antibodies

Target	Conjugate	Clone	Reactivity	Host	Company
CD11b	-	M1/70	Human	Rat	BD Bioscience, Germany
CD14	FITC	HCD14	Human	Mouse	BioLegend CNS, Inc., USA
CD33	-	1c7/1	Human	Mouse	Cedarlane Laboratories, Canada
CD33	-	P67.6	Human	Mouse	Santa Cruz Biotechnology, Inc., USA
CD33	-	P67.6	Human	Mouse	BioLegend CNS, Inc., USA
CD33	-	P67.6 Fab	Human	Mouse	Sanofi, France
CD33	-	WM53	Human	Mouse	Abcam, UK
CD33	-	WM53	Human	Mouse	Exbio, Czech Republic
CD45	APC	HI30	Human	Mouse	BioLegend CNS, Inc., USA
FcγRI	APC	10.1	Human	Mouse	BioLegend CNS, Inc., USA
FcγRI	-	10.1	Human	Mouse	BioLegend CNS, Inc., USA
IBA1	-	polyclonal	Human	Rabbit	Synaptic Systems GmbH, Germany
SIRPα	-	SE7C2	Human	Mouse	Santa Cruz Biotechnology, Inc, USA
TREM2	-	polyclonal	Human	Goat	R&D Systems GmbH, Germany

2.1.8.2 Secondary antibodies and staining reagents

Conjugate/Name	Reactivity	Host	Company
Alexa Fluor 488	Rabbit IgG	Goat	Thermo Fisher Scientific Inc., USA

Conjugate/Name	Reactivity	Host	Company
Alexa Fluor 488	Rat IgG	Goat	Thermo Fisher Scientific Inc., USA
Alexa Fluor 647	Mouse IgG	Goat	Thermo Fisher Scientific Inc., USA
Cy3-Streptavidin	Biotin	*S. avidinii*	Jackson ImmunoResearch, UK
DAPI (20 mg/ml)	DNA	-	Sigma Aldrich Chemie GmbH, Germany
FcR Blocking Reagent	Human Fc Receptors	-	Miltenyi Biotec, Germany
Hoechst 33342	DNA	-	Thermo Fisher Scientific Inc., USA
PerCP/Cyanine5.5	Mouse IgG	Goat	BioLegend CNS, Inc., USA

2.1.8.3 Isotype controls

Isotype	Conjugate	Clone	Host	Company
IgG1, κ	-	F(ab')2	Mouse	Thermo Fisher Scientific Inc., USA
IgG1, κ	-	MOPC-21	Mouse	Abcam, UK or BioLegend CNS, Inc., USA
IgG	-	polyclonal	Goat	R&D Systems GmbH, Germany
IgG1, κ	APC	MOPC-21	Mouse	BioLegend CNS, Inc., USA
IgG1, κ	FITC	MOPC-21	Mouse	BioLegend CNS, Inc., USA

2.1.9 Oligonucleotides for In-Fusion cloning and Sanger sequencing

Name	Nucleotide Sequence (5' → 3')
EEF1A1 Infusion Fwd	GTACGGGCCAGATATACGCGGGCTCCGGTGCCCGTCAGTG
EEF1A1 Infusion Rev	AGCTTAAGTTTAAACGCTAGTCACGACACCTGAAATGGAA GAAAAAAACTTTGAACCACT
IRES Infusion Fwd	CCGTATTACAAATGAGGATCCCCCTCTCCCTCCCCCCCCC
IRES Infusion Rev	ACCATGGTGGCGAGATCCATGGTTGTGGCCATATTATCAT
GCaMP6m Infusion Fwd	ATGGATCTCGCCACCATGGTCGA
GCaMP6m Infusion Rev	CCACACTGGACTAGTGGATCTCACTTCGCTGTCATCATTT
EEF1A1 Sequencing Fwd	GACAATTGCATGAAGAATCT
EEF1A1 Sequencing Rev	AGCTTAAGTTTAAACGCTAG
IRES Sequencing Fwd	CAGGGTCAGAGGTCGGATGT

Name	Nucleotide Sequence (5' → 3')
IRES Sequencing Rev	GACTGCGTGACCTGTCTTATTCC
GCaMP6m Sequencing Fwd	CCCCGAACCACGGGGACGTG
GCaMP6m Sequencing Rev	GCGGCCGCCACTGTGCTG

2.1.10 Oligonucleotides for semi-quantitative real-time PCR

Target	Nucleotide Sequence Forward (5' → 3')	Nucleotide Sequence Reverse (5' → 3')
CD14	ACTTGCACTTTCCAGCTTGC	GCCCAGTCCAGGATTGTCAG
CD33M	GCTGTGGGCAGGGGC	CCTTCCCGGAACCAGTAACC
CD33$^{\Delta E2}$	CCCTGCTGTGGGCAGACTTG	GCACCGAGGAGTGAGTAGTCC
CD64	TCGACCCCCAGCTACAGAAT	ACCAGCTTATCCTTCCACGC
GAPDH	CTGCACCACCAACTGCTTAG	TTCAGCTCAGGGATGACCTT
IL1B	CCAGCTACGAATCTCCGACC	TGGACCAGACATCACCAAGC
IL6	GGCACTGGCAGAAAACAACC	GCAAGTCTCCTCATTGAATCC
IL8	CTGGCCGTGGCTCTCTTG	TTAGCACTCCTTGGCAAAACTG
IL10	CGGCGCTGTCATCGATTT	TTAAAGGCATTCTTCACCTGCTC
INPP5D	ATTTGACCAGCAGCTCTCCC	ACTGGAGGGATAAGGGAGGG
PTPN6	GGCACCATCATCCACCTCAA	AGGCTCTCACGCACAAGAAA
PTPN11	GCCTGCAAAACACGGTGAAT	AGCGTATAGTCATGAGCGGC
SIRPA	GGTCAGCAAAAGCCATGACC	GGCATTCTTCTCGGGCTCAT
TNF	AACCTCCTCTCTGCCATCAA	CCAAAGTAGACCTGCCCAGA
TREM2	TCTCCGGCTGCTCATCTTAC	CACAAGTTGTGCGTGCTGAC
TYROBP	CCGAGTCGCCTTATCAGGA	GACTGTCATGATTCGGGCT

2.1.11 Software and R packages

2.1.11.1 Software

Software	Company/Programmer (Publication)
Accuri C6 Plus Software	BD Biosciences, USA
BBDuk/BBMap v38.86	Joint Genome Institute/Brian Bushnell
Corel Draw 2019	Corel GmbH, Germany

Software	Company/Programmer (Publication)
FACStation	BD Biosciences, USA
FastQC v0.11.8	Babraham Bioinformatics/Simon Andrews
featureCounts/Subread v2.0.0	Yang Liao (Liao *et al*., 2014)
FlowJo v10	FlowJo LLC, USA
ImageJ2/Fiji v1.51	NIH, USA
IN Cell Analyzer 2200 v6.2	GE Healthcare Life Science, UK
Geneious v8.1	Biomatters Ltd, New Zealand
Microsoft Office 2016	Microsoft, Germany
MultiQC v1.7	Philip Ewels (Ewels *et al*., 2016)
NanoDrop 1000 v3.8.1	Thermo Fisher Scientific Inc., USA
Realplex v2.2	Eppendorf AG, Germany
R v4.0.2	The R Foundation, USA
RStudio v1.3.1056	RStudio, Inc., USA
SPSS Statistics v23.0.0.0	SPSS Inc., USA
STAR v2.7.3a	Alexander Dobin (Dobin *et al*., 2013)
Stata v15	Stata Corp LLC, USA

2.1.11.2 R packages

R package	Version	Developer/Publication
apeglm	1.10.0	Zhu, Ibrahim and Love, 2019
ChEA3	3.0.0	Keenan *et al.*, 2019
clusterProfiler	3.16.1	Yu *et al.*, 2012
DESeq	1.28.1	Love, Huber and Anders, 2014
fgsea	1.14.0	Sergushichev, Korotkevich and Sukhov, 2019
ggplot2	3.3.2	Wickham, 2016
org.Hs.eg.db	3.11.4	Carlson, 2019
pheatmap	1.0.12	Kolde, 2019
ReactomePA	1.32.0	Yu and He, 2016
RUVSeq	1.22.0	Risso *et al.*, 2014
visNetwork	2.0.9	Almende, Thieurmel and Titouan, 2019
WGCNA	1.69	Langfelder and Horvath, 2008

2.2 Methods

2.2.1 Cell culture

Cell culture work was performed under sterile cell culture hoods with laminar air flow. The cells were cultivated in humidified incubators at 37 °C and 5-6 % CO_2. For extended storage periods, cells were frozen in 1 ml of the cell-specific freezing medium (see section 2.1.7) in 1.8 ml cryovials at a density of 2-5 x 10^6 cells/ml. Storage for up to four weeks was done at -80 °C but for longer periods the cells were transferred to a -152 °C freezer.

2.2.1.1 Culture of Flp-In-293 cells

Flp-In-293 cells and constitutive CD33-DAP12-GCaMP6m expression cell lines were cultured according to an adapted version of the manufacturer's instructions. Briefly, the cells were thawed in pre-warmed 293 medium and centrifuged (400 x g, 3 min) followed by cultivation in 293 medium containing 100 µg/ml Zeocin. Constitutive CD33-DAP12-GCaMP6m expression cell lines were cultured in 293 medium + 150 µg/ml Hygromycin B. The cells were passaged when reaching 80-90 % confluency by chemical detachment using 0.25 % Trypsin/EDTA. The cells were frozen in 90 % FBS and 10 % DMSO in a CoolCell LX device at -80 °C for 24-48 hours. For long-term storage, the cells were placed in a -152 °C freezer.

2.2.1.2 Culture of human induced pluripotent stem cells

BIONi induced pluripotent stem cell (iPSC) lines were kindly provided by Janssen Pharmaceutica and were cultured in geltrex-coated six-well plates. The plates were pre-coated with 1 ml 180 µg/ml ice-cold geltrex in DMEM/F-12 per well for 30-60 minutes at room temperature. iPSCs were cultured in TESR-E8 medium with a complete medium change every 24 hours. When reaching about 80 % confluency, the cells were passaged by incubation with accutase or 0.5 mM EDTA in PBS for 3 minutes at room temperature. The detached cells were collected in a 15 ml falcon and centrifuged at 200 x g. The cell pellet was resuspended in fresh pre-warmed TeSR-E8 medium and plated into new geltrex-coated six-well plates. If the cells were passaged with accutase 10 µM ROCK inhibitor Y-27632 was added in addition to the culture for 24 hours.

2.2.1.3 Differentiation of human iPSC into microglia

The differentiation of iPSCs into iPSC-derived microglia (iPSdMiG) was performed according to an established protocol and submitted patent by LIFE & BRAIN GmbH (Mathews *et al*., *in preparation*; Patent ID EP20162230). Of note, some critical factors necessary for proper differentiation were omitted because of confidentiality reasons. For the differentiation into iPSdMiG BIONi iPSCs were detached when reaching 80 % confluency using 1 mg/ml collagenase IV for 30 minutes at 37 °C. The colonies were collected carefully in DMEM/F-12 and pelleted by gravity. The supernatant was aspirated, and the colonies were transferred onto non-coated 125 ml Erlenmeyer flasks to allow formation of 3D embryoid bodies (EBs). The EBs were cultured in EB basal medium for four days with changing supplements. Finally, on day 4 the EBs were seeded in APEL medium supplemented with cytokines into PLO and fibronectin-coated cell culture formats. Medium changes were performed 3 times a week. The cultures started to produce non-adherent iPSdMiG, i.e., in suspension, from week 4-6 after seeding of the EBs. Free-floating iPSdMiG were harvested every week for up to 3 months. The culture supernatant was collected through a 40 µm cell strainer and pelleted by centrifugation at 400 x g for 5 minutes. Subsequently, the iPSdMiG were plated in PLL-coated cell culture dishes of the desired format in iPSdMiG seeding medium supplemented with cytokines. 24 hours after plating the cells were used for experiments. The purity of every batch of iPSdMiG was analyzed by expression of myeloid markers CD11b, CD14 and CD45.

2.2.2 Generation of CD33 reporter cell lines

2.2.2.1 CD33-DAP12-GCaMP6m constructs

The CD33-DAP12 fusion protein constructs were generated as previously described (Mossad, 2016). Briefly, the full mRNA sequence of the human CD33/SIGLEC3 and the human TYROBP/DAP12 were obtained from the NCBI Gene Databank (Gene IDs 945 and 7305, respectively). The CD33-DAP12 fusion protein lacks the intracellular and the transmembrane domains of CD33, which were exchanged by the DAP12 sequence representing an ITAM domain. Two different CD33-DAP12 constructs were generated: CD33M-DAP12 and $CD33^{\Delta E2}$-DAP12 – the latter lacks the sialic binding domain (Figure 8A). Further, a point mutation was introduced into the DAP12 gene (p.D50A), which eliminates possible interactions with ITAM receptors, including TREM2, via the Site-directed mutagenesis kit following manufacturer's instructions

(Mossad, 2016). Within this thesis, the *cytomegalovirus* (*CMV*) promoter of pcDNA5/FRT was exchanged with the *eukaryotic translation elongation factor 1 alpha 1* (*EEF1A1*) promoter to prevent epigenetic silencing (Meilinger *et al*., 2009; Teschendorf *et al*., 2002). As a second step, a calcium-sensitive green fluorescent protein (GFP), *GCaMP6m* (T. W. Chen *et al*., 2013), was introduced into the new pcDNA5/FRT-EEF1A1-CD33-DAP12 expression vector separated from the CD33-DAP12 fusion protein via an *internal ribosome entry site* (*IRES*). The In-Fusion primers were designed using Geneious v8.1 with 20 bp homologous arms at both ends, which matched the insertion site in the plasmid.

2.2.2.2 Amplification of target sequences

The target sequences were amplified using customized primers (see section 2.1.9) and a pLenti-EEF1A1-GFP plasmid for *EEF1A1* or pGP-CMV-GCaMP6m for *GCaMP6m*. In detail, 20 ng of plasmid (0.5 µl) was added together with 10 µM of each primer (1 µl each) and 22.5 µl of Accuprime Pfx SuperMix to a final reaction volume of 25 µl. The PCR was performed on a T3 thermocycler with the following program:

Table 1: PCR program for In-Fusion cloning

Step	Temperature	Time	Cycles
Initial Denaturation	95 °C	5 min	-
Denature	95 °C	30 s	35
Anneal	60 °C	30 s	
Extend	68 °C	90 s	
Final Extension	68 °C	10 min	-

2.2.2.3 Restriction digestion

Restriction digestion was performed with 500-1,000 ng of plasmid as input mixed with 1 µl of the restriction enzyme of choice and 2 µl of the recommended enzyme buffer. The reaction was filled up to 20 µl with ddH_2O, incubated for 1 hour at 37 °C and subsequently analyzed by agarose gel electrophoresis.

2.2.2.4 Agarose gel electrophoresis and gel extraction

Analysis of successful amplification of target sequences by PCR or restriction digestion of plasmids was performed using agarose gel electrophoresis. A 1 % agarose gel was prepared by solving 0.8 g of pure agarose powder in 80 ml of TAE buffer in a microwave

oven. When the liquid cooled down to approximately 55-60 °C, 4 µl of ethidium bromide (1:20,000) was added and subsequently the liquid was poured into a gel casting tray. If the samples should be used for In-Fusion cloning and excised from the gel, 8 µl of GelStar nucleic acid gel stain (1:10,000) was used instead of ethidium bromide. After the gel solidified it was placed into the gel electrophoresis running chamber and covered with TAE buffer. The samples were mixed with 4-5 µl of 6x loading dye and loaded onto the gel together with 2 µl of 1 kb Plus DNA Ladder as a control. The gel was run for 1 hour at 100 V and then analyzed using a Gel Doc 2000 system. For purification via gel electrophoresis the desired bands were then excised using a scalpel and DNA gel extraction was performed using the QIAquick Gel Extraction Kit according to manufacturer's instructions. Briefly, the excised gel pieces were weighted and 300 µl of Buffer QC was added per 100 mg of gel followed by incubation at 50 °C for 10 minutes or until the gel was completely dissolved. Subsequently, 1 gel volume of isopropanol was added, the liquid was transferred into a QIAquick spin column and centrifuged in a table-top centrifuge at 12,000 x g for 1 minute. After two washing steps with 750 µl Buffer PE the DNA was eluted with 20-50 µl of ddH_2O. Finally, the concentration and purity of the DNA was measured using a NanoDrop1000 spectrophotometer at 260 nm with a conversion factor of 1.0 equals 50 ng/µl DNA. The typical ratio for 260/280 was between 1.70-1.90 and for 260/230 > 1.90, which indicates pure DNA samples.

2.2.2.5 In-Fusion cloning of human EEF1A1 and GCaMP6m

For the exchange of the *CMV* promoter with the human *EEF1A1* promoter, 1 µg of pcDNA5/FRT (CD33M-DAP12 or $CD33^{\Delta E2}$-DAP12) was double digested with MluI-HF and NheI-HF in cutsmart buffer for 1 hour at 37 °C to cut out the *CMV* promoter region. For the incorporation of *IRES* and *GCaMP6m* the pcDNA5/FRT-EEF1A1 plasmids (CD33M-DAP12 or $CD33^{\Delta E2}$-DAP12) were digested with BamHI-HF in cutsmart buffer for 1 hour at 37 °C. The digested plasmids and the PCR fragments were analyzed and purified by agarose gel electrophoresis. The desired bands were excised, and gel extraction of the DNA was performed. The In-Fusion reaction was performed with a vector to insert molar ratio of 1:2. In detail, 50 ng of plasmid was used with the according mass of insert and 2 µl of In-Fusion HD Enzyme Premix in a 10 µl reaction. The reaction mix was incubated at 50 °C for 15 minutes and subsequently used for transformation.

2.2.2.6 Bacterial transformation and plasmid DNA isolation

For transformation of In-Fusion reactions, 2.5 µl of the reaction mix was incubated with 47.5 µl of Stellar competent cells for 30 minutes on ice and then heat-shocked for 45 seconds at 42 °C. Afterwards, the cells were placed on ice for 1 minute followed by addition of 450 µl pre-warmed SOC medium. The transformation reaction was then incubated for 1 hour at 37 °C in an Unimax 1010 with 190 rpm shaking. Finally, 100 µl suspension was plated on LB agar plates containing 50 µg/ml ampicillin and incubated overnight at 37 °C. For regular plasmid transformations 10 ng of plasmid was incubated with 50 µl Stellar competent cells. The next day, colonies were picked and expanded in 3 ml LB broth overnight at 37 °C with 190 rpm shaking. Subsequently, 2 ml of the bacterial suspension was collected for plasmid isolation using the QIAprep Spin Miniprep Kit according to manufacturer's instructions. Briefly, bacteria were pelleted in a 2 ml microcentrifugation tube by centrifugation at 6,800 x g for 3 minutes at room temperature followed by resuspension in 250 µl Buffer P1 and addition of 250 µl Buffer P2. The tube was mixed by inverting 4-6 times and incubated for 5 minutes at room temperature. Subsequently, 350 µl of Buffer N3 was added, mixed by inverting the tube 4-6 times and centrifuged at 18,000 x g for 10 minutes. Approximately 800 µl of the supernatant were transferred into a QIAprep 2.0 spin column and centrifuged at 18,000 x g for 30 seconds. Two washing steps were applied, the first with 500 µl Buffer PB and the second with 750 µl Buffer PE followed by removing the residual wash buffer by centrifugation. Finally, the plasmid DNA was eluted in 30 µl ddH_2O.

To obtain higher plasmid yields, validated clones were transformed into Stellar competent cells, inoculated in 200 ml LB broth, and cultured overnight at 37 °C with 190 rpm shaking. Plasmid isolation was subsequently performed using the NucleoBond Xtra Maxi Kit following manufacturer's instructions. In detail, the culture supernatant was centrifuged at 4000 x g for 15 minutes at 4 °C, and resuspended in 12 ml of Buffer RES. Then, 12 ml of Buffer LYS were added and mixed in a 50 ml falcon tube by inverting it 4-6 times. In the 5 minutes incubation phase, the NucleoBond Xtra column filter was equilibrated with 25 ml of Buffer EQU. To neutralize the reaction, 12 ml Buffer NEU was added to the 50 ml tube and thoroughly mixed. The lysate was loaded on the NucleoBond Xtra column filter. After it flowed through, the column filter was washed with 15 ml of Buffer EQU, the filter discarded, and the column washed again with 25 ml Buffer WASH. Elution of the bound plasmid DNA was realized by

adding 15 ml Buffer ELU. Subsequently, the eluted liquid was mixed with 10.5 ml isopropanol, vortexed and incubated for 2 minutes at room temperature. Afterwards, the mixture was loaded on the NucleoBond Finalizer Large, washed once with 4 ml 70 % ethanol and air-dried. Finally, the plasmid DNA was eluted using 500 µl TRIS. The concentration and purity of the DNA was measured using a NanoDrop1000 spectrophotometer at 260 nm with a conversion factor of 1.0 equals 50 ng/µl DNA. To analyze the plasmid, 500 ng of the plasmid DNA was then digested with indicated restriction digestion enzymes for 1 hour at 37 °C. Positive clones as well as amplified plasmids for stable transfection were further validated by Sanger sequencing by Microsynth Seqlab GmbH in Bonn.

2.2.2.7 Stable transfection of Flp-In-293 cells

In order to generate a CD33-DAP12-GCaMP6m reporter cell line, 3 x 10^6 Flp-In-293 cells were plated on a 100 mm cell culture dish and transfected the other day with Lipofectamine2000 in Opti-MEM according to manufacturer's instructions. The transfection mixture containing Lipofectamin2000, the pcDNA5/FRT-EEF1A1-CD33-DAP12-GCaMP6m plasmids and pOG44, encoding for the Flp recombinase at a molar ratio of 1:9 was pre-incubated in Opti-MEM separately for 5 minutes, then together for 20 minutes and subsequently incubated with the cells for 4 hours at 37°C. Afterwards, the transfection mixture was exchanged with pre-warmed 293 medium without antibiotics. 48 hours post transfection the cells were split to 25-30 % confluency. When the cells had attached to the dish, the culture medium was exchanged to 293 medium containing 150 µg/ml Hygromycin B to select for stable transfected clones. Approximately 20 clones per construct were then picked using a 100 µl pipette and expanded. Afterwards, the clones were examined for transgene expression by flow cytometry. For positive-tested clones two subclonal dilution steps were performed to ensure monoclonality and isogeneticity. Briefly, each subclonal dilution was performed by seeding positive clones at a density of 10-50 cells per ml in 100 mm cell culture dishes. After expansion, a few colonies were picked and reanalyzed for transgene expression. Retested positive clones were then used to perform calcium imaging experiments.

2.2.3 Detection of extracellular protein expression by flow cytometry

Stable transfected 293 cells were seeded 48 hours prior experiment in 6-well plates at a density of 3 x 10^5 cells per well. IPSdMiG were seeded 24 hours prior experiment in

6-well plates in iPSdMiG seeding medium at a density of 0.5-1 x 10^6 cells per well. Prior to the staining, antibodies (see section 2.1.8) were evaluated for the best concentration by antibody titration.

For the staining procedure, the cells were washed three times with PBS and mechanically detached using a cell lifter. Subsequently, the stable transfected 293 samples were incubated with the primary antibody against CD33 (clones 1c7/1, WM53 or P67.6, all 5 µg/ml) for 1 hour on ice followed by two washing steps with PBS and 30 minutes incubation with 5 µg/ml of the secondary antibody PerCP/Cy5.5-conjugated goat-anti-mouse IgG in PBS in darkness on ice. IPSdMiG were pre-incubated with 1:10 FcR Blocking Reagent in FACS staining buffer for 15 minutes on ice. Subsequently, the cells were incubated with directly conjugated antibodies FITC-CD14 (20 µg/ml), APC-CD45 (0.45 µg/ml) and APC-FcγRI (4 µg/ml) or unconjugated antibodies CD11b, CD33 and SIRPα (all 5 µg/ml) in FACS staining buffer containing 1:20 FcR Blocking Reagent for 1 hour on ice in darkness. Following two washing steps with PBS samples with unconjugated primary antibodies were incubated with either Alexa Fluor 488-conjugated goat-anti-rat IgG or Alexa Fluor 647-conjugated goat-anti-mouse IgG secondary antibodies in FACS staining buffer supplemented with 1:40 FcR Blocking Reagent for 30 minutes on ice in darkness. As controls either directly-conjugated isotype or secondary antibody-treated samples were used. Prior to the measurement, the samples were again washed two times with PBS and finally resuspended in 200 µl PBS. Fluorescence intensity was determined by flow cytometry (BD FACSCalibur/BD Accuri C6 Plus) and analyzed using FlowJo v10.

2.2.4 Calcium imaging in CD33 reporter cell lines

For calcium imaging, stable CD33-DAP12-GCaMP6m-expressing reporter cell lines were seeded in PLL-coated 96 well µ-plates at a density of 2 x 10^4 cells per well in 293 medium containing Hygromycin B. 48 hours after seeding the cells were prepared for imaging by washing with 1x PBS and incubating with Hoechst 33342 (5 µg/ml) in HBSS for 10 minutes at 37°C. The staining solution was exchanged to the imaging solution 100 µl HBSS + 1 % FBS per well for calcium imaging. Images were taken using an IN Cell Analyzer 2200 system with a Nikon 20X, numerical aperture 0.45, Plan Fluor, ELWD, Corr Collar 0-2.0, CFI/60 objective with one by one binning and the polychroic changer set to QUAD1. Images were taken for 95 seconds with f = 1 Hz. Brightfield and Hoechst 33342 images were only taken at the beginning and the end.

50 µl of dATP (100 µM), CD33 or isotype antibodies (10 µg/ml; see section 2.1.8.1; P67.6 from Santa Cruz) were automatically added to the cells after 5 seconds of baseline imaging in a 3 x solution. The Images were analyzed using FIJI for ImageJ and calcium signal was calculated using the *ΔF/F(t)* (Equation 1) as previously reported (Jia *et al*., 2011) with τ_0 = 1 seconds, τ_1 = 4 seconds and τ_2 = 9 seconds. For the statistical analysis, the area under curve (AUC) and the maximum *ΔF/F(t)* signal were calculated for each antibody in each independent experiment.

(A) $$F(t) = \frac{1}{N}\sum_{ROI} f_i(t)$$

(B) $$F_0(t) = \left\{ min\left(\overline{F(x)}\right) \middle| (t-\tau_2) < x < t \right\} \quad where\ \overline{F(x)} = \frac{1}{\tau_1}\int_{x-\frac{\tau_1}{2}}^{x+\frac{\tau_1}{2}} F(\tau)d\tau$$

(C) $$R(t) = \frac{F(t) - F_0(t)}{F_0(t)}$$

(D) $$\Delta F/F(t) = \frac{\int_0^t R(t-\tau)\times\omega(\tau)d\tau}{\int_0^t \omega(\tau)d\tau} \quad where\ \omega(\tau) = exp\left\{-\frac{|\tau|}{\tau_0}\right\}$$

Equation 1: The *ΔF/F(t)* calculation according to Jia *et al*., 2011.
(A) Calculation of the mean fluorescence intensity of a region of interest at the time point *t*. **(B)** The minimum $\overline{F(x)}$, which is in the range of *t – τ2* and smaller than *x* and *t* gives the time-dependent baseline $F_0(t)$. **(C)** The relative change in fluorescence intensity at the time point t is calculated by the quotient of the mean fluorescence intensity *F(t)* minus the time-dependent baseline $F_0(t)$ divided by the time-dependent baseline $F_0(t)$. **(D)** Noise filtering of the function is achieved by an exponentially weighted moving average over *R(t)* from 0 to *t*.

2.2.5 *In silico* comparison of iPSdMiG with human primary microglia

2.2.5.1 Sample preparation, mRNA sequencing, trimming, alignment, and read count generation

RNA for mRNA sequencing was kindly provided by Dr. Mona Mathews (iPSdMiG samples (31F, C133S4, C14 lines; n = 3 each)), Dr. Jens Kopatz and Jonas Winkler (THP1 samples; n = 6) as well as Jianbin Wen and Dr. Michael Peitz (iPSC samples (C14 line; n = 3)). RNA was diluted to 100 ng/µl. Library preparation and subsequent mRNA sequencing were performed at the NGS Core Facility at the University Hospital in Bonn. Briefly, quality control was performed using a TapeStation 2200 and library preparation was realized with a total input of 100 ng RNA using Lexogen's QuantSeq 3' mRNA-Seq Library Prep Kit FWD for Illumina. Subsequent mRNA sequencing was performed on a HiSeq 2500 V4 with 1-2 x 10^7 single-end reads. Base calling was

performed with bcl2fastq2 [v2.20]. For *in silico* comparison of iPSdMiG with human primary microglia (n = 39) and cortices (n = 16) (Galatro *et al*., 2017) as well as with iPSC-derived microglia-like cells (iMGL; n = 9) (Abud *et al*., 2017), raw read data (fastq files) were downloaded from the gene expression omnibus (GEO) databank (accession numbers GSE99074 (Galatro *et al*., 2017) and GSE89189 (Abud *et al*., 2017)). The entire analysis was performed within the Ubuntu 20.04.1 LTS operating system using selected open-source software. Quality of mRNA sequencing was analyzed using FastQC [v0.11.8]. Adapter contaminations as well as poor quality bases were trimmed using BBDuk from BBMap [v38.86]. Afterwards, STAR [v2.7.3a (Dobin *et al*., 2013)] with standard parameters was used to align the reads to the *Homo sapiens* reference genome hg38 (GRCh38) with the ensemble gene annotation version 97. The aligned reads were used for counting of reads per gene by featureCounts/Subread [v2.0.0 (Liao *et al*., 2014)] ignoring multimapping reads. The summaries of every single step were collected and summarized using MultiQC [v1.7 (Ewels *et al*., 2016)].

2.2.5.2 Differential expression, enrichment, and weighted gene correlation network analyses

The following analyses were performed within the R environment using R [v4.0.3 (R Core Team, 2020)] and RStudio [v1.3.1056 (RStudio Team, 2020)]. During the analysis, one outlier was identified in the human primary microglia dataset by Euclidean clustering of sample distances, which was consequently excluded from the analysis. First, low abundance genes were filtered by excluding genes with less than 5 counts in at least 2 samples. Then, the unwanted variance, which occurs because of different library preparation protocols and kits as well as different sequencing sites and machines, was removed using RUVSeq [v1.22.0 (Risso *et al*., 2014)]. For exploratory data analysis and weighted gene correlation network analyses (WGCNA) variance-stabilized RUVSeq-corrected data was used. Differential expression analysis was performed using the DESeq2 package [v1.28.1 (Love *et al*., 2014)] and apeglm [v1.10.0 (Zhu *et al*., 2019)] with the individual samples as contrast. Here, the RUVSeq correction factor was used within the DESeq design formula – as suggested by Love and colleagues – to eliminate the unwanted variance (Love *et al*., 2014). The human primary microglia were then directly compared to iPSdMiG and differentially expressed genes ($|\log2FC| \geq 1$ and FDR-adjusted p value ≤ 0.01) were used for pathway enrichment analysis with clusterProfiler [v3.16.1 (Yu *et al*., 2012)] and reactomePA

[v1.32.0 (Yu & He, 2016)]. For transcription factor enrichment analysis, the microglial core signature of iPSdMiG and human primary microglia was retrieved separately by individual comparisons of both samples with a very distinct cell type, here iPSCs (Galatro *et al*., 2017). Subsequently, for each comparison genes with $\log_2$FC ≥ 3 and FDR-adjusted *p* value ≤ 0.001 were extracted as the microglial core signature. Of note, for these analyses the different iPSdMiG lines were pooled and analyzed as one set of data. The microglia core signature was then used to identify regulatory elements such as transcription factors using ChEA3 (Keenan *et al*., 2019). The results were plotted using visNetwork [v2.0.9 (Almende *et al*., 2019)]. Finally, WGCNA was performed to identify clusters of co-expressed genes between the different cell types using the WGCNA package [v1.69 (Langfelder & Horvath, 2008)]. The identified co-expression modules were subsequently analyzed for enriched pathways by clusterProfiler and reactomePA. Again, within this analysis the three iPSdMiG lines were pooled and analyzed as one set of data.

2.2.6 Detection of phosphorylated and total SYK levels

For detection of phosphorylated SYK (pSYK) and total SYK (tSYK) levels, iPSdMiG were seeded in flat bottom 96 well plates at a density of 2 x 10^4 cells per well as described above. The next day, the cells were treated with either 10 µg/ml anti-FcγRI, anti-TREM2, or isotype control antibodies in iPSdMiG seeding medium for 5 minutes at 37 °C prior to cell lysis or left untreated. For ITAM/ITIM pathway interference experiments, CD33 antibodies (10 µg/ml; P67.6 from BioLegend) were co-incubated together with anti-TREM2 (5 µg/ml) in iPSdMiG seeding medium for 5 minutes at 37 °C. PSYK levels were detected by the AlphaLISA SureFire Ultra p-SYK (Tyr525/526) Assay Kit and normalized to the values of total SYK using the AlphaLISA SureFire Ultra Total SYK Assay Kit according to the 2-plate assay protocol for adherent cells. Briefly, the culture supernatant was discarded, 50 µl Lysis Buffer was added, and the cells were lysed on a plate shaker at 350 rpm for 10 minutes at room temperature. 10 µl of the cell lysate was used per reaction. All samples were measured as technical duplicates in 384-well OptiPlates. Subsequently, 5 µl of Acceptor Mix was added per reaction to the 10 µl cell lysate, sealed with Topseal-A adhesive film, and incubated for 1 hour at room temperature in darkness. Afterwards, 5 µl Donor Mix was added per reaction and again incubated for 1 hour at room temperature in darkness. Finally, the plate was measured using the standard AlphaLISA settings on a PerkinElmer EnVision

2104 system. For the analysis, the technical duplicates were averaged and the pSYK signal was normalized to the total SYK signal. Further, each condition was normalized to the wild type control or isotype treated control.

2.2.7 Gene transcription analysis by semi-quantitative real-time PCR

2.2.7.1 RNA isolation

IPSdMiG were seeded at a density of 4 x 10^5 cells per well in 6-well plates 24 hours prior to the experiment in iPSdMiG seeding medium. Total RNA from iPSdMiG was isolated using the standard phenol-chloroform-extraction method. Briefly, the cells were incubated with 1 ml QIAzol lysis reagent for 5 minutes and transferred to 2 ml microcentrifugation tubes. Subsequently, 200 µl chloroform was added, mixed thoroughly, and incubated for 3 minutes at room temperature. Then, the suspension was centrifuged at 13,000 x g for 10 minutes at 4 °C. Approximately 500 µl of the upper colorless aqueous phase was collected in a new 1.5 ml microcentrifugation tube and mixed with 500 µl isopropanol. For precipitation of the RNA, the samples were incubated at least 2 hours (to overnight) at -20 °C and then pelleted by centrifugation at 13,000 x g for 15 minutes at 4 °C. The supernatant was decanted, the pellet washed two times with 70 % ethanol, and centrifuged at 13,000 x g for 5 minutes. Afterwards, the RNA pellet was air-dried for at least 15 minutes or until no liquid remained and solved in 25 µl DEPC-treated water. RNA concentration was measured using a NanoDrop1000 at 260 nm with a conversion factor of 1.0 equals 40 ng/µl RNA. The typical ratio for 260/280 was between 1.90-2.10 and for 260/230 > 1.90, which indicates pure RNA samples.

2.2.7.2 cDNA synthesis

Isolated RNA was reverse transcribed to cDNA using the SuperScript III First-Strand Synthesis Kit following manufacturer's instructions. In short, 1 µg RNA was incubated with 1 µl random hexamer primers and 1 µl 10 mM dNTPs at 65 °C for 5 minutes and then placed for 1 minute on ice. Afterwards, 4 µl of 5 x single strand buffer, 2 µl of dithiothreitol (DTT) and 1µl of 200 U/ml superscript III reverse transcriptase were added per sample. The conversion of RNA to cDNA was performed using a T3 Thermocycler at 50 °C for 1 hour followed by enzyme inactivation at 85 °C for 5 min. Finally, the cDNA was diluted to 100-200 ng/µl.

2.2.7.3 Semi-quantitative real-time polymerase chain reaction analysis

The generated cDNA was used to analyze gene transcript levels of *CD14*, *CD33M, CD33$^{\Delta E2}$*, *C-X-C motif chemokine ligand 8* (*CXCL8*/*IL-8*), *Fc fragment of IgG receptor Ia* (*FCGR1A*), *interleukin* (*IL*) *1B*, *IL6*, *IL10*, *inositol polyphosphate-5-phosphatase D* (*INPP5D*), *protein tyrosine phosphatase non-receptor type 6* (*PTPN6*), *PTPN11*, *signal regulatory protein alpha* (*SIRPA*), *tumor necrosis factor* (*TNF*), *triggering receptor expressed on myeloid cells 2* (*TREM2*), and *transmembrane immune signaling adaptor TYROBP* (*TYROBP*) using semi-quantitative real-time polymerase chain reaction (qRT-PCR). *Glyceraldehyde 3-phosphate dehydrogenase* (*GAPDH*) was used as housekeeping gene. Maxima SYBR Green qPCR Master Mix was used with 2 µl of cDNA and the respective gene-specific primers (see 2.1.10). For *CD14*, *IL10*, *TNF*, and *TYROBP* the primer sequences were used from previous publications (Alias *et al*., 2012; Brosig *et al*., 2015; Krakauer *et al*., 2008; Malvandi *et al*., 2013). The ABI 5700 Sequence Detection System was used for amplification and detection (95 °C, 10 seconds; 40 cycles of 95 °C for 15 seconds, 60 °C for 30 seconds and 72 °C for 30 seconds). Relative gene transcription was quantified by calculating the $\Delta\Delta C_t$ calculation (Equation 2) with *GAPDH* as internal control. Each value was normalized to the wild type control condition.

(A) $$\Delta C_t = C_{t\,Target\,Gene} - C_{t\,Reference\,Gene}$$

(B) $$\Delta\Delta C_t = \Delta C_{t\,Stimulation} - \Delta C_{t\,Control}$$

(C) $$Expression\,Fold\,Change = 2^{-\Delta\Delta C_t}$$

Equation 2: The $\Delta\Delta C_t$ method to calculate differences in mRNA expression levels after qRT-PCR. (A) In a first step the threshold cycle of the target gene is subtracted by the threshold cycle of the reference gene, which results in the ΔC_t. **(B)** Then, the ΔC_t of the stimulation sample is subtracted by the ΔC_t of the control sample, which results in the $\Delta\Delta C_t$. **(C)** The final result is obtained by raising 2 to the power of $-\Delta\Delta C_t$.

2.2.8 Phagocytosis assays

2.2.8.1 Phagocytosis of pHrodo Red Staphylococcus aureus BioParticles

IPSdMiG were seeded at a density of 2 x 10^4 cells per well of an ibidi 96-well µ-plate as described above and incubated with 100 µl of 0.5 mg/ml pHrodo Red *Staphylococcus aureus* BioParticles resuspended in iPSdMiG seeding medium for 90 minutes at 37 °C according to manufacturer's instructions. Afterwards, the cells were washed three times with 1x PBS and incubated with 5 µg/ml Hoechst 33342 for 10 minutes at 37 °C. Subsequently, the cells were washed two times with 1x PBS and

finally 200 µl PBS was added to each well. Nine pictures were randomly taken for each experimental condition using an IN Cell Analyzer 2200 system, and the intensity of the collected images was determined by FIJI for ImageJ as integrated density using a semi-automatic analysis pipeline. The background was subtracted in each image and normalized to the number of Hoechst 33342-positive nuclei. Each ratio was normalized to the wild type control condition.

2.2.8.2 Preparation of aggregated amyloid β_{1-42}

Prior to phagocytosis experiments, aggregated amyloid β_{1-42} ($A\beta_{1-42}$) was prepared. Biotinylated $A\beta_{1-42}$ was incubated for 72 hours at 37 °C to cause formation of a mixture of oligomeric, protofibrillar, and fibrillar $A\beta_{1-42}$ species.

2.2.8.3 Phagocytosis of amyloid β_{1-42}

Phagocytosis experiments were performed as previously described (Shahraz *et al*., 2015). Briefly, 2 x 10^4 iPSdMiG were seeded per well of an ibidi 96-well µ-plate as described above and incubated with 2 µM biotinylated $A\beta_{1-42}$ in iPSdMiG seeding medium for 90 minutes at 37 °C. Afterwards, the cells were washed with PBS and fixed with ice cold 4 % PFA for 15 minutes, followed by incubation with blocking solution for 1 hour at room temperature. Then, iPSdMiG were incubated with rabbit anti-IBA1 (2 µg/ml) overnight at 4 °C in antibody staining solution followed by 3 washing steps with PBS and the incubation with Alexa Fluor 488-conjugated goat-anti-rabbit IgG (2.5 µg/ml) and Cy3-conjugated streptavidin (2.5 µg/ml) in PBS for 2 hours at room temperature. Afterwards, the cells were washed two times with PBS, counterstained with DAPI (1:10,000) in PBS for 30 seconds and washed again two times with PBS. For each condition, nine images were randomly taken using an IN Cell Analyzer 2200 system. Relative $A\beta_{1-42}$ phagocytosis was determined using FIJI for ImageJ by calculating the ratio of $A\beta_{1-42}$ particles in cells to the total number of cells. Each ratio was normalized to the wild type control condition.

2.2.9 Dihydroethidium staining for detection of reactive oxygen species.

Analysis of reactive oxygen species (ROS) was performed as previously described (Shahraz *et al*., 2015). In short, the cells were seeded at a density of 2 x 10^4 cells per well of an ibidi 96-well µ-plate as described above. Subsequently, the cells were pre-treated with 4 mM N-acetylcysteine (NAC) in iPSdMiG seeding medium for 1 hour at 37 °C or left untreated. Afterwards, iPSdMiG were treated with 20 µg unlabeled

Staphylococcus aureus BioParticles in 100 µl iPSdMiG seeding medium per well for 15 minutes at 37 °C with or without NAC or left untreated. After removing the supernatant, the cells were washed three times with Krebs-HEPES-buffer and all conditions were treated with 30 µM dihydroethidium (DHE) in Krebs-HEPES-buffer for 15 minutes at 37 °C. Then, the cells were washed three times with Krebs-HEPES-buffer fixed with ice cold 4 % PFA containing 0.25 % glutaraldehyde for 15 minutes, washed three times with PBS and counterstained with DAPI (1:10,000) in PBS for 30 seconds. Finally, after two additional PBS washing steps, each well was filled with 200 µl of PBS. On the same days nine pictures per well were randomly taken for each condition with the IN Cell Analyzer 2200 system and DHE intensity from the collected images was determined by FIJI for ImageJ as the integrated density using a semi-automatic analysis pipeline. The background was subtracted in each image and the DHE intensity was normalized to the number of DAPI-positive nuclei of every image. The average of all nine individual images of each experimental condition was then normalized to the untreated (UT) wild type condition.

2.2.10 Graphical visualization and statistical analysis

Results are presented as mean ± *standard error of the mean* (*SEM*) and plotted using Prism v8 or R v4.0.2 with colorblind-friendly colors. Statistical analysis was performed with Stata v15 or SPSS v23 as indicated in the figure legend and described below. The data was checked for normal distribution by Shapiro-Wilk test and for equality of variances by Levene's test prior to analysis. Welch's ANOVA with Games-Howell post hoc was used for the CD33 antibody study and many qRT-PCR data, as the null hypothesis of equal variances was rejected. Kruskal-Wallis H test was used if the null hypothesis of normal distribution was rejected. Student's *t*-test or one-/two-way ANOVA followed by Bonferroni post hoc was used for statistical analysis of data not violating normal distribution and equality of variances hypotheses. *** represents $p \leq 0.001$, ** represents $p \leq 0.01$ and * represents $p \leq 0.05$.

3 Results

3.1 Human induced pluripotent stem cell-derived microglia as a model system

Microglia are the only resident innate immune cells of the CNS and have pleiotropic functions in order to fight invading pathogens and maintain homeostasis (Klein *et al*., 2008; Nimmerjahn *et al*., 2005). Recently, genome-wide association studies linked several microglial gene variants to neurodegenerative diseases, such as AD (Hollingworth *et al*., 2011; Lambert *et al*., 2013; Naj *et al*., 2011). Accumulating evidence suggests that activated microglia can be either causal or consequential of these CNS diseases but their contribution to disease progression is generally undisputed. Consequently, the interest in microglia and microglial model systems to study CNS diseases is increasing. However, large quantities of human primary microglia from patients and healthy controls are scarcely available due to the limited quantities of donor material. As a result, a new field emerged addressing the need of human microglia model systems using induced pluripotent stem cells (iPSCs). In the recent years, several protocols were developed describing the generation of microglial precursors or microglia-like cells from iPSCs. These protocols had in common that the cells need a comparably long period of up to 14 days of co-culture with neurons or monoculture with a cocktail of distinct cytokines (among them IL-34) to gain microglial identity (Abud *et al*., 2017; Haenseler *et al*., 2017; Muffat *et al*., 2016). In addition, it was described that human primary microglia quickly lose expression of key microglial markers once they were removed from neural-rich *in vivo* environment and placed into *in vitro* culture (Bennett *et al*., 2018), thereby questioning approaches to generate microglia in the absence of neural cells.

Within this thesis, a protocol for generation of microglia from human iPSCs was utilized, in which the microglia arose in a neuron-enriched environment, mimicking the *in vivo* development. This circumvented the need for an extended co-culture with neurons or monoculture with cytokines, therefore providing ready-to-use microglia directly harvested from the differentiation culture (Mathews *et al*., *in preparation*; Patent ID EP20162230).

3.1.1 Generation of induced pluripotent stem cell-derived microglia

Human induced pluripotent stem cell-derived microglia (iPSdMiG) were generated via induction of primitive hematopoiesis and differentiation of neuroepithelial cells in embryoid bodies (EBs). The EBs were then seeded into adherent culture and iPSdMiG arose and matured in a multi-lineage glial and neural progenitor-enriched co-culture, which mimics the *in vivo* environment. Around 4-6 weeks after initiating the differentiation from iPSCs, suspension microglia were harvested from the supernatant and directly seeded for experiments (Figure 4). Production of iPSdMiG into the supernatant continued for up to week 20, allowing for multiple harvests from the same

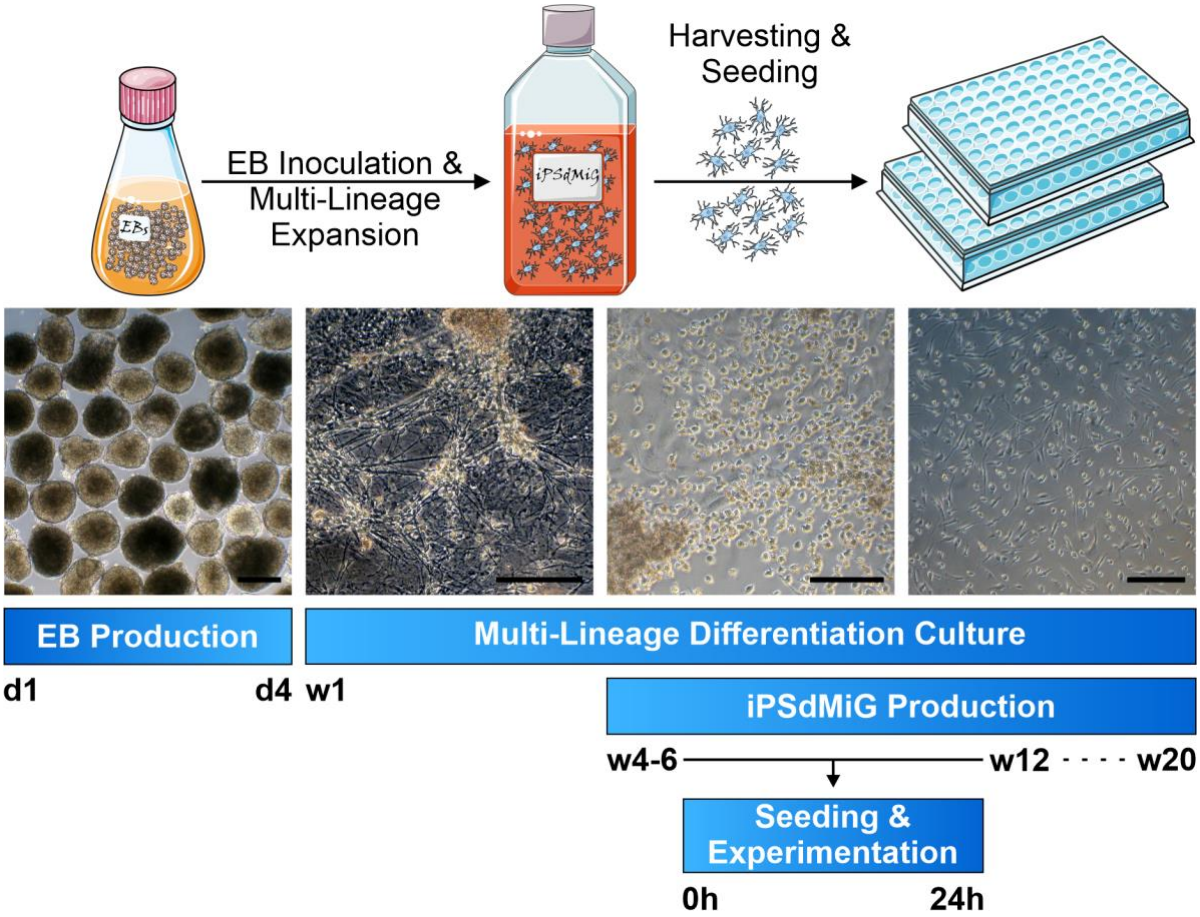

Figure 4: Schematic drawing and exemplary images depicting the generation of iPSdMiG. Embryoid body (EB) formation was induced from 80 % confluent iPSC cultures. EBs were cultured for 4 days in with changing supplements (left). Seeding of EBs onto pre-coated cell culture formats let to outgrowth of cells from multiple lineages (middle left). 4-6 weeks after seeding iPSdMiG were visible as free-floating shiny cells (middle right), and were produced majorly in the following 7-week peak production phase until week 12. However, iPSdMiG production continued with lower numbers even until week 20. Harvested iPSdMiG from the supernatant were plated in a desired cell culture format for experiments with a minimal time of 24 hours of culturing (right). Scale bars = 200 µm. d = day; EB = embryoid body; iPSdMiG = induced pluripotent stem cell-derived microglia; w = week. Illustrations partly adapted or modified from Servier Medical Art.

differentiation culture. Once harvested, iPSdMiG were seeded in respective plate formats for 24 hours to allow adherence of the suspension cells.

3.1.2 *In silico* comparison of iPSdMiG with human microglia and macrophages

The main objective of the generation of a new model system is to closely resemble the primary cells, which are meant to be modeled. Thus, a comparison of iPSdMiG to human primary microglia is indispensable. The state-of-the-art technique for comparing several cell types is to compare their transcriptome by mRNA sequencing. As primary human brain tissue was unavailable, comparisons to human primary microglia were performed *in silico* by using a previously published dataset of *ex vivo* isolated human primary microglia and cortex samples (Galatro *et al*., 2017). In addition, data from a current cutting-edge protocol for developing human microglial-like cells from iPSCs (iMGL) (Abud *et al*., 2017) was used as comparison as well as samples from human iPSCs and THP1 macrophages – a commonly used *in vitro* source for human monocytes-derived macrophages (Chanput *et al*., 2014). For iPSdMiG samples, RNA from three different iPSC lines previously generated by LIFE & BRAIN GmbH was used (31F, C133S4 ad C14).

3.1.2.1 Comparison using exploratory data analyses

Following trimming, alignment, and read count generation, exploratory data analysis was used as a first tool to investigate the data. Dimensionality reduction using principal component analysis (PCA) with the 5,000 most variable genes showed that the individual samples clustered together very well. Merely the human primary microglia samples displayed a slightly higher variance. Of note, iPSdMiG samples were grouped according to their iPSC background but located in very close proximity to the human primary microglia and apart from iMGL, THP1 macrophages, iPSCs, and human cortex samples. The variance on PC1 (67.3 %) described the differences between the myeloid samples (microglia and macrophages) and iPSCs as well as, to a much bigger extend, the cortex samples. Only 6.4 % of the variance (PC2) was due to differences between human primary microglia, iPSdMiG, iMGL, THP1 macrophages and iPSCs (Figure 5A). To gain more insight into the differences between the individual myeloid cell types, the cortex samples were removed from the PCA. Interestingly, even in absence of the cortex samples iPSdMiG samples clustered in close proximity to human primary microglia and both together farther apart from iMGL, THP1

macrophages and iPSC samples. Thereby, PC1 described 29.6 % of the variance and separated iPSCs, THP1 macrophages, and iMGL from human primary microglia and

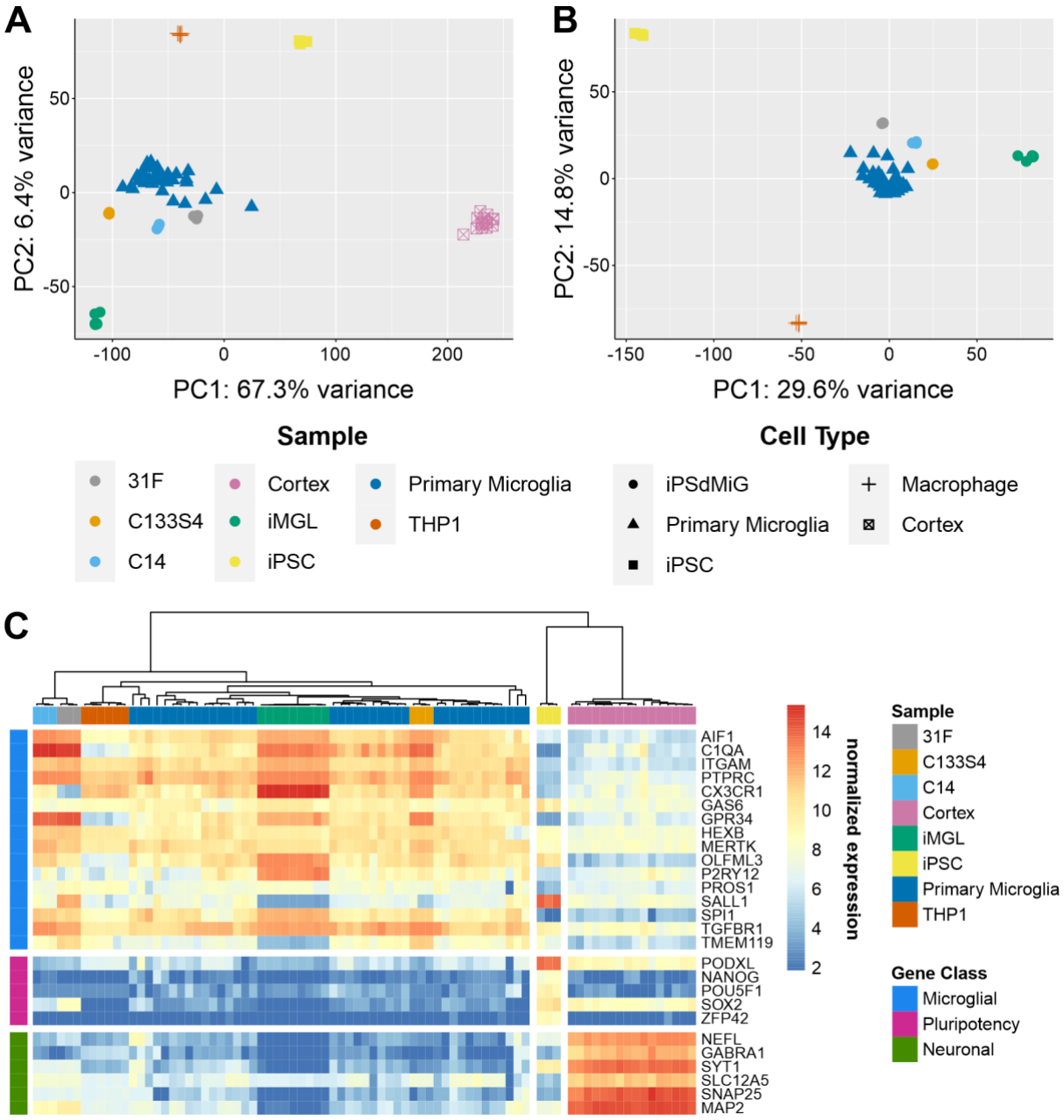

Figure 5: Exploratory data analysis highlighted similarities between iPSdMiG and human primary microglia.

(A) Principal component analysis showed clustering of iPSdMiG in very close proximity to human primary microglia and farther apart from other cells including THP1 and iMGL. **(B)** Principal component analysis excluding the cortex samples led to clustering of iPSdMiG in very close proximity to human primary microglia and a bit closer towards iMGL. **(C)** The heatmap of lineage-specific genes showed an overall prominent expression of microglial but not neuronal or stem cell-related genes in iPSdMiG, iMGL and human primary microglia. 31F n = 3; C133S4 n = 3; C14 n = 3; Cortex n = 16; iMGL n = 9; iPSC n = 3; Primary Microglia n = 38; THP1 n = 6. iMGL = iPSC-derived microglia-like cells; iPSC = induced pluripotent stem cell; iPSdMiG = iPSC-derived microglia; PC = principal component.

iPSdMiG. PC2 described 14.8 % of the overall variance and separated the microglial samples from iPSCs and THP1 macrophages (Figure 5B).

Next, the transcription of lineage-specific markers was analyzed and displayed via a heatmap. The selection consisted of 16 previously published microglial markers (*AIF1*, *C1QA*, *ITGAM* [*CD11B*], *PTPRC* [*CD45*], *CX3CR1*, *GAS6*, *GPR34*, *HEXB*, *MERTK*, *OLFML3*, *P2RY12*, *PROS1*, *SALL1*, *SPI1* [*PU.1*], *TGFBR1* and *TMEM119*) (Butovsky *et al*., 2014), 5 pluripotency markers (*PODXL* [*TRA-1-60*], *NANOG*, *POU5F1* [*OCT4*], *SOX2* and *ZFP42*) and 6 neuronal markers (*NEFL, GABRA1*, *SYT1*, *SLC12A4*, *SNAP25* and *MAP2*). IPSdMiG, iMGL and human primary microglia exhibited an overall similar gene transcription pattern. Merely a subset of genes, e.g., *C1QA* and *GPR34* were transcribed stronger in iPSdMiG and iMGL compared to human primary microglia. In iPSC and cortex samples, microglial genes were absent or only slightly transcribed. *SALL1*, although described as a microglia-specific marker, showed exceptionally high expression in iPSCs. Pluripotency markers were mainly observed in iPSC but *PODXL* and *SOX2* were also found in cortex samples. Cortex samples displayed high transcription of neuronal markers while low to no transcription was observed in THP1 and iMGL samples. Some iPSdMiG and human primary microglia samples showed comparatively low expression of neuronal marker genes, e.g., *SLC12A5* and *MAP2* (Figure 5C).

Together, PCA and investigation of lineage-specific genes suggested that iPSdMiG and human primary microglia are more alike compared to any other tested sample.

3.1.2.2 Enriched pathways and transcription factors

PCA and heatmaps are useful tools for getting an overview over multidimensional and large datasets. However, in order to closely investigate relations between different samples, differential expression (DE) analysis was performed. First, human primary microglia were compared to iPSdMiG (31F, C133S4, and C14 samples pooled), genes with $|\log2FC| \geq 1$ and FDR-adjusted p value ≤ 0.01 were extracted as DE genes and consequently analyzed for over-represented/enriched pathways. The top 10 results consisted of pathways belonging to respiration and protein translation including “Respiratory electron transport, ATP synthesis by chemiosmotic coupling, and heat production by uncoupling proteins” or “Eukaryotic Translation Initiation” but no immunity-related or microglia-specific pathways were enriched (Figure 6A). In a second approach iPSdMiG and human primary microglia were individually compared

to the iPSC samples and filtered for their individual microglia core signature. Herein, only highly significant and highly upregulated genes (log2FC ≥ 3 and FDR-adjusted *p* value ≤ 0.001) were considered to be important for the microglial identity. The microglial core signature of iPSdMiG consisted of 1402 genes and the core signature of human primary microglia of 5820 genes. These genes were then used to identify transcription factors, which drive these transcriptome changes as upstream regulators. Out of the top 20 identified enriched transcription factors, iPSdMiG and human primary

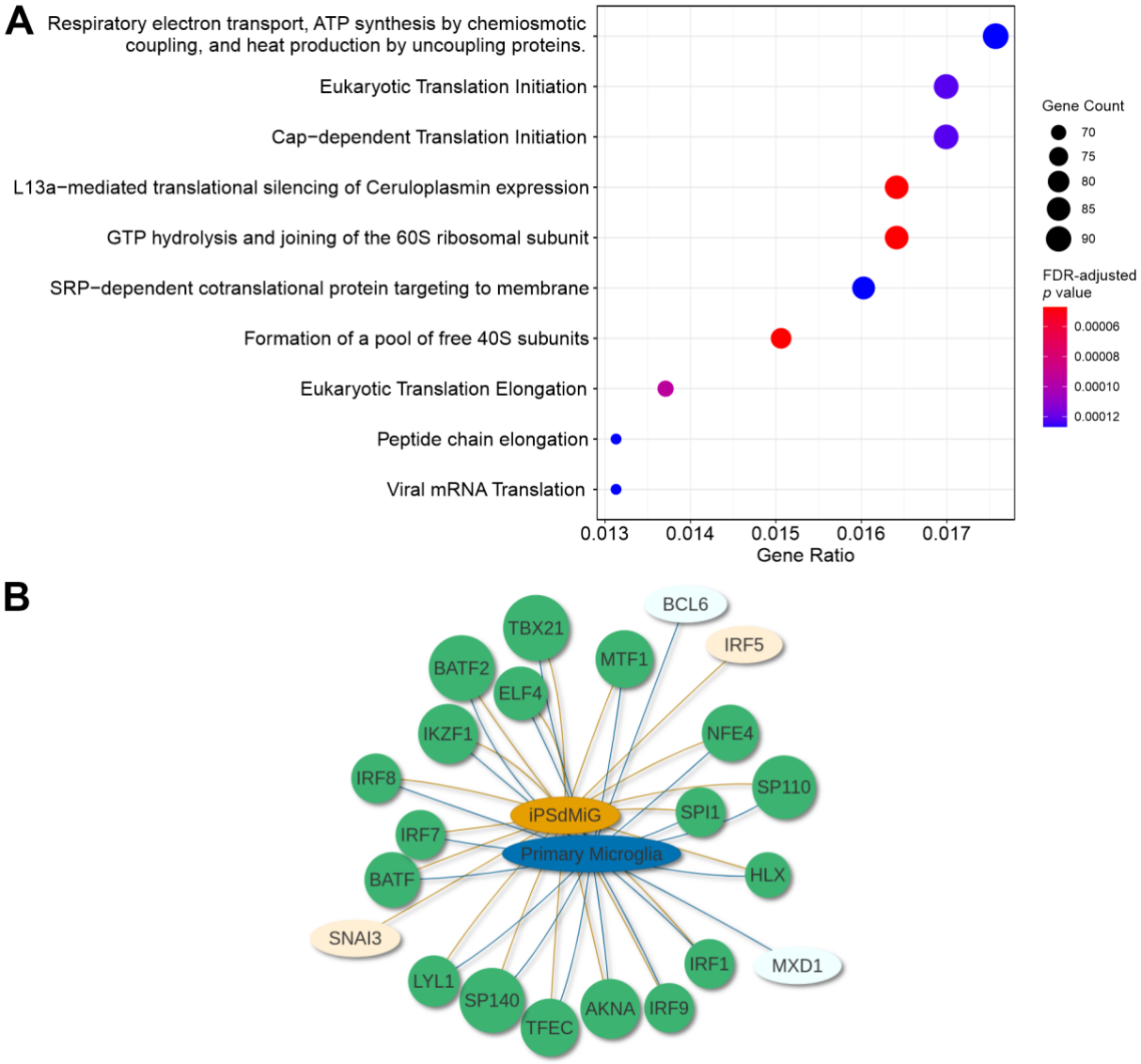

Figure 6: Pathway and transcription factor enrichment analyses of iPSdMiG and human primary microglia suggest a similar transcriptome.
(A) Differentially expressed genes between iPSdMiG and human primary microglia were enriched in pathways mainly belonging to translation. **(B)** Transcription factor analysis using the individual core signature of iPSdMiG and human primary microglia revealed that they shared 90 % of the enriched transcription factors (green). iPSdMiG n = 9; Primary Microglia n = 38. iPSdMiG = induced pluripotent stem cell-derived microglia.

microglia shared 18, among them well-known microglial/myeloid transcription factors SPI (PU.1) and IRF8 as well as other IRF family members (Figure 6B).
Thus, the transcriptome of iPSdMiG and human primary microglia did not differ in immunity-related or microglia-specific pathways and their cellular identity is orchestrated by a highly similar set of key transcription factors.

3.1.2.3 Co-expression of genes in iPSdMiG and human primary microglia

In addition to highlighting differences by DE analysis, a comparison of co-expressed genes was used as a measure to further determine how similar the samples or cell types were to each other. To assess gene co-expression, weighted gene correlation network analysis (WGCNA) was performed with the top 20,000 most variable genes. WGCNA identified 11 different co-expression modules and a grey module, which consisted of all genes not belonging to any other module. Thereby, the three largest modules besides the grey module were the turquoise module with 9685 genes, the blue module with 1272 genes and the brown module with 1240 genes. Module-trait relationships with the samples as trait data identified the cortex samples to be highly correlated with the turquoise module (0.97, $p = 1 \times 10^{-48}$). The highest module correlation of iPSdMiG and human primary microglia was with the blue module (0.47, $p = 8 \times 10^{-6}$ and 0.34, $p = 0.002$, respectively). iMGL were highly correlated with the yellow and red module (0.82, $p = 1 \times 10^{-20}$ and 0.72, $p = 4 \times 10^{-14}$, respectively) and weakly correlated with the blue module (0.24, $p = 0.03$). THP1 macrophages and iPSC were highly correlated with the magenta or pink module, respectively (0.91, $p = 1 \times 10^{-32}$ or 0.96, $p = 2 \times 10^{-44}$, respectively) (Figure 7A). Next, modules of interest were investigated for enriched pathways. The turquoise module, which correlated with the cortex samples, was enriched in neuronal-related pathways including “Neuronal System”, “Transmission across Chemical Synapses”, and “Neurotransmitter receptors and postsynaptic signal transmission” (Figure 7B). The blue module, which moderately correlated with iPSdMiG as well as human primary microglia and weakly correlated with iMGL exhibited an overrepresentation of genes belonging to immunity-related pathways, among them “Innate Immune System”, “Signaling by Interleukins”, and “Toll-like Receptor Cascades” (Figure 7C). The pink module, which correlated with iPSC samples, was enriched in genes belonging to extracellular space and pluripotent stem cells including “Extracellular matrix organization”, “Transcriptional regulation of

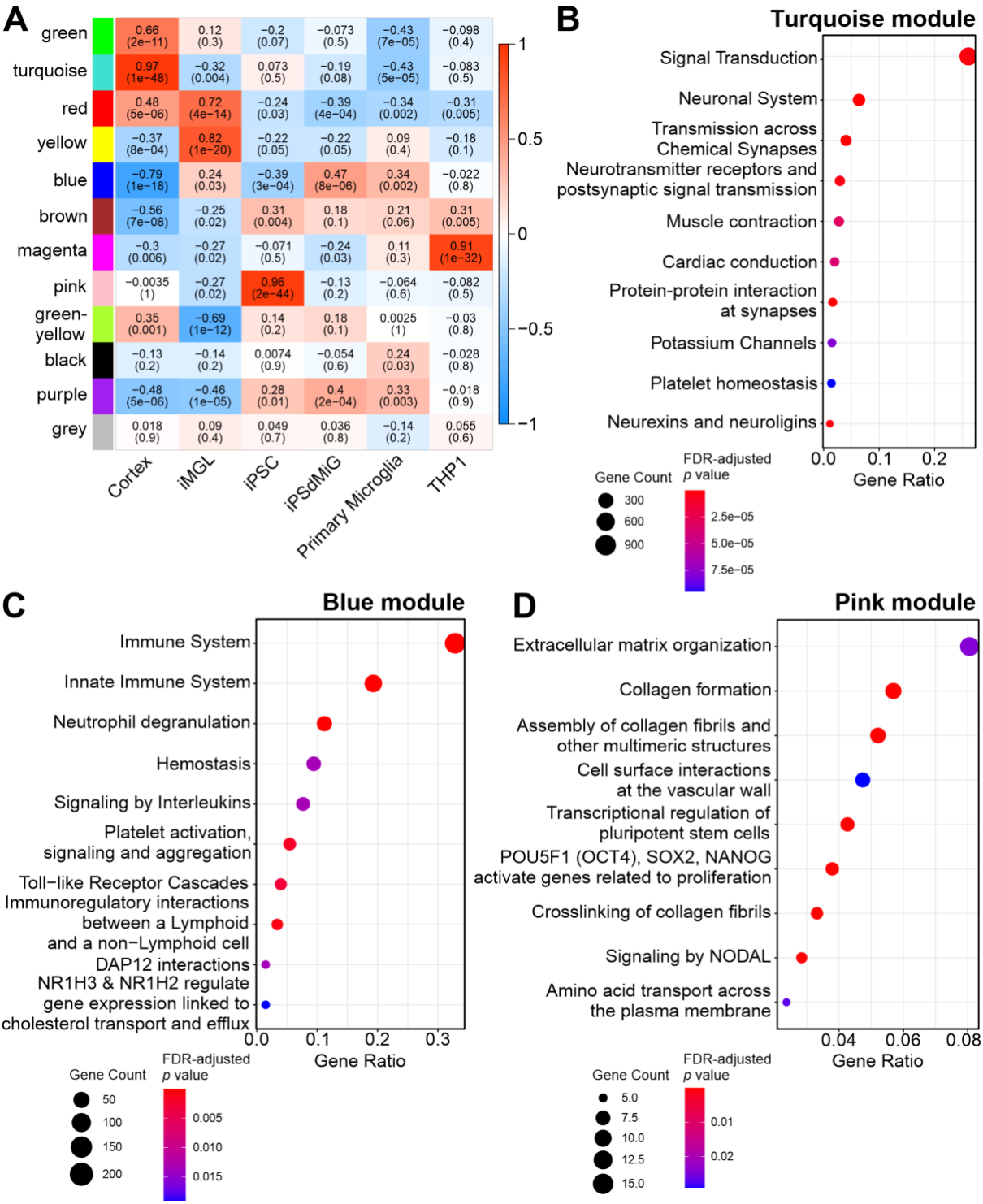

Figure 7: WGCNA identified an immunity-related module co-expressed in iPSdMiG, human primary microglia, and iMGL.

(A) Module-trait relationship revealed three modules of main interest: the turquoise module, which correlated with the cortex, the blue module, which correlated with iMGL, iPSdMiG, and human primary microglia and the pink module, which correlated with iPSCs. **(B)** The turquoise module showed overrepresentation of neuronal pathways following enrichment analysis. **(C)** Pathway enrichment of the blue module resulted in identification of immunity-related pathways. **(D)** The pink module was enriched for pathways associated with pluripotency maintenance and extracellular matrix. Cortex n = 16; iPSdMiG n = 9; iMGL n = 9; iPSC n = 3; Primary Microglia n = 38; THP1 n = 6. iMGL = iPSC-derived microglia-like cells; iPSC = induced pluripotent stem cell; iPSdMiG = iPSC-derived microglia.

pluripotent stem cells", and "POU5F1 (OCT4), SOX2, NANOG activate genes related to proliferation" (Figure 7D). Other modules – including modules, which showed high correlation with iMGL or THP1 macrophages – were enriched in genes belonging to transcriptional regulation by RUNX1 (magenta module), (RNA) metabolism, translation, or respiration (see Appendix Table 2).

Taken together, WGCNA identified a single module (blue), which correlated with all three microglia samples in this comparison and was enriched in immunity-related pathways. Interestingly, iPSdMiG and human primary microglia but not iMGL showed a higher correlation with this module than with any other module. Moreover, this data provides further evidence that iPSdMiG transcriptionally resembled human primary microglia. Differences in transcriptional activity were only attributed to respiration and protein translation. In addition, iPSdMiG and human primary microglia showed similar gene transcript levels of lineage-specific markers, clustered in very close proximity in the PCA and had a similar set of enriched transcription factors shaping their cellular identity. Therefore, iPSdMiG represent a bona fide *in vitro* model system of human primary microglia.

Nevertheless, to identify modulators of human CD33 signaling a stable CD33-expressing reporter cell line was generated and analyzed (see section 3.2) before investigating iPSdMiG carrying CD33 variants (see section 3.3).

3.2 CD33 reporter cell line identified agonistic CD33 antibodies

Understanding the putative contribution of a receptor and its signaling to a disease is a manifold but vital task. Identification of molecules or antibodies modulating receptor signaling is crucial in elucidating signaling value on cellular behavior as well as its druggability for therapeutic intervention in diseases. In the first step, these studies are usually performed in reporter cell lines, which overexpress the receptor of interest. The benefit of these reporter cell lines is multifarious including signal amplification by protein overexpression, low costs, and high reproducibility (Gervaix *et al*., 1997; Richards *et al*., 1999; G. Q. Wang *et al*., 2006).

Within this thesis, a human CD33 reporter cell line was generated and analyzed for CD33 activation by a panel of CD33-specific antibodies. Activation of CD33 results in phosphorylation of its intracellular ITIM and ITIM-like domains and subsequent recruitment and activation of protein tyrosine phosphatases. These protein tyrosine

phosphatases can directly dephosphorylate the ITIM and ITIM-like domains (Taylor *et al*., 1999; Walter *et al*., 2008), which might impede efficient analysis. Therefore, the ITIM and ITIM-like domains of CD33 with fast and transient signaling were replaced by the activatory ITAM signaling domain of TYROBP/DAP12. ITAM signaling typically leads to an increase in intracellular calcium levels, which was therefore analyzed as an indicator for CD33 activation in the CD33 reporter cell lines.

Elements of the results within this section were submitted for publication to *Scientific Reports* on 10th November 2020 (Wißfeld *et al*., *in revision*).

3.2.1 Generation of CD33-DAP12-GCaMP6m reporter cell lines

3.2.1.1 Cloning of the expression plasmid pcDNA5/FRT-EEF1A1-CD33-DAP12-GCaMP6m

Two CD33-DAP12 constructs – CD33M-DAP12 and CD33$^{\Delta E2}$-DAP12 – were previously generated by exchanging the transmembrane and intracellular domains of CD33 with the correspondent domains of TYROBP/DAP12 (Figure 8A) (Mossad, 2016). CD33M represents full-length CD33 and is the most commonly expressed CD33 isoform in the Caucasian population. Alternative splicing of exon 2 of CD33 results in expression of CD33$^{\Delta E2}$ the second commonly expressed CD33 isoform in the Caucasian population. Exon 2 of CD33 largely encodes for the sialic acid-binding domain. Hence, CD33$^{\Delta E2}$ lacks the sialic acid-binding domain (Figure 8A).

The two *CD33-DAP12* constructs were cloned into the expression vector pcDNA5/FRT, which enables stable integration of the *CD33-DAP12* constructs into the genome of the cell line of interest if co-transfected together with a plasmid containing the Flp recombinase (pOG44). Agarose gel electrophoresis after digestion of the expression plasmids with restriction digestion enzyme EcoRI showed the presence of CD33M-DAP12 or CD33$^{\Delta E2}$-DAP12 due to a shift in the band heights at either 5,227 + 883 bp (CD33M-DAP12) or 4,846 + 883 bp (CD33$^{\Delta E2}$-DAP12) compared to 4,195 + 883 bp for the empty vector control (Figure 8B). Two additional cloning steps were performed. First, the strong viral *CMV* promoter was exchanged with the *EEF1A1* promoter to stabilize CD33-DAP12 gene transcription because viral promoters in eukaryotic expression systems are prone to be epigenetically silenced by, e.g., hypermethylation, which finally results in loss of transgene expression (Meilinger *et al*., 2009; Teschendorf *et al*., 2002). Second, a genetically engineered

calcium indicator was introduced, which makes live cell staining for calcium imaging redundant.

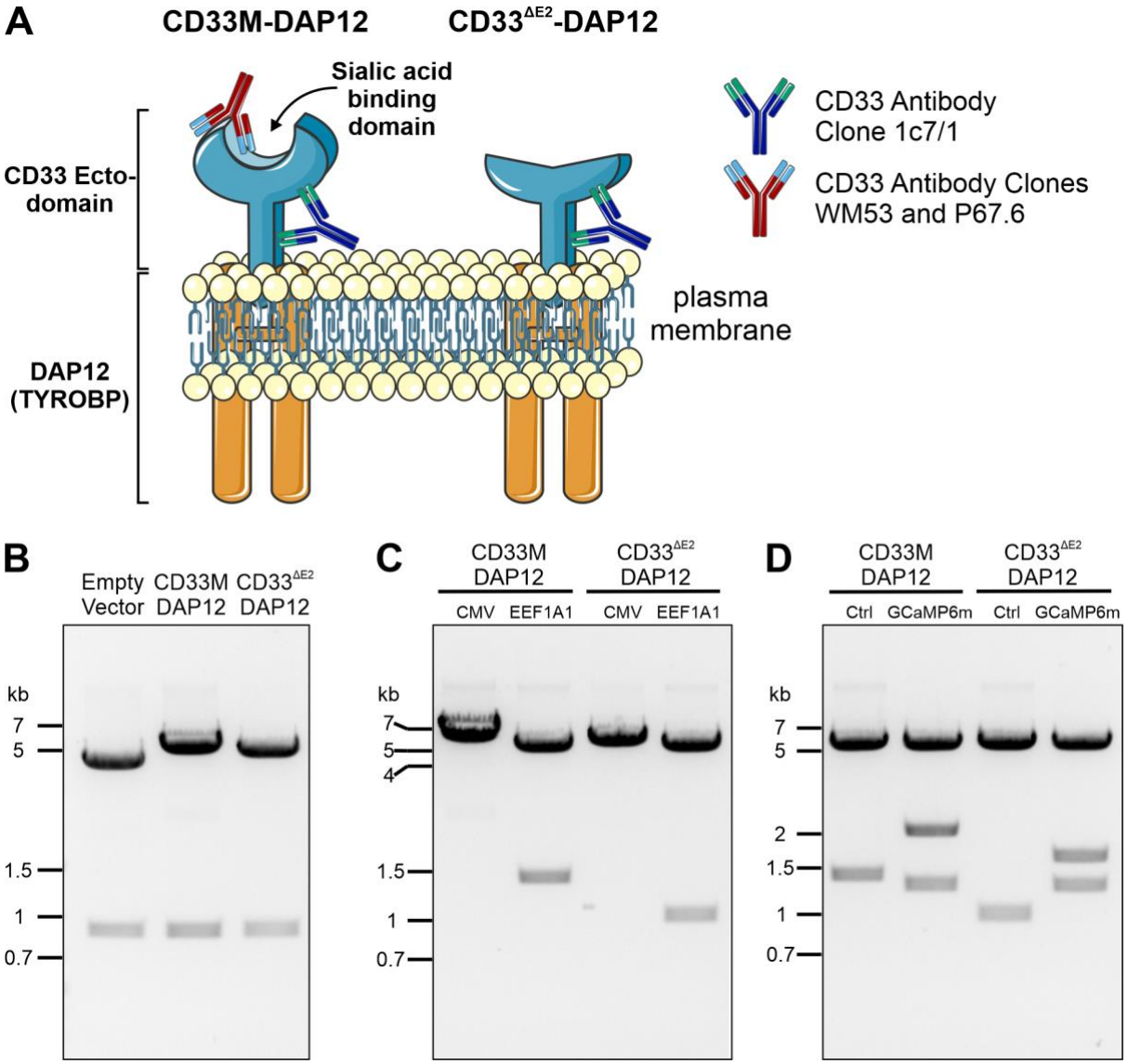

Figure 8: Generation of CD33 reporter cell line constructs analyzed by restriction digestion.
(A) Schematic drawing of the two CD33-DAP12 fusion proteins and antibody binding. The extracellular part of full-length CD33 (CD33M) or exon 2-deleted CD33$^{\Delta E2}$ were fused to the transmembrane and intracellular domain of TYROBP (DAP12). CD33M can be recognized by CD33-specific antibodies 1c7/1, WM53 and P67.6 while CD33$^{\Delta E2}$ is only detected by 1c7/1. **(B)** Representative agarose gel image of restriction digestion of CD33M-DAP12 and CD33$^{\Delta E2}$-DAP12 cloned into expression vector pcDNA5/FRT with EcoRI. CD33M-DAP12 and CD33$^{\Delta E2}$-DAP12-positive plasmids showed a higher band than the empty vector control plasmid. **(C)** Representative agarose gel electrophoresis image displaying the restriction digestion of *EEF1A1*-incorporated versus *CMV* plasmids with XhoI. *EEF1A1*-positive plasmids showed an additional second band compared to *CMV* plasmid with only one band. **(D)** Representative agarose gel image of restriction digestion following cloning of GCaMP6m into pcDNA5/FRT-CD33-DAP12 plasmids. XhoI restriction digestions resulted in an additional third band in GCaMP6m-positive plasmids instead of two bands for negative plasmids. *CMV* = cytomegalovirus; Ctrl = control; DAP12 = DNAX-activation protein; *EEF1A1* = eukaryotic translation elongation factor 1 alpha 1; GCaMP6m = calcium-sensitive green fluorescent protein; TYROBP = transmembrane immune signaling adaptor TYROBP.

Successful substitution of *CMV* with *EEF1A1* was demonstrated by agarose gel electrophoresis after restriction digestion with XhoI. Thereby, *CMV* plasmids exhibited only a single band and *EEF1A1*-containing plasmids an additional band at 1,339 bp (CD33M-DAP12) or 958 bp (CD33$^{\Delta E2}$-DAP12; Figure 8C). The calcium-sensitive green fluorescent protein variant GCaMP6m was introduced as genetically engineered calcium indicator into the pcDNA5/FRT-EEF1A1-CD33-DAP12 plasmids. Independent expression of CD33-DAP12 and GCaMP6m was realized by insertion of an *internal ribosome entry site* (*IRES*) motif between *CD33-DAP12* and *GCaMP6m*. Integration of the *IRES-GCaMP6* motif after *CD33-DAP12* was confirmed by agarose gel electrophoresis after restriction digestion with XhoI. Positive clones exhibited three instead of two bands after restriction digestion with XhoI at the height of 5,283 + 1,954 + 1,234 bp (CD33M-DAP12-GCaMP6m) or 5,279 + 1,573 + 1,234 bp (CD33$^{\Delta E2}$-DAP12-GCaMP6m) following agarose gel electrophoresis (Figure 8D).
Thus, the expression vector pcDNA5/FRT containing the two *CD33-DAP12* constructs was successfully modified to ensure constitutive CD33-DAP12 expression in eukaryotic expression systems. Furthermore, introduction of the genetically engineered calcium indicator GCaMP6m mitigates the need for long staining procedures to detect of intracellular calcium levels.

3.2.1.2 Constitutive CD33-DAP12 and GCaMP6m expression in Flp-In-293 cells

After confirmation of the correct target sequence by Sanger sequencing, the two new CD33-DAP12-IRES-GCaMP6m constructs were stably transfected into Flp-In-293 cells by co-transfection together with pOG44. Selection of stable integration of the constructs into the host genome was performed by resistance to antibiotic Hygromycin B. Individual clones were picked, expanded, and analyzed for CD33 surface expression by flow cytometry. Subsequently, two subclonal dilution steps were performed for positive clones and CD33 expression was analyzed anew by flow cytometry (Figure 9). Using different CD33-specific antibody clones, the two CD33-DAP12 constructs could be distinguished by their binding affinities. As described above, CD33M represents full-length CD33 and can be bound by all three tested antibody clones, namely 1c7/1, WM53 and P67.6. Clone 1c7/1 binds CD33 in the C2 domain and thus can also detect the shorter CD33$^{\Delta E2}$ form. However, clones WM53 and P67.6 bind an epitope within the sialic acid-binding domain, which is absent in CD33$^{\Delta E2}$ and hence are not able to stain CD33$^{\Delta E2}$-expressing cells (Figure 8A).

Accordingly, CD33M-DAP12-expressing cells showed high CD33 surface expression detected by all three tested CD33-specific antibodies whereas in CD33$^{\Delta E2}$-DAP12 cells surface expression of CD33 was only measured by CD33 antibody clone 1c7/1 (Figure 9A). Quantification of flow cytometry results showed 91.53 ± 1.64 % CD33-

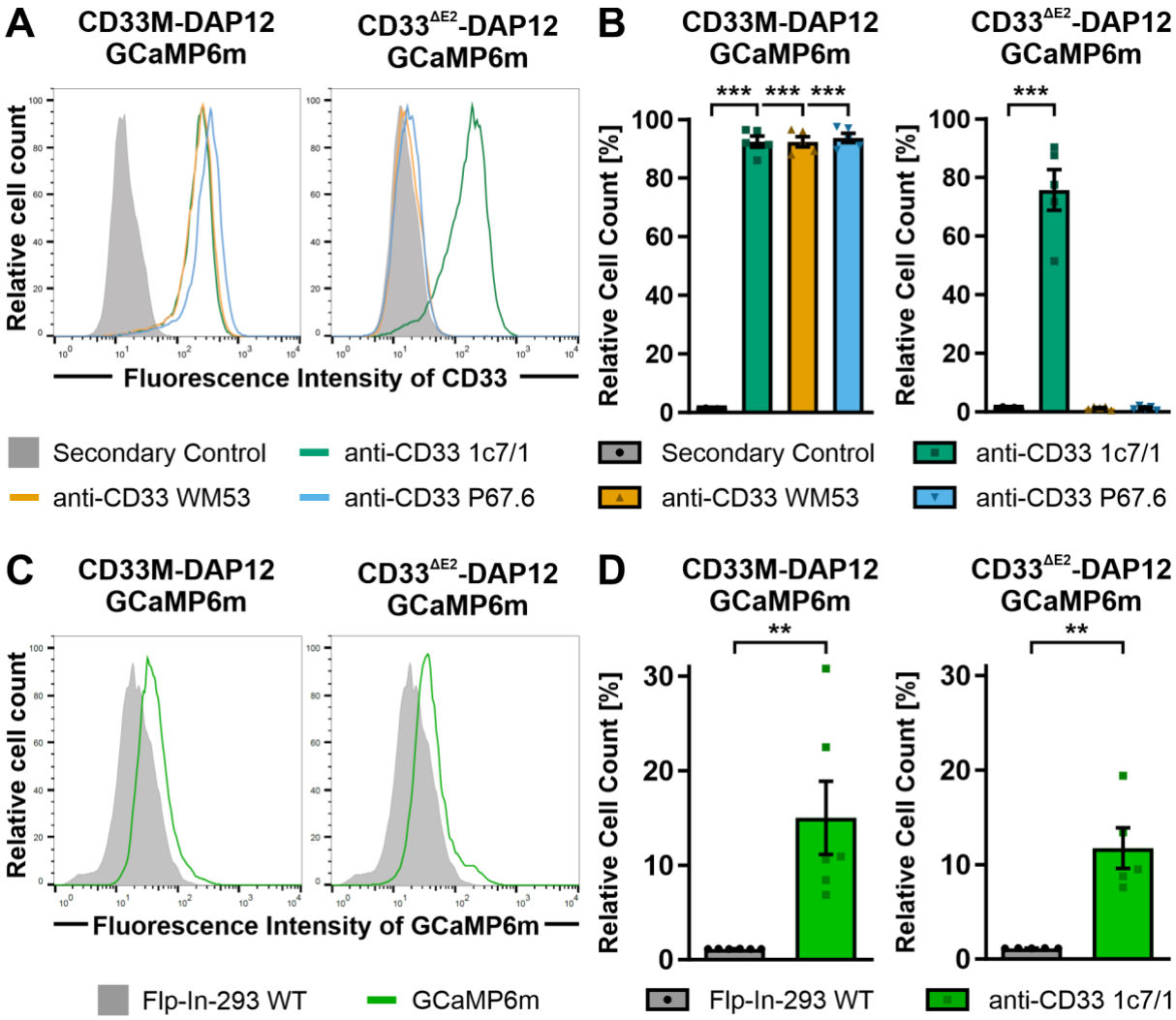

Figure 9: Flow cytometry analysis showing CD33-DAP12 and GCaMP6m expression in reporter cell lines.

(A) Histogram plots of CD33 expression in CD33-DAP12-GCaMP6m reporter cells analyzed by flow cytometry. CD33M-DAP12-expressing cells were stained by all tested antibodies while CD33$^{\Delta E2}$-DAP12-expressing cells were only stained by CD33 antibody clone 1c7/1. **(B)** Quantification of CD33 surface expression revealed all tested antibodies showed a high percentage of CD33-positive cells in CD33M-DAP12-expressing cells. Only CD33 antibody clone 1c7/1, but neither WM53 nor P67.6, showed high staining in CD33$^{\Delta E2}$-DAP12-expressing cells. **(C)** Histogram plots of GCaMP6m expression in CD33-DAP12-GCaMP6m reporter cells analyzed by flow cytometry. Both lines showed a slight endogenous GCaMP6m fluorescence. **(D)** Quantification of endogenous GCaMP6m expression revealed a similar percentage of GCaMP6m-positive cells in CD33M-DAP12 and CD33$^{\Delta E2}$-DAP12-expressing cells. Data are presented as mean ± *SEM* of 5-6 independent experiments. *** represents $p \leq 0.001$ and ** represents $p \leq 0.01$ determined by Welch's ANOVA followed by Games-Howell post hoc test. DAP12 = DNAX-activation protein; GCaMP6m = calcium-sensitive green fluorescent protein.

positive cells detected by antibody clone 1c7/1 as well as 93.72 ± 1.55 % or 92.42 ± 1.89 % of CD33-positive cells in CD33M-DAP12-expressing cells by antibody clones WM53 or P67.6, respectively. In contrast, in CD33$^{\Delta E2}$-DAP12-expressing cells CD33 antibody clones WM53 and P67.6 detected 1.29 ± 0.23 % or 1.32 ± 0.28 % of CD33-positive cells, respectively. Antibody clone 1c7/1, however, detected 75.72 ± 6.93 % of CD33-positive cells in CD33$^{\Delta E2}$-DAP12-expressing cells (Figure 9B). Interestingly, faint but detectable GCaMP6m fluorescence was observed in both CD33M-DAP12 and CD33$^{\Delta E2}$-DAP12-expressing cell lines resulting in a slight shift of the histogram (Figure 9C). In detail, 15.02 ± 3.88 % or 11.73 ± 2.15 % of GCaMP6m-positive cells were measured in CD33M-DAP12-expressing or CD33$^{\Delta E2}$-DAP12-expressing cell lines compared to parental Flp-In-293 WT cells (Figure 9D).
Thus, constitutive expression of the CD33-DAP12 fusion protein construct together with GCaMP6m was successfully demonstrated.

3.2.2 Agonistic CD33 antibodies identified by calcium imaging in CD33 reporter cell line

In the CD33-DAP12 reporter cell system, CD33 activation results in an increased phosphorylation of SYK and PI3K via DAP12/TYROBP signaling. Consequently, activation of DAP12 leads to PLCγ2-dependent generation of IP_3 and DAG, and thus, an increase in intracellular calcium levels from the ER and other organelles (Figure 10A) (Linnartz & Neumann, 2013; McVicar *et al*., 1998; Peng *et al*., 2010; Wu *et al*., 2000). The commercially available CD33 antibody clones 1c7/1, WM53, P67.6, and P67.6 F(ab), which was kindly generated and provided by Sanofi, were tested for their ability to stimulate CD33. In addition, dATP (100 µM) and IgG1 or IgG1 F(ab')2 were used as a positive and isotype antibody controls, respectively. Extracellular dATP leads to increased intracellular calcium levels via the purinergic P2 receptor family. Thereby, PI3K is also involved in downstream signaling and intracellular calcium release (Burnstock, 1990; Dalziel & Westfall, 1994).
The relative change in fluorescence over time *ΔF/F(t)* of the isotype control antibodies (IgG1 and IgG1 F(ab')2) did not show any remarkable change in both cell lines. However, addition of 100 µM dATP led to a very sharp increase in *ΔF/F(t)* in CD33M-DAP12 and CD33$^{\Delta E2}$-DAP12-expressing cells, as expected. Interestingly, addition of the CD33-specific antibodies 1c7/1 and P67.6 but not WM53 or P67.6 F(ab) led to a strong increase in *ΔF/F(t)* in CD33M-DAP12 cells. In CD33$^{\Delta E2}$-DAP12-expressing

cells, however, none of the tested CD33 antibodies evoked an increase in intracellular calcium levels (Figure 10B+C). Quantification of the area under curve (AUC) by calculation of the integral of each individual *ΔF/F(t)* curve revealed a significant

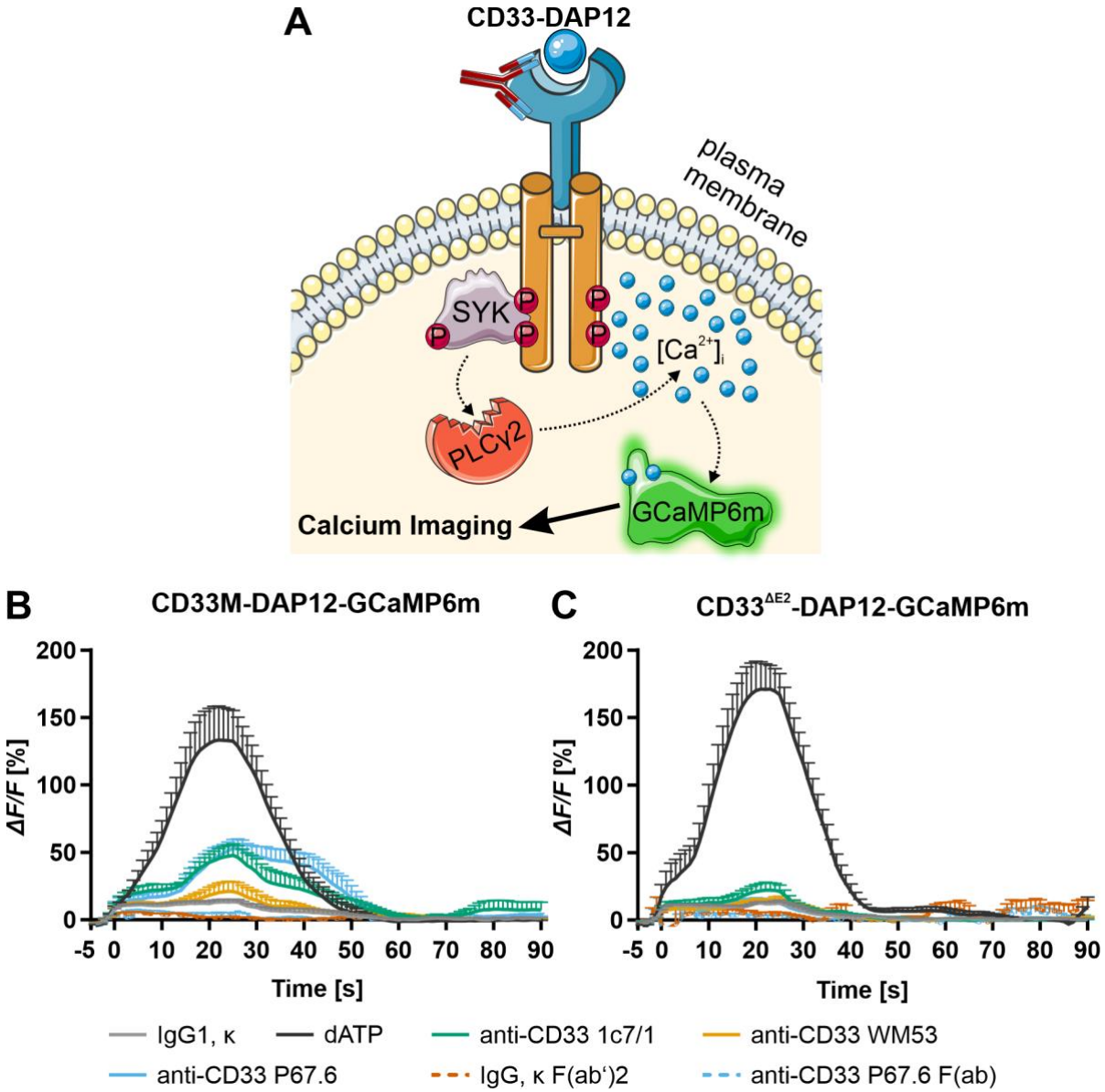

Figure 10: Calcium imaging in CD33-DAP12-GCaMP6m reporter cell lines identified agonistic CD33 antibodies.

(A) Molecular function of the CD33 reporter cell lines. Activation of the CD33-DAP12 chimeric construct results in ITAM-mediated signaling, which finally leads to the release of intracellular calcium via SYK and PLCγ2. Then, the calcium increase is measured by GCaMP6m fluorescence intensity. **(B)** XY-plot of *ΔF/F(t)* in CD33M-DAP12-expressing cells. Addition of dATP as well as CD33-specific antibodies 1c7/1 and P67.6 led to a change in *ΔF/F(t)* signal compared to IgG control. **(C)** XY-plot of *ΔF/F(t)* in $CD33^{\Delta E2}$-DAP12-expressing cells. Only addition of dATP led to a change in *ΔF/F(t)* signal compared to IgG control. Data are presented as mean + *SEM* of 4-8 independent experiments. $[Ca^{2+}]_i$ = intracellular calcium ions; DAP12 = DNAX-activation protein; GCaMP6m = calcium-sensitive green fluorescent protein; PLCγ2 = phospholipase C gamma 2; P = phosphate; SYK = spleen-associated tyrosine kinase.

increase in intracellular calcium levels of dATP-treated CD33M-DAP12 cells compared to IgG1 treatment (dATP 6.22 ± 0.49 versus IgG1 1.00 ± 0.17, $p = 0.002$). Further, a selective increase in intracellular calcium transients was observed after 1c7/1 and P67.6 treatment in CD33M-DAP12-expressing cells (1c7/1 2.72 ± 0.49, $p = 0.15$ and P67.6 3.92 ± 0.64, $p = 0.04$). Interestingly, addition of CD33 antibodies WM53 and P67.6 F(ab) did not result in any notable response (1.33 ± 0.19 and 1.19 ± 0.10, WM53 and P67.6 F(ab), respectively; Figure 11A). As a second quantification method the maximum *ΔF/F(t)* signal was determined and compared.

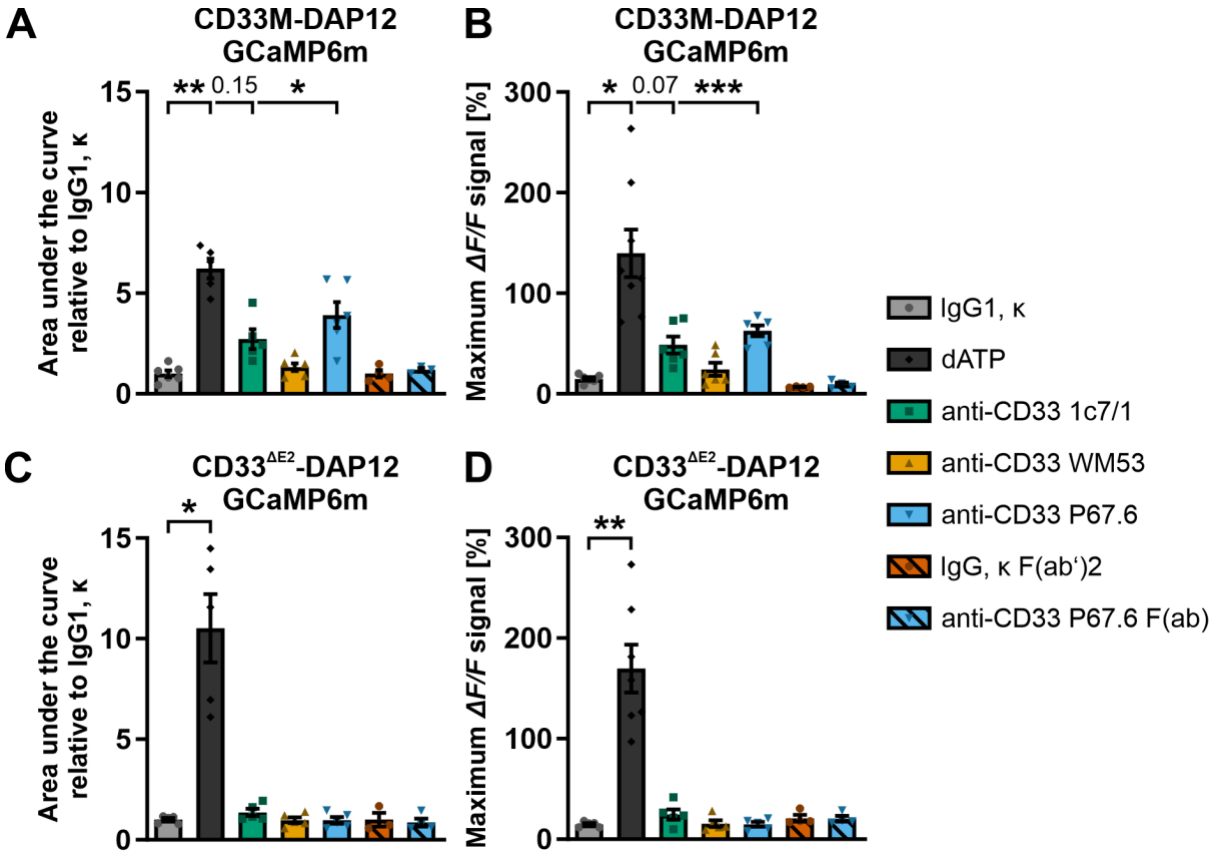

Figure 11: Quantification of calcium imaging in CD33-DAP12-GCaMP6m reporter cell lines identified agonistic CD33 antibodies.

(A) Quantification of *ΔF/F(t)* signal in CD33M-DAP12-expressing reporter cells as the AUC. Increased AUC was observed when CD33M-DAP12-expressing reporter cells were treated with dATP, anti-CD33 1c7/1 and anti-CD33 P67.6 compared to IgG1, κ. **(B)** Quantification of CD33M-DAP12 activation as the maximum *ΔF/F(t)* signal resulted in an elevated signal in dATP, anti-CD33 1c7/1 and anti-CD33 P67.6-treated CD33M-DAP12-expressing cells compared to IgG1, κ. **(C)** Quantification of *ΔF/F(t)* signal in $CD33^{\Delta E2}$-DAP12-expressing reporter cells as AUC showed an increased value compared to IgG1, κ only when adding dATP to the cells. **(D)** Quantification of $CD33^{\Delta E2}$-DAP12 activation as the maximum *ΔF/F(t)* signal resulted in an elevated signal in dATP-treated $CD33^{\Delta E2}$-DAP12-expressing cells compared to IgG1, κ. Data are presented as mean ± *SEM* of 3-8 independent experiments. *** represents $p \leq 0.001$, ** represents $p \leq 0.01$ and * represents $p \leq 0.05$ determined by Welch's ANOVA followed by Games-Howell post hoc test. AUC = area under curve; DAP12 = DNAX-activation protein; GCaMP6m = calcium-sensitive green fluorescent protein.

Similar to AUC, treatment of CD33M-DAP12 cells with 100 µM dATP increased the *ΔF/F(t)* signal to 139.76 ± 23.57 % (p = 0.01 compared to IgG1 isotype control with 14.86 ± 1.70 %). CD33 antibodies 1c7/1 and P67.6 elevated the *ΔF/F(t)* signal to 48.70 ± 8.39 % (p = 0.07 compared to IgG1) and 62.57 ± 5.37 % (p < 0.001 compared to IgG1), respectively. Addition of CD33 antibody clones WM53, P67.6 F(ab) as well as IgG1 F(ab')2 to CD33M-DAP12-expressing cells did not lead to a remarkable response (24.34 ± 6.53 %, 9.31 ± 1.88 %, or 6.27 ± 0.27 %, WM53, P67.6 F(ab), or IgG1 F(ab')2 respectively; Figure 11B). In CD33$^{\Delta E2}$-DAP12-expressing cells treatment with 100 µM dATP resulted in an increase of the AUC to 10.51 ± 1.69 (versus IgG1 1.00 ± 0.08, p = 0.03). There was no significant elevation of the AUC evoked by treatment of CD33$^{\Delta E2}$-DAP12-expressing cells with any of the tested CD33-specific antibodies. In detail, addition of CD33 antibody clones 1c7/1, WM53, P67.6, or P67.6 F(ab) resulted in an AUC of 1.36 ± 0.18, 0.98 ± 0.14, 0.97 ± 0.17, or 0.86 ± 0.20 relative to IgG1 control, respectively (Figure 11C). Changes in the maximum *ΔF/F(t)* signal were in line with the AUC data. Addition of 100 µM to CD33$^{\Delta E2}$-DAP12-expressing cells led to a significant increase in the maximum *ΔF/F(t)* signal to 169.67 ± 23.78 % (p = 0.006 compared to IgG1 isotype control with 14.74 ± 1.29 %). The maximum *ΔF/F(t)* signal upon treatment of CD33$^{\Delta E2}$-DAP12-expressing cells with CD33 antibody clones 1c7/1, WM53, P67.6, or P67.6 F(ab) was 24.64 ± 5.11 %, 15.43 ± 3.31 %, 14.88 ± 2.32 %, or 20.39 ± 2.80 %, respectively and thus, did not statistically differ from the IgG1 control values (Figure 11D).

Taken together, the CD33 reporter cell lines were able to identify CD33 antibody clone P67.6 as agonistic and antibody clone 1c7/1 as potentially agonistic CD33 antibodies.

3.2.3 Validation of CD33-agonistic antibodies in human iPSdMiG

Reporter cell lines have some advantages over primary cells or other *in vitro* cultured cell lines, which endogenously express the protein of interest such as reduced background noises in the simple assay systems as well as the overexpression of the protein of interest. However, their advantages are intertwined with their limitations. Activation of the CD33 reporter cell line lacks the recruitment and activation of phosphatases since activation of TYROBP/DAP12 results in recruitment of ITAM-associated SYK. Thus, it is indispensable to validate this artificial system with an orthogonal assay. For this reason, human iPSdMiG, which closely resembled human primary microglia on transcriptome level (see section 3.1), were analyzed for CD33

pathway activation by assessing the phosphorylation status of ITAM-associated SYK. Thereby, CD33 pathway activation in iPSdMiG results in activation of protein tyrosine phosphatases, which in turn dephosphorylate SYK (see Figure 3).

3.2.3.1 CD33 transcription and surface expression in human iPSdMiG

Wild type (WT), isogenic CD33 knockout ($CD33^{-/-}$) and isogenic homozygous exon 2-deleted CD33 ($CD33^{\Delta E2}$) expressing human iPSdMiG were analyzed for activation of CD33 by the panel of CD33-specific antibodies. Initially, transcription and expression of CD33 were evaluated to validate expression of the specific variants. CD33M mRNA levels were significantly decreased in $CD33^{-/-}$ and $CD33^{\Delta E2}$ compared to WT iPSdMiG from 1.00 ± 0.01 to 0.11 ± 0.04 or 0.16 ± 0.04 (both $p < 0.001$ compared to WT), respectively (Figure 12A). Using $CD33^{\Delta E2}$-specific primers (spanning exon-exon junction 1/3) $CD33^{\Delta E2}$ transcripts were mainly detected in $CD33^{\Delta E2}$ iPSdMiG (WT 0.25 ± 0.02, $CD33^{-/-}$ 0.12 ± 0.02, both $p < 0.001$ compared to $CD33^{\Delta E2}$ with 1.00 ± 0.01). Interestingly, WT iPSdMiG showed significantly increased $CD33^{\Delta E2}$ mRNA levels compared to $CD33^{-/-}$ iPSdMiG ($p = 0.002$; Figure 12B). Flow

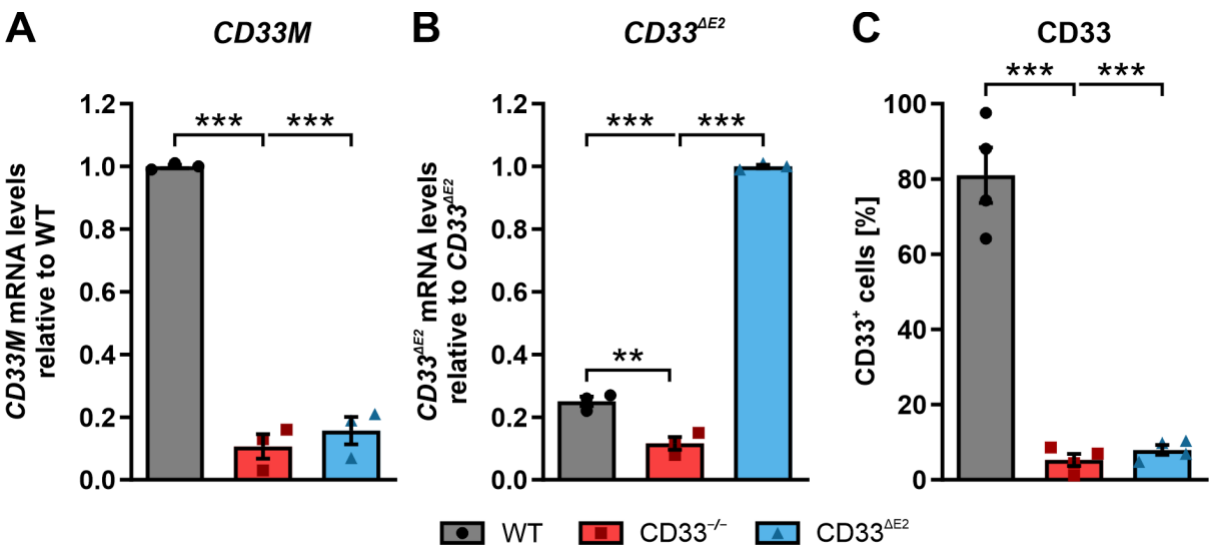

Figure 12: CD33 transcription and expression in BIONi lines analyzed by qRT-PCR and flow cytometry.

(A) Gene transcript levels of full-length *CD33M* were diminished in $CD33^{-/-}$ (red) or $CD33^{\Delta E2}$-expressing iPSdMiG (blue) compared to wild type iPSdMiG (grey). **(B)** Exon 2-deleted *CD33* (*$CD33^{\Delta E2}$*) mRNA levels were nearly absent in $CD33^{-/-}$ iPSdMiG (red) and diminished in WT iPSdMiG (grey) compared to $CD33^{\Delta E2}$-expressing iPSdMiG (blue). **(C)** CD33 surface expression analyzed by flow cytometry showed nearly absent CD33 surface expression in $CD33^{-/-}$ (red) or $CD33^{\Delta E2}$-expressing iPSdMiG (blue) compared to wild type iPSdMiG (grey). Data are presented as mean ± *SEM* of 3-4 independent experiments. *** represents $p \leq 0.001$ and ** represents $p \leq 0.01$ determined by Welch's ANOVA followed by Games-Howell post hoc test.

cytometry analysis for CD33 did not show notable CD33 surface expression in CD33$^{-/-}$ (5.30 ± 1.62 %, p = 0.003) or CD33$^{\Delta E2}$ iPSdMiG (7.96 ± 1.30 %, p = 0.004) compared to WT iPSdMiG (80.98 ± 7.38 %; Figure 12C). Hence, CD33$^{-/-}$ and CD33$^{\Delta E2}$ iPSdMiG lost CD33 surface expression.

3.2.3.2 CD33 antibody clones P67.6 and 1c7/1 activate CD33 in human iPSdMiG

In theory, the ITIM signaling following CD33 activation is able to directly antagonize ITAM signaling by dephosphorylating ITAMs and key kinases of the ITAM signaling pathway, such as SYK (see Figure 3). Hence, phosphorylated SYK (pSYK) was measured to analyze CD33 signaling to overcome limitations in measurement of fast and transient ITIM phosphorylation kinetics. PSYK levels in unstimulated iPSdMiG were only slightly elevated compared to the background signal (data not shown). Therefore, pSYK levels were increased by stimulation of ITAM-associated receptor TREM2 by an agonistic anti-TREM2 antibody.

IgG control-treated WT iPSdMiG (anti-TREM2 Ctrl) showed low levels of pSYK/tSYK compared to anti-TREM2-treated WT iPSdMiG (IgG Ctrl 3.37 ± 0.28 % compared to anti-TREM2/IgG1 100 ± 3.06 %; Figure 13A). Co-treatment of WT iPSdMiG with anti-TREM2 and CD33-specific antibodies 1c7/1 or P67.6 decreased pSYK/tSYK levels to

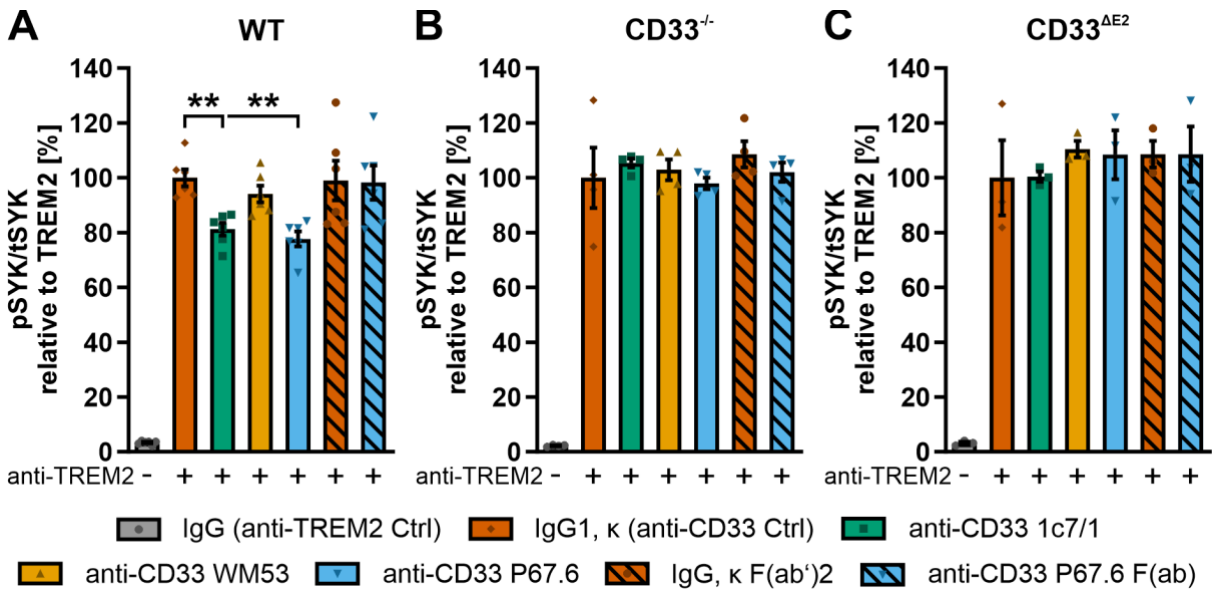

Figure 13: CD33 activation in iPSdMiG by agonistic CD33 antibodies measured via pSYK/tSYK. **(A)** Anti-TREM2 treatment triggered an increase in pSYK/tSYK, which was dampened by CD33-specific antibodies 1c7/1 (green) and P67.6 (blue) in WT full-length CD33-expressing iPSdMiG. This effect was absent in CD33$^{-/-}$ **(B)** or CD33$^{\Delta E2}$-expressing iPSdMiG **(C)**. Data are presented as mean ± *SEM* of 3-6 independent experiments. ** represents $p \leq 0.01$ determined by Welch's ANOVA followed by Games-Howell post hoc test.

81.24 ± 2.35 % (p = 0.01) or 77.69 ± 2.75 % (p = 0.004), respectively, indicating CD33 activation by these antibodies. Co-treatment of WT iPSdMiG with anti-TREM2 and CD33 antibody clones WM53 or P67.6 F(ab) did not alter pSYK/tSYK levels (WM53 94.08 ± 3.06 % and P67.6 F(ab) 98.26 ± 6.27 %; Figure 13A). Interestingly, the effect of the CD33-specific antibody clones 1c7/1 and P67.6 was not observed in $CD33^{-/-}$ or $CD33^{\Delta E2}$ iPSdMiG. In detail, treatment of $CD33^{-/-}$ iPSdMiG with anti-TREM2 elevated pSYK/tSYK levels compared to IgG control-treated cells from 2.23 ± 0.15 % to 100 ± 11.01 %. Co-treatment of $CD33^{-/-}$ iPSdMiG with anti-TREM2 and CD33-specific antibodies did not change pSYK/tSYK levels (1c7/1 105.40 ± 1.61 %, WM53 102.93 ± 3.79 %, P67.6 97.94 ± 2.14 %, and P67.6 F(ab) 102.01 ± 3.50 %; Figure 13B). Similarly, $CD33^{\Delta E2}$ iPSdMiG exhibited increased pSYK/tSYK levels following anti-TREM2 treatment (IgG Ctrl 3.13 ± 0.50 % versus anti-TREM2/IgG1 100 ± 13.74 %). Co-treatment of $CD33^{\Delta E2}$ iPSdMiG with anti-TREM2 and CD33-specific antibodies did not show a notable effect (1c7/1 100.42 ± 1.84 %, WM53 110.46 ± 3.04 %, P67.6 108.40 ± 8.94 %, and P67.6 F(ab) 108.61 ± 10.14 %; Figure 13C).

Thus, CD33-specific antibody clones 1c7/1 and P67.6 were able to functionally activate CD33 signaling and directly antagonize ITAM signaling induced by stimulation of TREM2 with a specific antibody.

3.3 The role of CD33 in human microglia

Recently, polymorphisms in the CD33 gene were linked to AD by genome-wide association studies (Hollingworth *et al*., 2011; Lambert *et al*., 2013; Naj *et al*., 2011). Thereby, increased expression $CD33^{\Delta E2}$, which lacks the sialic acid-binding domain, was found to be protective (Griciuc *et al*., 2013; Malik *et al*., 2013). In line with this hypothesis, expression levels of full-length CD33M positively correlated with increased Aβ plaque load in the brains of AD patients (Bradshaw *et al*., 2013; Griciuc *et al*., 2013) and CD33M-expressing macrophages and microglia exhibited decreased cargo uptake *in vitro* (Bhattacherjee *et al*., 2019). However, there is still only little known about CD33 signaling and, to date, its function in microglia is not fully understood. This thesis aims to elucidate the function of CD33 signaling in microglia and its consequences for AD progression. For this purpose, CD33M (WT), CD33 knockout ($CD33^{-/-}$), and exon 2-deleted CD33 ($CD33^{\Delta E2}$) iPSdMiG were functionally analyzed

and compared by investigating alterations in gene transcription and expression of ITIM and ITAM-associated receptors or adapter molecules, ITAM pathway activation, cytokine gene transcription, phagocytosis, and ROS production.

Elements of the results within this section and Figure 12 of the preceding section were accepted for publication in *GLIA* on 8th January 2021 (Wißfeld *et al*., 2021).

3.3.1 CD33 influenced ITIM/ITAM-associated molecule gene transcription

Regulatory signaling axes, including the ITIM-ITAM signaling axis, are well-balanced and tightly-controlled systems (Linnartz *et al*., 2010; Linnartz & Neumann, 2013). The absence of a signaling partner on one side of these systems often triggers

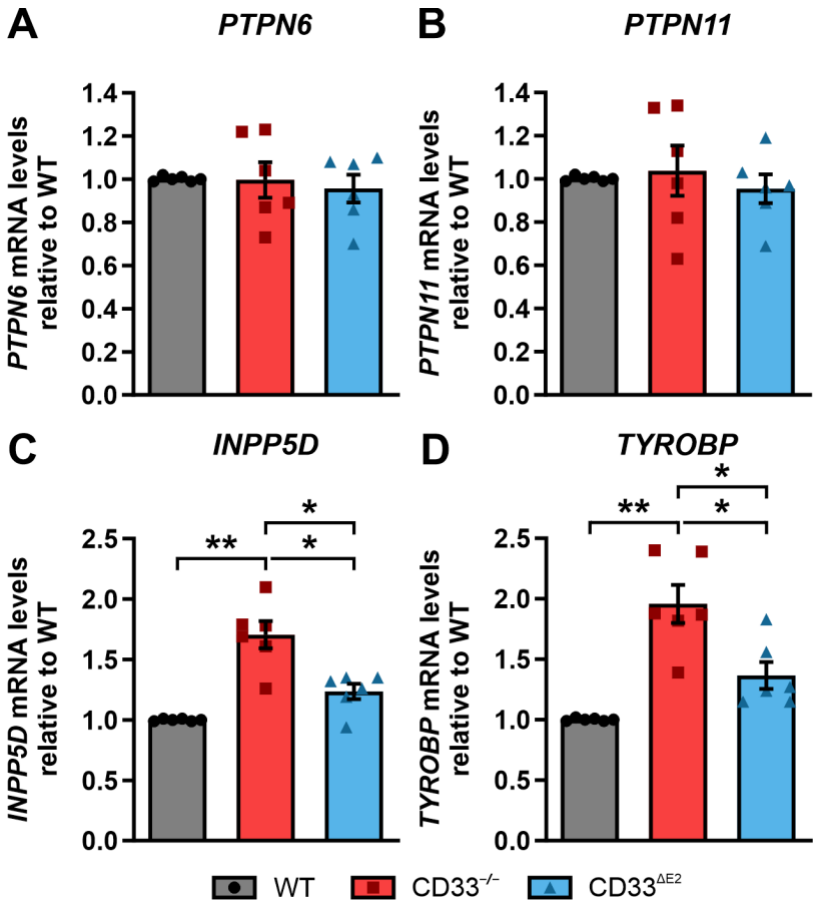

Figure 14: ITIM and ITAM adapter molecule gene transcription analyzed by qRT-PCR.
(A) Gene transcript levels of *PTPN6* were unchanged in CD33$^{-/-}$ (red) or CD33$^{\Delta E2}$-expressing iPSdMiG (blue) compared to wild type iPSdMiG (grey). **(B)** No difference was observed in *PTPN11* mRNA levels in CD33$^{-/-}$ (red) or CD33$^{\Delta E2}$-expressing iPSdMiG (blue) compared to wild type iPSdMiG (grey). **(C)** *INPP5D* mRNA levels were increased in CD33$^{-/-}$ (red) and mildly increased in CD33$^{\Delta E2}$-expressing iPSdMiG (blue) compared to wild type iPSdMiG (grey). **(D)** Gene transcript levels of *TYROBP* were increased in CD33$^{-/-}$ (red) and mildly increased in CD33$^{\Delta E2}$-expressing iPSdMiG (blue) compared to wild type iPSdMiG (grey). Data are presented as mean ± *SEM* of 6 independent experiments. ** represents $p \leq 0.01$ and * represents $p \leq 0.05$ determined by Welch's ANOVA followed by Games-Howell post hoc test. PTPN = protein tyrosine phosphatase non-receptor type; INPP5D = inositol polyphosphate-5-phosphatase D; TYROBP = transmembrane immune signaling adapter TYROBP.

compensatory regulation in form of up- or downregulation of associated proteins – a phenomenon known as genetic compensation response (GCR) (Rossi *et al*., 2015). To test for any GCR downstream of CD33, gene transcript levels of ITIM-associated adapter proteins *PTPN6/SHP1*, *PTPN11/SHP2*, and *INPP5D/SHIP1* as well as ITAM-containing *TYROBP/DAP12* were investigated. Knockout of CD33 ($CD33^{-/-}$) or expression of exon 2-deleted CD33 ($CD33^{\Delta E2}$) did not alter gene transcript levels of *PTPN6* ($CD33^{-/-}$ 1.00 ± 0.08 and $CD33^{\Delta E2}$ 0.95 ± 0.06 compared to WT 1.00 ± 0.00; Figure 14A) or *PTPN11* ($CD33^{-/-}$ 1.04 ± 0.12 and $CD33^{\Delta E2}$ 0.95 ± 0.07 compared to WT 1.00 ± 0.00; Figure 14B). However, the mRNA levels of *INPP5D* as well as *TYROBP* were significantly increased in $CD33^{-/-}$ and with much lower magnitude in $CD33^{\Delta E2}$ iPSdMiG. In detail, *INPP5D* was upregulated in $CD33^{-/-}$ iPSdMiG to 1.71 ± 0.11 compared to WT (1.00 ± 0.00, $p = 0.003$) and $CD33^{\Delta E2}$ iPSdMiG (1.23 ± 0.06, $p = 0.032$ compared to WT and $p = 0.016$ compared to $CD33^{-/-}$; Figure 14C). Further, in $CD33^{-/-}$ iPSdMiG *TYROBP* mRNA transcripts were significantly increased to 1.96 ± 0.16 compared to WT (1.00 ± 0.01, $p = 0.004$) and $CD33^{\Delta E2}$ iPSdMiG (1.37 ± 0.11, $p = 0.032$). In addition, *TYROBP* mRNA levels were significantly increased in $CD33^{\Delta E2}$ compared to WT iPSdMiG ($p = 0.049$; Figure 14D). Hence, knockout of *CD33* and with a lower magnitude expression of $CD33^{\Delta E2}$ in iPSdMiG led to upregulation of *INPP5D* and *TYROBP* mRNA levels.

3.3.2 CD33 affected microglial receptor transcription and expression

In a similar way, differential CD33 expression in form of absence of CD33 ($CD33^{-/-}$) or expression of $CD33^{\Delta E2}$ might affect gene transcription and protein expression of microglial receptors, including activatory receptors TREM2 (*TREM2*), CD14 (*CD14*), and FcγRI (*FCGR1A*) as well as inhibitory receptors CD45 (*PTPRC*) and SIRPα (*SIRPA*). Semi-quantitative real-time PCR revealed upregulation of the gene transcripts of ITAM-associated receptor *TREM2* in $CD33^{-/-}$ (2.92 ± 0.66, $p = 0.012$ compared to WT and $p = 0.03$ compared to $CD33^{\Delta E2}$) but not in $CD33^{\Delta E2}$ iPSdMiG (1.25 ± 0.22) compared to WT iPSdMiG (1.00 ± 0.01; Figure 15A). Increased mRNA levels in $CD33^{-/-}$ and $CD33^{\Delta E2}$ iPSdMiG were detected for TLR co-receptor *CD14* and partly for ITAM-associated receptor *FCGR1A*. In detail, knockout of *CD33* increased *CD14* gene transcript levels to 2.99 ± 0.23 ($p = 0.001$) and expression of $CD33^{\Delta E2}$ in iPSdMiG to 2.31 ± 0.31 ($p = 0.024$) compared to WT (1.00 ± 0.01; Figure 15B). *FCGR1A* mRNA levels were elevated in $CD33^{-/-}$ (8.13 ± 1.54) and tended to be

increased in CD33$^{\Delta E2}$ iPSdMiG (2.23 ± 0.24) compared to WT (1.00 ± 0.01, $p < 0.001$ compared to CD33$^{-/-}$ and $p = 0.153$ compared to CD33$^{\Delta E2}$; Figure 15C). In addition, *FCGR1A* mRNA levels in CD33$^{-/-}$ iPSdMiG tended to be increased compared to CD33$^{\Delta E2}$ iPSdMiG ($p = 0.153$). Furthermore, gene transcript levels of ITIM-bearing *SIRPA* tended to be increased in CD33$^{-/-}$ but not CD33$^{\Delta E2}$ iPSdMiG (CD33$^{-/-}$ 1.59 ± 0.25 with $p = 0.15$ and CD33$^{\Delta E2}$ 1.13 ± 0.11 compared to WT 1.00 ± 0.00; Figure 15D).

On protein level, all three iPSdMiG lines were highly positive for microglial receptors CD14, CD45, FcγRI, and SIRPα with more than 90 % of positive cells (except for CD14

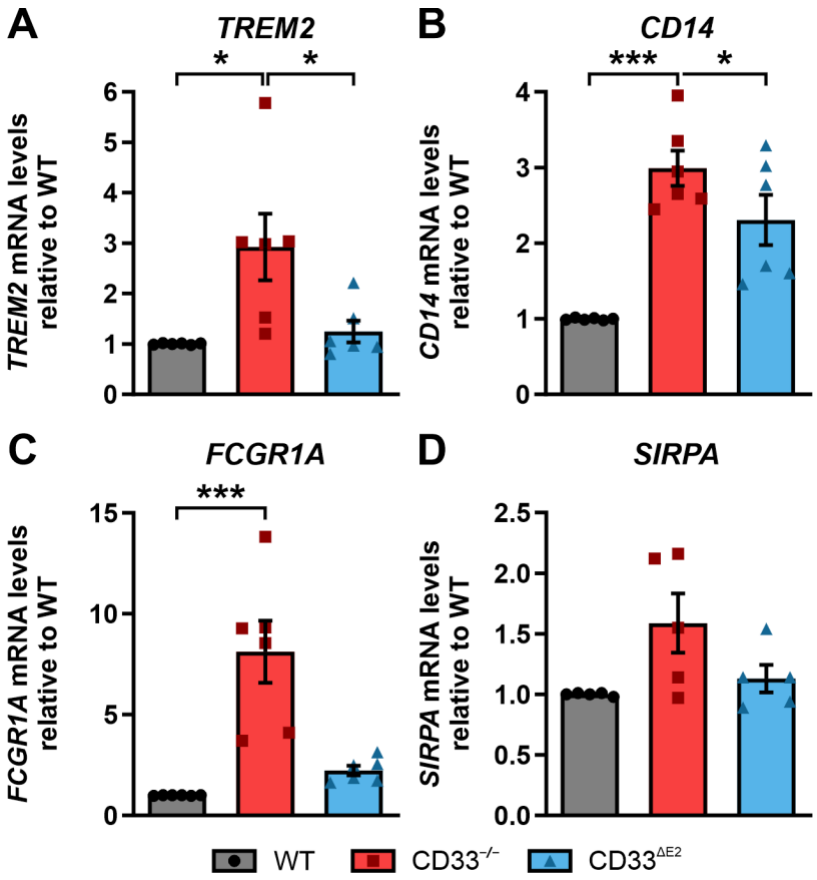

Figure 15: Elevated myeloid receptor mRNA levels in CD33$^{-/-}$ iPSdMiG analyzed by qRT-PCR. **(A)** Gene transcript levels of *TREM2* were increased in CD33$^{-/-}$ (red) but not CD33$^{\Delta E2}$-expressing iPSdMiG (blue) compared to wild type iPSdMiG (grey). **(B)** Increased *CD14* mRNA levels were observed in CD33$^{-/-}$ (red) and CD33$^{\Delta E2}$-expressing iPSdMiG (blue) compared to wild type iPSdMiG (grey). **(C)** *FCGR1A* mRNA levels were increased in CD33$^{-/-}$ (red) but only tended to be increased in CD33$^{\Delta E2}$-expressing iPSdMiG (blue) compared to wild type iPSdMiG (grey). **(D)** Gene transcript levels of *SIRPA* tended to be increased in CD33$^{-/-}$ (red) but not in CD33$^{\Delta E2}$-expressing iPSdMiG (blue) compared to wild type iPSdMiG (grey). Data are presented as mean ± *SEM* of 5-6 independent experiments. *** represents $p \leq 0.001$ and * represents $p \leq 0.05$ determined by Welch's ANOVA followed by Games-Howell post hoc test or Kruskal-Wallis *H* test (*FCGR1A*). *FCGR1A = Fc fragment of IgG receptor Ia*; *SIRPA = signal regulatory protein alpha*; *TREM2 = triggering receptor expressed on myeloid cells 2*.

in CD33$^{\Delta E2}$ iPSdMiG with 88.23 ± 3.00 %, Figure 16A-D) without statistically significant differences quantified by flow cytometry. However, differences in the average protein load per cell measured as geometric mean fluorescence intensity (MFI) were observed. Here, the MFI of CD14, CD45, FcγRI, and SIRPα was increased in CD33$^{-/-}$ iPSdMiG (CD14 2.37 ± 0.34, CD45 1.72 ± 0.15, FcγRI 2.79 ± 0.33, and SIRPα 1.44 ± 0.23) compared to WT (CD14 1.00 ± 0.22 with $p = 0.009$, CD45 1.00 ± 0.10 with $p = 0.006$, FcγRI 1.00 ± 0.29 with $p = 0.003$, and SIRPα 1.00 ± 0.25 with $p = 0.555$) and CD33$^{\Delta E2}$ iPSdMiG (CD14 0.84 ± 0.14 with $p = 0.007$, CD45 0.76 ± 0.03

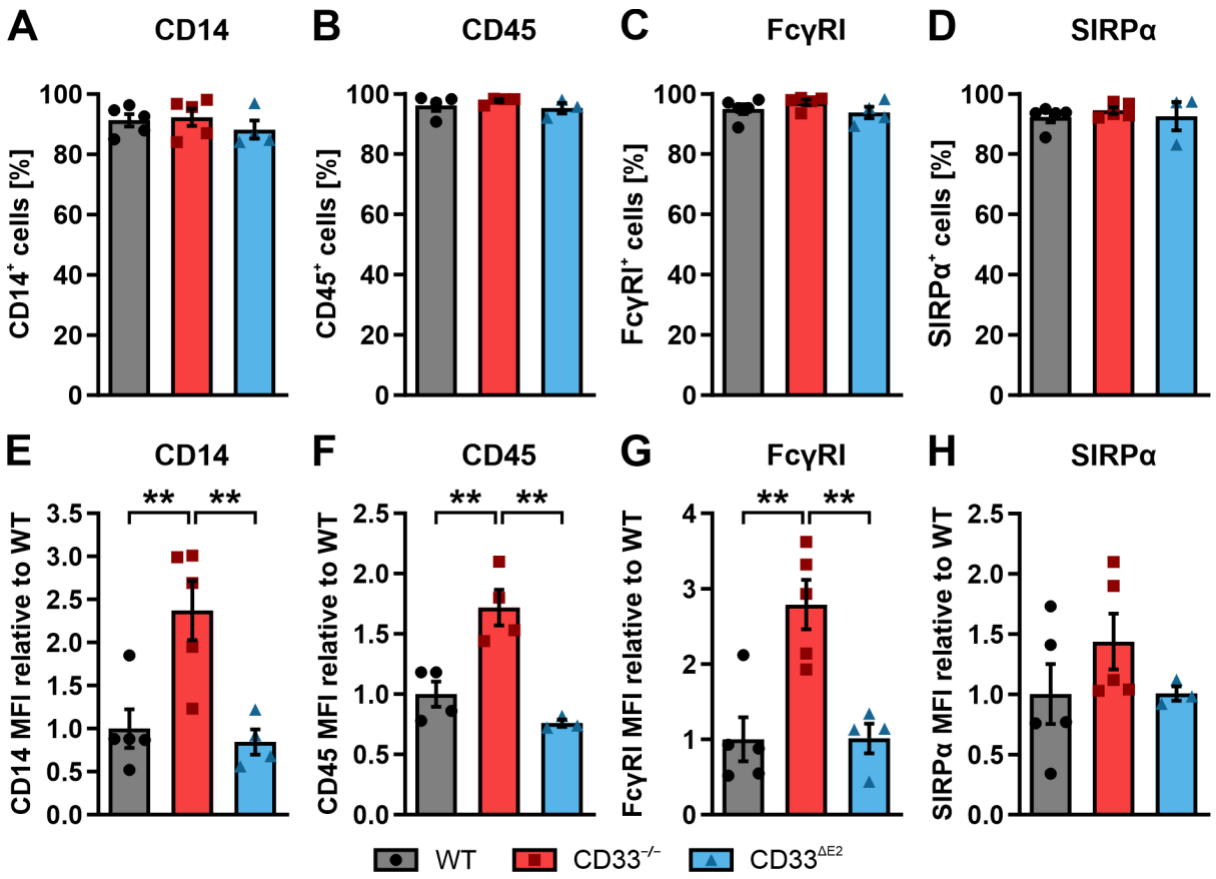

Figure 16: Myeloid receptor surface expression levels were increased in CD33$^{-/-}$ iPSdMiG. Quantification of surface expression by flow cytometry as percentage of positive cells of myeloid receptors **(A)** CD14, **(B)** CD45, **(C)** FcγRI and **(D)** SIRPα showed very percentages of positive cells in all three iPSdMiG lines without statistically significant differences. **(E)** Increased CD14 surface expression determined via MFI was observed in CD33$^{-/-}$ (red) but not CD33$^{\Delta E2}$-expressing iPSdMiG (blue) compared to wild type iPSdMiG (grey). **(F)** MFI quantification showed increased CD45 surface expression in CD33$^{-/-}$ (red) but not in CD33$^{\Delta E2}$-expressing iPSdMiG (blue) compared to wild type iPSdMiG (grey). **(G)** FcγRI surface expression determined by MFI was increased in CD33$^{-/-}$ (red) but not in CD33$^{\Delta E2}$-expressing iPSdMiG (blue) compared to wild type iPSdMiG (grey). **(H)** Quantification of the MFI of SIRPα staining showed SIRPα surface expression tended to be increased in CD33$^{-/-}$ (red) but not in CD33$^{\Delta E2}$-expressing iPSdMiG (blue) compared to wild type iPSdMiG (grey). Data are presented as mean ± *SEM* of 3-5 independent experiments. ** represents $p \leq 0.01$ determined by one-way ANOVA followed by Bonferroni post hoc test. FcγRI = Fc fragment of IgG receptor Ia; MFI = geometric mean fluorescence intensity; SIRPα = signal regulatory protein alpha.

with $p = 0.002$, FcγRI 1.01 ± 0.20 with $p = 0.004$, and SIRPα 1.01 ± 0.06 with $p = 0.752$; Figure 16E-H).

Taken together, knockout of *CD33* in iPSdMiG induced upregulation of mRNA levels activatory receptors *TREM2*, *CD14*, and *FCGR1A*. Expression of CD33$^{\Delta E2}$ in iPSdMiG only resulted in upregulation of *CD14* gene transcripts. Interestingly, CD33$^{-/-}$ iPSdMiG showed a higher surface expression of CD14, CD45, FcγRI, and SIRPα compared to WT and CD33$^{\Delta E2}$ iPSdMiG, although the percentage of positive cells was undistinguishably high in all three lines.

3.3.3 Increased ITAM pathway activation in CD33$^{-/-}$ and CD33$^{\Delta E2}$ iPSdMiG

As shown in section 3.2.3.2 induction of the CD33 signaling cascade by activation of CD33 is able to directly antagonize ITAM signaling by, e.g., dephosphorylation of SYK. Loss of CD33 resulted in the increased gene transcription or protein expression of ITAM-associated TYROBP, TREM2 and FcγRI but also of ITIM-associated INPP5D and SIRPα, whereas in CD33$^{\Delta E2}$-expressing iPSdMiG only *CD14* mRNA levels were increased. These changes – in conjunction with loss of CD33 surface expression – are able to modulate ITIM/ITAM downstream signaling in either direction, inhibitory or activatory. To assess whether deletion of CD33 or expression of CD33$^{\Delta E2}$ in iPSdMiG affected the ITIM-ITAM signaling axis, phosphorylation of SYK was determined as pSYK/tSYK. An increased SYK phosphorylation was observed in untreated CD33$^{-/-}$ (1.56 ± 0.11, $p = 0.002$) and CD33$^{\Delta E2}$ iPSdMiG (1.43 ± 0.08, $p = 0.013$) compared to WT iPSdMiG (1.00 ± 0.08; Figure 17A). Activation of the ITAM signaling axis by a TREM2-specific antibody elevated the pSYK/tSYK level in all lines compared to the isotype control antibody (WT from 1.00 ± 0.11 to 26.48 ± 5.05 with $p = 0.036$, CD33$^{-/-}$ from 1.95 ± 0.21 to 92.19 ± 8.45 with $p < 0.001$ and CD33$^{\Delta E2}$ from 1.30 ± 0.05 to 43.36 ± 5.95 with $p < 0.001$). Furthermore, the pSYK/tSYK levels in TREM2-treated CD33$^{-/-}$ iPSdMiG were significantly increased compared to both, TREM2-treated WT and CD33$^{\Delta E2}$ iPSdMiG (both $p < 0.001$ compared to CD33$^{-/-}$). The pSYK/tSYK levels in TREM2-treated CD33$^{\Delta E2}$ iPSdMiG were not significantly altered compared to TREM2-treated WT iPSdMiG ($p = 0.39$; Figure 17B). Likewise, treatment with a FcγRI-specific antibody increased pSYK/tSYK levels in iPSdMiG compared to the isotype control-treated cells (WT from 1.00 ± 0.10 to 8.30 ± 0.64 with $p = 0.047$, CD33$^{-/-}$ from 1.59 ± 0.13 to 40.32 ± 3.80 with $p < 0.001$ and CD33$^{\Delta E2}$ from 1.44 ± 0.13 to 13.23 ± 0.78 with $p < 0.001$). In addition, the pSYK/tSYK levels in FcγRI-treated

CD33$^{-/-}$ iPSdMiG were significantly increased compared to both FcγRI-treated WT and CD33$^{\Delta E2}$ iPSdMiG (both $p < 0.001$ compared to CD33$^{-/-}$). However, the increased pSYK/tSYK levels in FcγRI-treated CD33$^{\Delta E2}$ iPSdMiG were insignificant compared to FcγRI-treated WT iPSdMiG ($p = 0.57$; Figure 17C).

Thus, increased phosphorylation of SYK was observed following *CD33* knockout or expression of CD33$^{\Delta E2}$ in iPSdMiG. Stimulation with a TREM2-specific or FcγRI-specific antibody showed increased pSYK/tSYK levels in CD33$^{-/-}$ iPSdMiG compared to both, WT and CD33$^{\Delta E2}$ iPSdMiG.

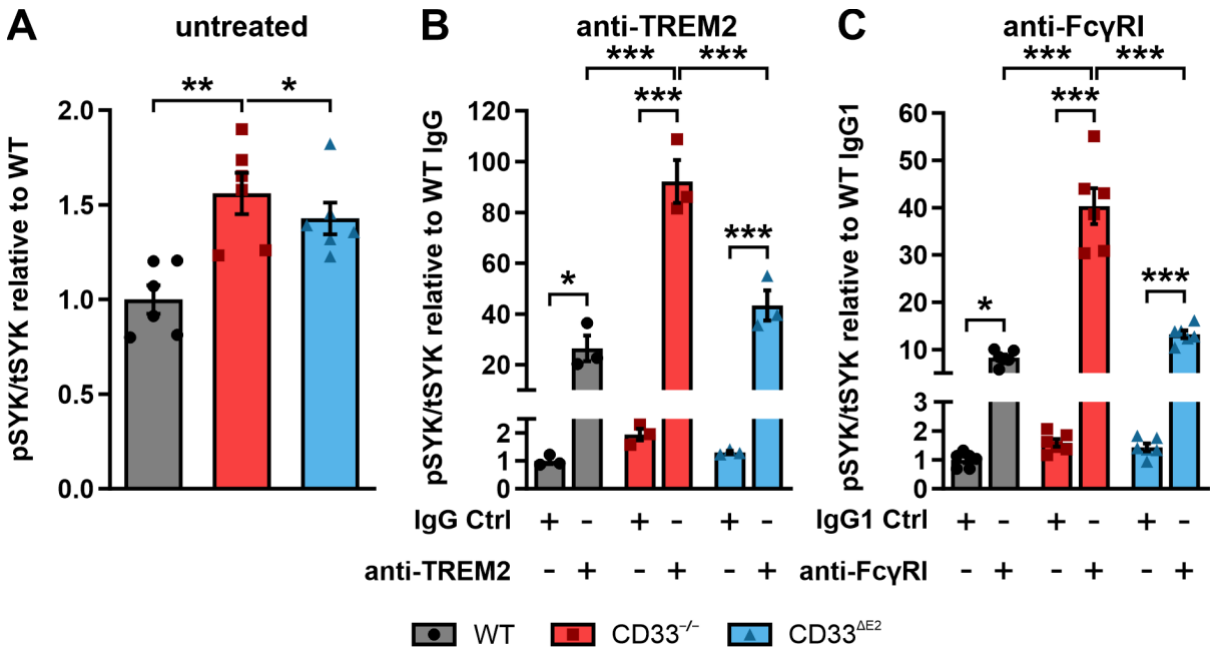

Figure 17: ITAM pathway activation measured in CD33$^{-/-}$ and CD33$^{\Delta E2}$ iPSdMiG by pSYK/tSYK. **(A)** Untreated CD33$^{-/-}$ (red) and CD33$^{\Delta E2}$-expressing iPSdMiG (blue) exhibited elevated pSYK/tSYK levels compared to wild type iPSdMiG (grey) measured by AlphaLISA. **(B)** Treatment of iPSdMiG with a TREM2-specific antibody for 5 minutes resulted in elevated pSYK/tSYK levels in all three lines compared to IgG Ctrl-treated samples. CD33$^{-/-}$ iPSdMiG (red) showed a significantly higher increase compared to wild type (grey) and CD33$^{\Delta E2}$-expressing iPSdMiG (blue). **(C)** Treatment of iPSdMiG with a FcγRI-specific antibody for 5 minutes resulted in elevated pSYK/tSYK levels in all three lines compared to IgG1 Ctrl-treated samples. CD33$^{-/-}$ iPSdMiG (red) showed a significantly higher increase compared to wild type (grey) and CD33$^{\Delta E2}$-expressing iPSdMiG (blue). Data are presented as mean ± *SEM* of 3-6 independent experiments. *** represents $p \leq 0.001$, ** represents $p \leq 0.01$ and * represents $p \leq 0.05$ determined by one-way ANOVA followed by Bonferroni post hoc test. FcγRI = Fc fragment of IgG receptor Ia; IgG Ctrl = isotype control; pSYK = phosphorylated spleen-associated tyrosine kinase; TREM2 = triggering receptor expressed on myeloid cells 2; tSYK = total SYK.

3.3.4 Upregulated inflammatory cytokine and chemokine gene transcription in CD33$^{-/-}$ and CD33$^{\Delta E2}$ iPSdMiG

Loss of CD33 surface expression in CD33$^{-/-}$ and CD33$^{\Delta E2}$ iPSdMiG resulted in a slight increase in SYK phosphorylation. Consequently, increased pSYK levels could lead to

an increased or more pronounced activation of the microglial cells. Cytokine and chemokine production are hallmarks of activated microglia and upregulated quickly in response to an immunogenic stimulus but also chronically in case of an imbalanced signaling system (reviewed in Hanisch, 2002). Therefore, production of *TNF* (TNF-α), *IL1B* (IL-1β), *IL6*, *CXCL8* (CXCL8/IL-8), and *IL10* was investigated in iPSdMiG on gene transcript level using semi-quantitative real-time PCR. Knockout of *CD33* in iPSdMiG resulted in an increase in the mRNA transcription of the cytokines *TNF* (1.61 ± 0.18, $p = 0.039$), *IL1B* (1.67 ± 0.15, $p = 0.021$), *IL6* (10.52 ± 1.62, $p = 0.005$),

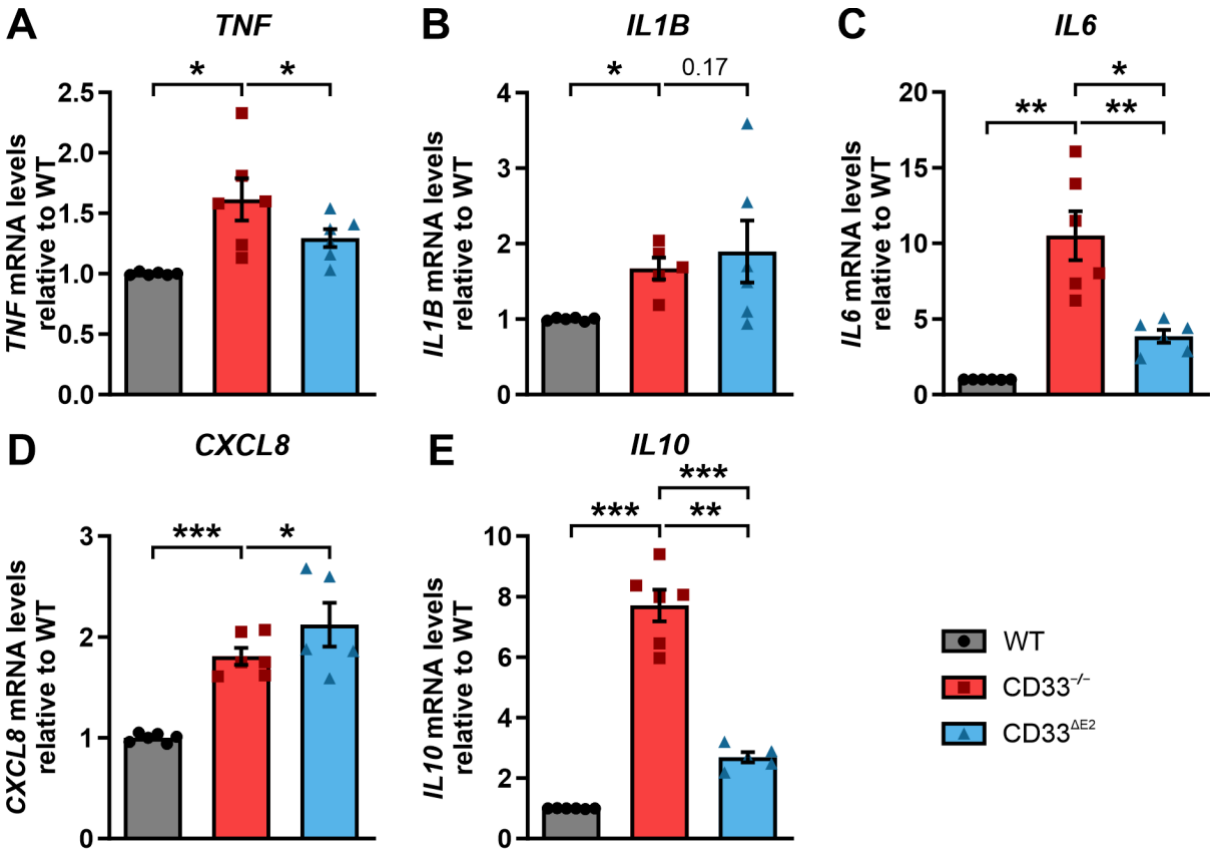

Figure 18: Cytokine mRNA levels were increased in CD33$^{-/-}$ and CD33$^{\Delta E2}$ iPSdMiG assessed by qRT-PCR.
(A) Upregulated *TNF* mRNA levels were observed in CD33$^{-/-}$ (red) and with lower magnitude in CD33$^{\Delta E2}$-expressing iPSdMiG (blue) compared to wild type iPSdMiG (grey). **(B)** Gene transcript levels of *IL1B* were increased in CD33$^{-/-}$ (red) and tended to be increased in CD33$^{\Delta E2}$-expressing iPSdMiG (blue) compared to wild type iPSdMiG (grey). **(C)** *IL6* mRNA levels were sharply increased in CD33$^{-/-}$ (red) and moderately in CD33$^{\Delta E2}$-expressing iPSdMiG (blue) compared to wild type iPSdMiG (grey). **(D)** Gene transcript levels of *CXCL8* were upregulated in CD33$^{-/-}$ (red) and CD33$^{\Delta E2}$-expressing iPSdMiG (blue) compared to wild type iPSdMiG (grey). **(E)** *IL10* mRNA levels were sharply increased in CD33$^{-/-}$ (red) and moderately in CD33$^{\Delta E2}$-expressing iPSdMiG (blue) compared to wild type iPSdMiG (grey). Data are presented as mean ± *SEM* of 5-6 independent experiments. *** represents $p \leq 0.001$, ** represents $p \leq 0.01$ and * represents $p \leq 0.05$ determined by Welch's ANOVA followed by Games-Howell post hoc test. *CXCL8 = C-X-C motif chemokine ligand 8*; *IL = interleukin*; *TNF = tumor necrosis factor*.

IL10 (7.71 ± 0.52, $p < 0.001$), and the chemokine *CXCL8* (1.81 ± 0.08, $p < 0.001$) compared to WT iPSdMiG (*TNF* 1.00 ± 0.01, *IL1B* 1.00 ± 0.01, *IL6* 1.00 ± 0.00, *IL10* 1.00 ± 0.00, and *CXCL8* 1.00 ± 0.02; Figure 18A-E). In CD33$^{\Delta E2}$ iPSdMiG upregulation of cytokine and chemokine mRNA transcription was less consistent. Gene transcript levels of *IL1B* (1.89 ± 0.41 with $p = 0.168$; Figure 18B) and *CXCL8* (2.12 ± 0.22 with $p = 0.014$; Figure 18D) were upregulated or tended to be upregulated compared to WT iPSdMiG with a similar magnitude as observed in CD33$^{-/-}$ iPSdMiG. In contrast, upregulation of *TNF* (1.29 ± 0.07 with $p = 0.024$ compared to WT; Figure 18A), *IL6* (3.85 ± 0.43 with $p = 0.003$ compared to WT; Figure 18C) and *IL10* (3.07 ± 0.41 with $p = 0.009$ compared to WT; Figure 18E) tended to be lower or were significantly lower compared to CD33$^{-/-}$ iPSdMiG (for *TNF* $p = 0.281$, for *IL6* $p = 0.019$ and for *IL10* $p < 0.001$).

Altogether, both CD33$^{-/-}$ as well as CD33$^{\Delta E2}$ iPSdMiG exhibited increased cytokine gene transcript levels compared to WT iPSdMiG. However, in CD33$^{\Delta E2}$ iPSdMiG a dampened increase in mRNA levels of *TNF*, *IL6* and *IL10* compared to CD33$^{-/-}$ iPSdMiG was observed whereas *IL1B* and *CXCL8* did not vary compared to CD33$^{-/-}$ iPSdMiG.

3.3.5 Increased phagocytic capacity of CD33$^{-/-}$ and CD33$^{\Delta E2}$ iPSdMiG

Uptake of particles such as bacteria, debris or aggregated proteins is a key competence of microglia. This process is referred to as phagocytosis. As knockout of *CD33* or expression of CD33$^{\Delta E2}$ in iPSdMiG exhibited increased phosphorylation of SYK and increased gene transcript levels of selected cytokines as a sign of cellular activation, phagocytosis of pHrodo-labeled *S. aureus* BioParticles was investigated. PHrodo is a pH-sensitive dye, which is non-fluorescent outside the cell (at pH 7.4) but fluoresces brightly upon uptake in acidic phagolysosomes. Thus, live cell imaging was performed after incubation with pHrodo-conjugated BioParticles and fluorescence intensity was measured as a representation of phagocytic activity.

Knockout of *CD33* as well as expression of CD33$^{\Delta E2}$ in iPSdMiG resulted in an increased baseline phagocytosis of pHrodo-conjugated *S. aureus* BioParticles compared to WT iPSdMiG. In detail, CD33$^{-/-}$ and CD33$^{\Delta E2}$-expressing iPSdMiG exhibited with 2.37 ± 0.12 ($p = 0.001$) and 1.96 ± 0.15 ($p = 0.008$), respectively, a significantly elevated phagocytic capacity compared to WT iPSdMiG (1.00 ± 0.21; Figure 19A+B). *S. aureus* BioParticles trigger TLR-mediated phagocytosis via, e.g.,

recognition of lipoteichoic acid as component of the cell wall of *S. aureus*. TLR signaling is a strong and powerful pro-inflammatory activator triggered by an

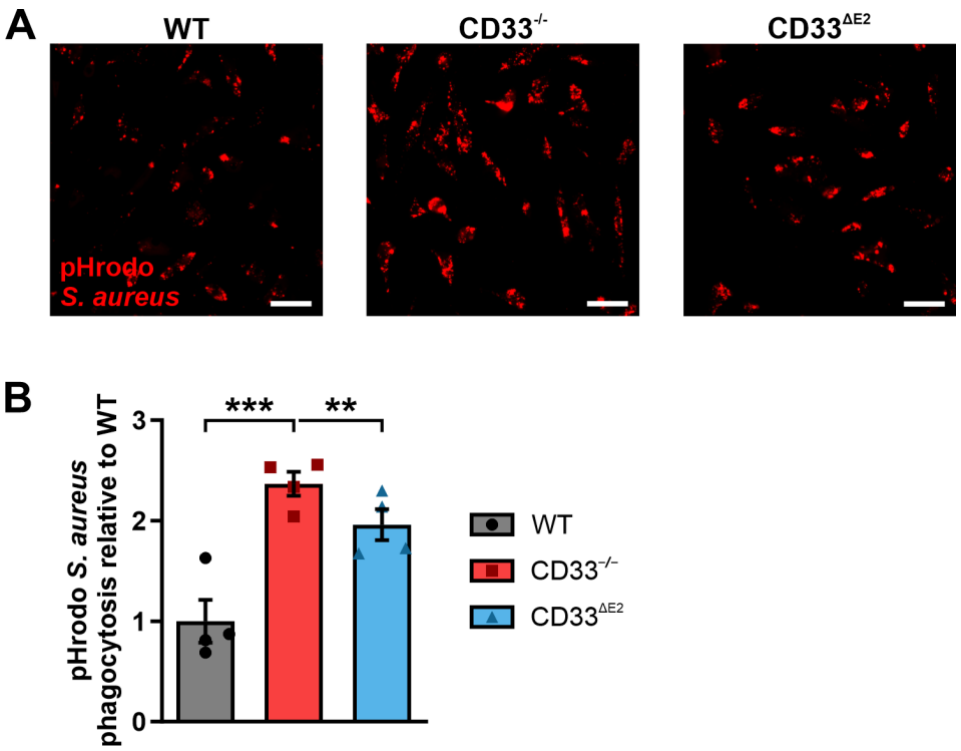

Figure 19: PHrodo *S. aureus* BioParticles phagocytosis was increased in CD33$^{-/-}$ and CD33$^{\Delta E2}$ iPSdMiG.
(A) Microscopy images of living iPSdMiG showing red fluorescent pHrodo BioParticles present in acidic lysosomes. Representative image out of 4 independent experiments. Scale bars = 50 µm. **(B)** Quantification of pHrodo BioParticles fluorescence intensity showed an increased phagocytic capacity in CD33$^{-/-}$ (red) and CD33$^{\Delta E2}$-expressing iPSdMiG (blue) compared to wild type iPSdMiG (grey). Data are presented as mean ± *SEM* of 4 independent experiments. *** represents $p \leq 0.001$ and ** represents $p \leq 0.01$ determined by one-way ANOVA followed by Bonferroni post hoc test.

exogenous stimulus such as invading pathogens (Long *et al*., 2009). Therefore, the response to an endogenous disease-related stimulus, here aggregated Aβ$_{1\text{-}42}$, was also investigated. Likewise, CD33$^{-/-}$ and CD33$^{\Delta E2}$-expressing iPSdMiG exhibited with 1.67 ± 0.11 ($p = 0.001$) and 1.42 ± 0.06 ($p = 0.021$), respectively, a significantly increased aggregated Aβ$_{1\text{-}42}$ uptake compared to WT iPSdMiG (1.00 ± 0.08; Figure 20A+B). Overall, CD33$^{-/-}$ and CD33$^{\Delta E2}$-expressing iPSdMiG showed an increased phagocytic capacity compared to WT iPSdMiG.

3.3.6 Elevated phagocytic oxidative burst triggered by loss of *CD33*

Invading pathogens activate a variety of pro-inflammatory pathways once recognized by microglia. Phagocytosed pathogens trigger the production and release of ROS, which can be both, beneficial in terms of acute pathogen clearance as well as

detrimental in terms of causing collateral damage to neurons due to chronic release (P. R. Angelova & Abramov, 2018; Shukla *et al*., 2011). It is known that ROS can be

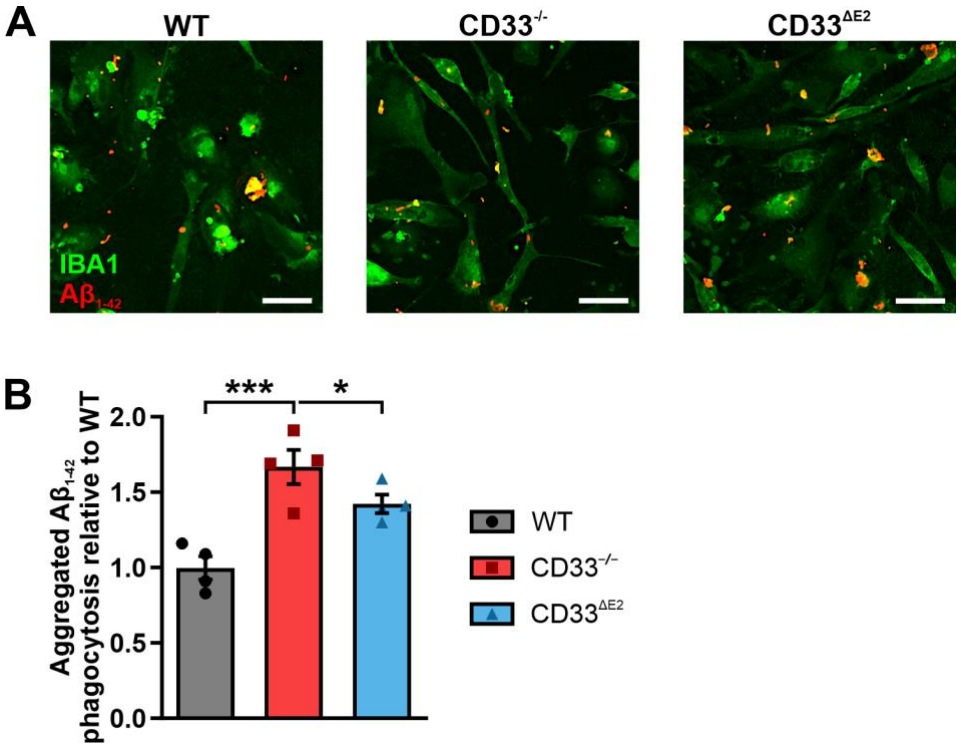

Figure 20: $A\beta_{1-42}$ phagocytosis was increased in $CD33^{-/-}$ and $CD33^{\Delta E2}$ iPSdMiG .
(A) Microscopy images of IBA1-stained iPSdMiG (green) showing red-fluorescent aggregated $A\beta_{1-42}$. Representative image out of 4 independent experiments. Scale bars = 50 µm. **(B)** Quantification of aggregated $A\beta_{1-42}$ phagocytosis showed an increased phagocytic capacity in $CD33^{-/-}$ (red) and $CD33^{\Delta E2}$-expressing iPSdMiG (blue) compared to wild type iPSdMiG (grey). Data are presented as mean ± *SEM* of 4 independent experiments. *** represents $p \leq 0.001$ and * represents $p \leq 0.05$ determined by one-way ANOVA followed by Bonferroni post hoc test. Aβ = amyloid β; IBA1 = ionized calcium-binding adapter molecule 1.

induced by ITAM signaling (Mocsai *et al*., 2006; Wakselman *et al*., 2008). Therefore, $CD33^{-/-}$ and $CD33^{\Delta E2}$-expressing iPSdMiG were investigated for ROS production by DHE staining. Oxidized DHE intercalates with the cell's DNA and starts to fluoresce in the red spectrum. Interestingly, there was no change observed in untreated $CD33^{-/-}$ and $CD33^{\Delta E2}$-expressing iPSdMiG ($CD33^{-/-}$ 1.11 ± 0.06 and $CD33^{\Delta E2}$ 0.89 ± 0.09 compared to WT 1.00 ± 0.05). Treatment of iPSdMiG with unlabeled *S. aureus* BioParticles increased ROS production in WT iPSdMiG to 1.50 ± 0.06 ($p = 0.003$ compared to untreated), in $CD33^{-/-}$ iPSdMiG to 2.02 ± 0.11 ($p < 0.001$ compared to untreated) and in $CD33^{\Delta E2}$ iPSdMiG to 1.35 ± 0.05 ($p = 0.11$ compared to untreated). The ROS increase after *S. aureus* BioParticles treatment was significantly increased in $CD33^{-/-}$ iPSdMiG compared to WT ($p = 0.002$) and $CD33^{\Delta E2}$ iPSdMiG ($p < 0.001$).

Treatment with the antioxidant NAC attenuated the *S. aureus* BioParticles-induced ROS increase (WT 1.18 ± 0.04 with $p = 0.234$, CD33$^{-/-}$ 1.32 ± 0.08 with $p < 0.001$, and CD33$^{\Delta E2}$ 1.01 ± 0.19 with $p = 0.722$ compared to *S. aureus* BioParticles treatment only; Figure 21).

Thus, knockout of *CD33* but not expression of CD33$^{\Delta E2}$ in iPSdMiG resulted in an increased production of ROS following *S. aureus* BioParticles treatment.

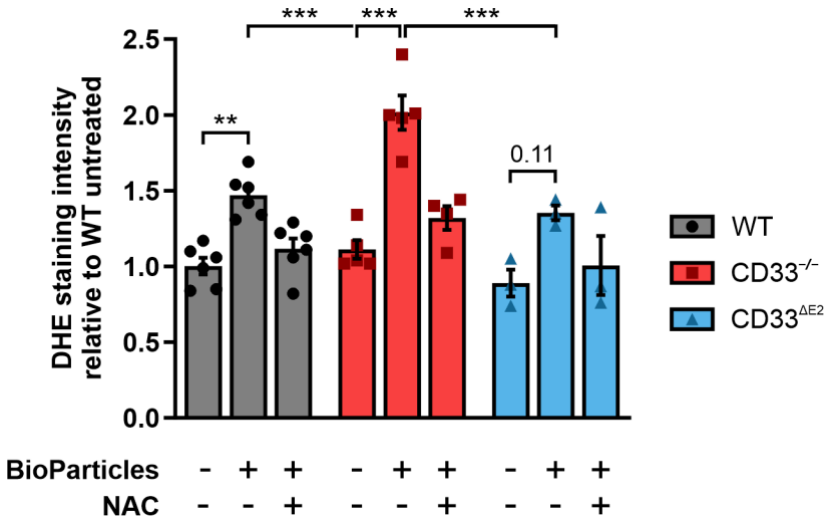

Figure 21: ROS production analyzed by DHE staining showed increased oxidative burst in CD33$^{-/-}$ iPSdMiG.

Quantification of DHE staining intensity showed that the three iPSdMiG lines did not differ in constitutive production of ROS. Treatment with unlabeled *S. aureus* BioParticles for 15 minutes increased ROS production in all three iPSdMiG lines with a higher magnitude in CD33$^{-/-}$ iPSdMiG (red) compared to CD33$^{\Delta E2}$-expressing iPSdMiG (blue) and wild type iPSdMiG (grey). Treatment with NAC attenuated BioParticles-induced ROS production. Data are presented as mean ± *SEM* of 3-6 independent experiments. *** represents $p \leq 0.001$ and ** represents $p \leq 0.01$ determined by one-way ANOVA followed by Bonferroni post hoc test. DHE = dihydroethidium; NAC = N-acetylcysteine; ROS = reactive oxygen species.

4 Discussion

Microglial contribution to the progression of neurodegenerative diseases, such as Alzheimer's disease, is widely undisputed. Genetic risk factors for late-onset Alzheimer's disease were found to be mainly of microglial origin (Hollingworth et al., 2011; Lambert et al., 2013; Naj et al., 2011). Thus, how these microglial risk genes contribute to AD development and progression is a major question of today's AD research. Among others, CD33 is one of these risk genes. It is mainly expressed in cells of myeloid origin including macrophages and microglia. CD33 attracted scientific attention for its abundance on acute myeloid leukemia (AML) cells and was therefore studied intensively. Several phase III clinical trials targeting CD33 with cytotoxic agent-conjugated antibodies in AML had to be discontinued due to lack of improved clinical outcome (Feldman *et al*., 2005; Petersdorf *et al*., 2013; Ravandi, 2011). Despite intense investigation for CD33-targeting antibody-drug conjugates only little is known about the function of CD33 in microglia in general and in particular in AD. Recently, it was shown that CD33 surface expression levels as well as the number of $CD33^{+}$ microglia positively correlate with increased Aβ plaque load (Bradshaw *et al*., 2013; Griciuc *et al*., 2013) suggesting a modulation of CD33 expression or CD33 signaling might be beneficial in AD. To therapeutically intervene in CD33 expression or signaling it is indispensable to find modulators of CD33 signaling and to study the consequences of alterations of CD33 signaling or expression in detail. This project aimed to develop a novel CD33 reporter cell line to identify modulators of CD33 signaling. Further, iPSC-derived microglia were characterized by *in silico* RNA-sequencing analysis and utilized to study the role of CD33 and the AD-protective variant $CD33^{\Delta E2}$ in human microglia.

4.1 IPSdMiG transcriptionally resemble human primary microglia

Previously, many studies use humanized AD mouse models, such as APP/PS1 and 5xFAD, to investigate disease onset, progression, and microglial contribution (Esquerda-Canals *et al*., 2017; Götz *et al*., 2018). However, these animal models exhibit limitations regarding the successful translation of critical findings to humans. Of note, at least 15 of the human AD-related genes do not have a clear ortholog in mice, including CD33 (Mancuso *et al*., 2019). As a result, the scientific community started to focus more closely on human microglia-like cells differentiated from iPSCs.

To date, there are several protocols published describing the generation of microglia/macrophage precursors or microglia/macrophage-like cells (Abud *et al*., 2017; Haenseler *et al*., 2017; Muffat *et al*., 2016). However, they lack a fundamental characteristic of human microglia – their maturation in neuronal tissue. Recently, it was shown that freshly isolated *ex vivo* human microglia, which were placed in *in vitro* culture, rapidly and heavily downregulate gene transcript levels of characteristic microglial receptors (Bennett *et al*., 2018). Many of the current protocols try to surrogate the long maturation in neuronal tissue by either supplementation of cytokines, such as IL-34, or culture of microglial precursors with neuronal cells for up to 14 days. The protocol utilized within this thesis generates microglia together with neuronal and endothelial cells, which enables microglial generation and maturation directly among neuronal cells within the same culture paradigm (Mathews *et al*., *in preparation*; Patent ID EP20162230).

Characterization of these iPSC-derived microglia showed a very high expression of myeloid markers CD14, CD45, FcγRI and SIRPα. Thus, a pure microglia population can be harvested from culture supernatants without noticeable neuronal or endothelial cell contamination as these cells remain attached to the cell culture format. Comparison of iPSC-derived microglial with human primary microglia was performed in other publications, too (Abud *et al*., 2017; Haenseler *et al*., 2017; Muffat *et al*., 2016). However, in many instances the human primary microglia were cultured *in vitro* in a similar or the same medium as the iPSC-derived microglia for several days (Abud *et al*., 2017; Muffat *et al*., 2016). This is known to induce transcriptomic changes, which render the primary cells more similar to the iPSC-derived microglia they should be compared to (Januszyk *et al*., 2015). Thus, the best-available samples are freshly *ex vivo* isolated non-cultured primary microglia. Consequently, RNA sequencing samples from freshly isolated human primary microglia (Galatro *et al*., 2017) were used for *in silico* comparison with iPSdMiG since fresh donor material was not available. As comparison to a different protocol, RNA sequencing data of iMGL (Abud *et al*., 2017) were used. The protocol by Abud and colleagues is a widely used cutting-edge protocol, which claims high transcriptomic similarity to human primary fetal and adult microglia. However, these human primary fetal and adult microglia samples were cultured for a period of nine days *in vitro* (Abud *et al*., 2017), which might completely change their transcriptome. Thus, only iMGL but not human primary fetal and adult microglia samples from Abud and colleagues were included in this analysis.

IPSdMiG clustered in very close proximity to human primary microglia samples in the principal component analysis regardless of in- or exclusion of the cortex samples demonstrating a high similarity between the two samples. Interestingly, the different iPSdMiG lines were separated very well from each other, which might be attributed to donor-specific differences that can be also seen in the spread-out human primary microglia samples. Surprisingly, iMGL samples clustered farther apart from human primary microglia, which might be explained by the characteristic of PCAs to highlight differences. However, when the cortex samples were removed, iMGL moved closer towards the iPSdMiG-human primary microglia cluster but THP1 macrophages and iPSCs remained far off. THP1 cells are a widely used human cancer cell line for investigation of monocyte and macrophage pathways. Treatment of THP1 cells with phorbol 12-myristate 13-acetate (PMA) confers them into a macrophage-like phenotype (Chanput *et al*., 2014; Daigneault *et al*., 2010). However, they show no overlap with human primary microglia in principal component analysis, which might be explained by the different origin. THP1 cells are peripheral blood monocytes, which were obtained from the blood of a boy, who suffered from acute monocytic leukemia (Tsuchiya *et al*., 1980). Thus, these cells originate from the definitive or second wave of hematopoiesis whereas microglia emerged from the primitive hematopoiesis (Ginhoux *et al*., 2010; Kierdorf *et al*., 2013). Previous comparison of iPSC-derived microglia-like cells with blood monocytes using PCA also showed no overlap between the microglial-like cells and monocytes (Abud *et al*., 2017; Haenseler *et al*., 2017).

The identity of a cell can be predicted by the expression of so-called lineage-specific markers – genes or proteins, which are typically expressed in distinct cell types or lineages. Gene transcript levels of the microglial markers defined by Butovsky and colleagues (Butovsky *et al*., 2014) were mostly high in iPSdMiG, iMGL, and human primary microglia and comparable low in iPSC and cortex samples. Using different iPSC-derived microglia protocols, discrepancies in expression of some of these microglial markers between iPSC-derived microglia and blood monocytes was shown before (Abud *et al*., 2017; Haenseler *et al*., 2017). In general, THP1 macrophages displayed a lower expression of microglial genes compared to the human primary microglia. This again highlights differences between the THP1 macrophages and the human primary microglia. *SALL1* showed low transcription levels in most human primary microglia, iPSdMiG, and iMGL samples. However, it appeared to be highly transcribed in iPSCs. High expression of *SALL1* in embryonic stem cells was shown

before and recently *SALL1* was identified to regulate embryonic stem cell differentiation targeting similar transcription site as NANOG (Karantzali *et al*., 2011). In addition, other microglial markers such as *GAS6*, *HEXB*, *MERTK*, *OLFML3* and *TGFBR1* were also detected in iPSCs. For most of these genes, functions in embryonic development or (cancer) stem cell maintenance was already described before (Jin *et al*., 2017; Jung *et al*., 2016; Mullen & Wrana, 2017). Moderate transcription of many microglial genes was found in cortex samples, which might be attributed to the microglial cells present in the cortex. Gene transcripts of typical pluripotency markers were highly present in iPSCs and absent in iPSdMiG, iMGL, human primary microglia, and THP1 macrophages. Merely *PODXL* and *SOX2* were moderately transcribed in cortex samples. *PODXL* is a cell surface glycoprotein present on vascular endothelial cells of blood vessels where it is required for maintaining blood-brain barrier function during acute inflammation (Cait *et al*., 2019). *SOX2* is required for maintaining neural stem cell identity in the central nervous system, which are present in the subventricular and subgranular zone (Zhang & Cui, 2014). As expected, neuronal lineage markers were strongly transcribed in cortex samples due to high neuron content. However, there was also low to moderate transcript levels found in human primary microglia and iPSdMiG while iMGL did not show neuronal lineage marker transcription. There are two reasonable explanations for this phenomenon: On one hand, these transcripts could have been the result of small neuron contamination during isolation or harvesting procedures. On the other hand, they might have been attributed to phagocytosis of apoptotic or dead neuronal cells or debris as both cell types are in steady contact to neuronal cells. Considering the high expression of myeloid markers on iPSdMiG measured by flow cytometry and the fluorescence-activated cell sorting-based isolation of human primary microglia a contamination with neuronal cells might be negligible. Thus, looking at specific microglial marker transcription, human primary microglia, iPSdMiG, and iMGL resembled one another.

Pathway enrichment, also known as pathway overrepresentation analysis, is a powerful tool to group differentially expressed (DE) genes and get easily interpretable biological insights into transcriptome changes. Interestingly, pathway enrichment analysis of DE genes between iPSdMiG and human primary microglia did not result in any overrepresented immunity-related pathways within the most significant pathways. However, the two samples differed in respiration and protein translation-related

pathways. Consequently, iPSdMiG and human primary microglia had a highly similar immunity-related transcriptome profile.

Transcription factors are master regulators of gene transcription. Different cell types have a specific set of key transcription factors, which drive their cellular identity (Heinz *et al*., 2010; Stadhouders *et al*., 2019). In order to identify cellular identity-driving transcription factors of iPSdMiG and human primary microglia, highly upregulated and highly significant DE genes against iPSCs were extracted for each comparison, which represented their individual microglial core signatures (Galatro *et al*., 2017). IPSCs transcriptionally represent the most distinct cell type in the analysis and upregulated DE genes might be important for cellular identity of iPSdMiG and human primary microglia. Hence, they were chosen to be compared against each other. The lists of DE genes were investigated for enriched transcription factors, which can explain these changes in the transcriptome profile. Human primary microglia and iPSdMiG shared 90 % of these enriched transcription factors. Among them were SPI1 and IRF8, two master regulators of microglial identity (Kierdorf *et al*., 2013; Smith *et al*., 2013). In addition, BATF/BATF2 and other IRF family members, such as IRF1, IRF7, and IRF9, were enriched in both microglial core signatures. These transcription factors are important for macrophage and microglia effector function by controlling inflammatory processes (Cohen *et al*., 2014; Masuda *et al*., 2015; Ousman *et al*., 2005; Roy *et al*., 2015; Tanaka *et al*., 2015). The high overlap of enriched transcription factors might shape both cell types into a similar cellular identity.

Apart from the comparison of two cell types via DE genes, identification of correlated or co-expressed genes is a potent tool to find overall similarities (Langfelder & Horvath, 2008). WGCNA identified 11 co-expressed module of which the turquoise, magenta, and pink module seemed of higher interest as they were highly associated with only a single cell type. The turquoise module, correlated with cortex samples, was clearly enriched in neuronal-related pathways. RUNX1, which showed enriched pathways in the magenta module that correlated with THP1 macrophages, is a key driver of definitive hematopoiesis including the generation of monocyte-derived macrophages such as THP1 macrophages (Fujimoto *et al*., 2007; Okuda *et al*., 2001). POU5F1 (OCT4), SOX2, and NANOG signaling pathways, which were enriched in the pink module (correlated with iPSC samples), are known to be essential to maintain pluripotency of iPSCs (Heurtier *et al*., 2019; Takahashi & Yamanaka, 2006). Thus, pathway enrichment analysis identified that these modules consisted of genes

belonging to neuronal (turquoise module), definitive hematopoiesis (magenta module), and pluripotency pathways (pink module). IMGL highly correlated with the red and the yellow module, and weakly correlated with the blue module. Further, the cortex samples correlated moderately with the red module. Pathway enrichment showed the red and the yellow module consisted of translation, respiration, and metabolism-related pathways. The second largest module, the blue module, correlated in addition moderately with iPSdMiG and human primary microglia. This module was enriched in innate immunity-related pathways and thus highlights that a set of immunity-related genes is co-expressed in iPSdMiG, human primary microglia and to a lesser extend also in iMGL. Of note, iPSdMiG and human primary microglia showed the strongest correlation with the blue module. It is known that heterogeneous data, which might be the result of many different donor/lines, affects unsupervised statistical analysis such as used in WGCNA (Langfelder & Horvath, 2008). This might explain overall lower correlation coefficients in iPSdMiG and human primary microglia as the data of these two groups is more heterogenous than the data of other groups, which can be also seen in the PCA plot. Further, iPSdMiG and human primary microglia but not iMGL were weakly to moderately associated with the brown and the purple modules. These modules were enriched with genes belonging to RNA metabolism and translation. Thus, iPSdMiG and human primary microglia showed a high number of co-expressed genes identified by WGCNA.

Taken together, the generation of iPSdMiG from iPSCs within a neural environment gave rise to microglial cells closely resembling the transcriptome of non-cultured *ex vivo* human primary microglia. They shared a broad variety of transcription factors driving their cellular identity and showed similar transcript levels of key microglial genes. In a direct comparison to human THP1 macrophages and iMGL, human primary microglia had more co-expressed genes and gene modules in common with iPSdMiG than with any of the other tested samples. Hence, iPSdMiG are the preferable model system if investigating human microglia.

4.2 CD33 reporter cell line identifies agonistic CD33 antibodies

Receptor signaling can be studied in endogenous-expressing cells or in so-called reporter cell lines. The latter are usually common *in vitro* cell lines, such as HEK-293, CHO, or 3T3 cells, genetically engineered to overexpress the receptor of interest.

Reporter cell lines are easy to maintain, cost-effective, and provide an unlimited number of cells for studies. Another major advantage is that results are more reproducible (Gervaix *et al*., 1997; Richards *et al*., 1999; G. Q. Wang *et al*., 2006). The quality of cells is always similar, unlike primary cell material, which might be obtained from different donors (Pastor *et al*., 2010). Furthermore, reporter genes can be introduced such as calcium-sensitive GFP variants, which allow direct measurement of receptor signaling in living cells without the need of extensive and stressful live cell staining. Hence, a human chimeric CD33-DAP12 reporter cell line was generated in a Flp-In-293 background and analyzed for CD33 activation by a panel of CD33-specific antibodies.

CD33 signals via its ITIM domain, which becomes phosphorylated and subsequently recruits and activates phosphatases, including SHP1 or SHP2 (Linnartz & Neumann, 2013; McVicar *et al*., 1998; Peng *et al*., 2010; Wu *et al*., 2000). However, a reliable quantification of ITIM phosphorylation or phosphatase activity is difficult because it is a very transient and autoregulatory event, i.e., the activated phosphatases also dephosphorylate the ITIM domain (Taylor *et al*., 1999; Walter *et al*., 2008). In addition, reliable assay or readout systems, which can be also used for high-throughput screening of ITIM activation are missing so far. On the other hand, the complementary ITAM signaling results in SYK-PLCγ2-mediated transiently increased intracellular calcium levels, which is a broadly-used and reliable readout method to study cellular activation of reporter cell systems (Chambers *et al*., 2003). TYROBP/DAP12 is an ITAM-containing adapter molecule, which endogenously pairs with ITAM-associated receptors, such as TREM2 or FcγRI, and initiates signaling upon receptor activation (Kobayashi *et al*., 2016; Linnartz & Neumann, 2013). Consequently, the extracellular domain of full-length CD33M or exon 2-deleted variant CD33$^{\Delta E2}$ were fused to the transmembrane and intracellular domain of DAP12, thereby redirecting the inhibitory CD33 signaling towards activatory ITAM signaling. This approach was already successfully used to redirect NK cells towards tumor cells via an DAP12-containing chimeric antigen receptor (CAR) (Töpfer *et al*., 2015). In addition, the *CMV* promoter of the expression plasmid pcDNA5/FRT was successfully replaced by the human *EEF1A1* promoter to avoid epigenetic silencing of the viral *CMV* promoter, which would eventually result in loss of transcription of the gene of interest downstream of the silenced promoter (Meilinger *et al*., 2009; Teschendorf *et al*., 2002). In a last step,

the calcium-sensitive GFP variant, *GCaMP6m*, was introduced into the expression plasmid separated from the CD33-DAP12 fusion protein via an *IRES* motif, which results in a bicistronic expression cassette. The *IRES* motif enables independent translation of both proteins, CD33-DAP12 and GCaMP6m as it works as a ribosomal binding site to initiate translation (Bochkov & Palmenberg, 2006). Independent translation of CD33-DAP12 and GCaMP6m via an *IRES* motif was preferred over a 2A approach, which is a self-cleaving peptide sequence resulting in generation of two peptides during translation. 2A peptides have the disadvantage that incomplete cleavages might occur, which then results in fusion proteins. In addition, they alter the peptide sequence of both the upstream and the downstream protein (Kim *et al*., 2011). However, independent translation of CD33-DAP12 and GCaMP6m via an *IRES* motif might result in much lower translation efficiency of the gene following the *IRES* motif, here, GCaMP6m (Mizuguchi *et al*., 2000).

Stable transfected CD33-DAP12-GCaMP6m cell lines were investigated for CD33 surface expression by flow cytometry. Both, CD33M-DAP12 and $CD33^{\Delta E2}$-DAP12-expressing cell lines were highly positive for CD33 surface expression. However, CD33 antibody clones WM53 and P67.6 failed to detect $CD33^{\Delta E2}$ on $CD33^{\Delta E2}$-DAP12-expressing cells. Both, WM53 and P67.6 bind an epitope in the V-set immunoglobulin-like domain (Pérez-Oliva *et al*., 2011). Due to splicing of exon 2 the V-set immunoglobulin-like domain containing the sialic acid-binding domain is not present in $CD33^{\Delta E2}$. Thus, CD33 antibody clones WM53 and P67.6 were able to discriminate between CD33M-DAP12 and $CD33^{\Delta E2}$-DAP12-expressing cell lines by binding only to CD33M but not $CD33^{\Delta E2}$. Interestingly, $CD33^{\Delta E2}$ was found to be expressed on the cell surface of $CD33^{\Delta E2}$-DAP12 reporter cells. Recent findings showed that $CD33^{\Delta E2}$ is not transported to the plasma membrane but rather found in peroxisomes of blood neutrophils and monocytes (Siddiqui *et al*., 2017). However, a recent study comparing human and murine CD33 highlighted that the surface expression of murine CD33 is dependent on interaction with DAP12. Deletion of DAP12 in murine RAW264.7 cells resulted in loss of murine CD33 surface expression (Bhattacherjee *et al*., 2019). Consequently, fusing $CD33^{\Delta E2}$ to DAP12 might also stabilize the surface expression of the $CD33^{\Delta E2}$-DAP12 chimeric protein.

In addition to CD33 surface expression, a low GCaMP6m fluorescence intensity was observed in CD33-DAP12-GCaMP6m cell lines compared to the parental Flp-In-293 wild type cell line. GCaMP6m has a low baseline fluorescence and starts to fluoresce

brightly when binding calcium ions due to a conformational change (Chen *et al.*, 2013). Further, GCaMP6m might be much lower expressed than the CD33-DAP12 construct, which is known for the second open reading frame (ORF) of bicistronic IRES-spaced vectors (Mizuguchi *et al*., 2000). The low baseline fluorescence paired with lower protein expression might result in only a low percentage of positive cells.

Activation of the CD33-DAP12 reporter cell lines should result in a SYK-PI3K-PLCγ2-mediated increase of intracellular calcium levels (Linnartz & Neumann, 2013; McVicar *et al*., 1998; Peng *et al*., 2010; Wu *et al*., 2000). Both, CD33-DAP12-expressing cell lines showed a CD33-independent increase in intracellular calcium levels when adding dATP to the cells. Extracellular dATP binds to proteins belonging to the P2X and P2Y receptor family, which trigger a downstream response finally leading to the release of calcium ions from cellular compartments into the cytoplasm (Pubill *et al*., 2001; Weisman *et al*., 2012). A very low yet notable increase in the *ΔF/F(t)* signal over the baseline was observed for the negative controls IgG1 and IgG1 F(ab')2, which could be accounted to a technical artifact induced by automated compound addition. However, this small change in *ΔF/F(t)* was clearly distinguishable from the pronounced response to the strong stimulus of dATP. Further, CD33M-DAP12-expressing cells showed a selective increase in intracellular calcium levels upon addition of CD33-specific antibody clone P67.6 and a tendency for increased intracellular calcium levels for CD33-specific antibody clone 1c7/1. Interestingly, the *ΔF/F(t)* increase was only 30 - 50 % of the strength of the positive control dATP. This finding might indicate a not yet saturated reporter system at an antibody concentration of 10 µg/ml. CD33-specific antibodies WM53 and P67.6 F(ab) did not induce an increase in intracellular calcium levels compared to IgG1 controls, and $CD33^{\Delta E2}$-DAP12 cells were not activated by any of the tested CD33-specific antibody clones. These results were validated in human iPSdMiG where only the CD33-specific antibody clones 1c7/1 and P67.6 were able to antagonize TREM2-induced phosphorylation of SYK. Here, the effect of the two antibody clones was also restricted to the CD33M-expressing WT iPSdMiG. This proves a direct interaction between ITIM signaling of CD33 and ITAM signaling of TREM2, which was already hypothesized due to CD33 interaction with protein tyrosine phosphatases but not shown (Paul *et al*., 2000; Taylor *et al*., 1999). Absence of CD33M expression in $CD33^{-/-}$ or $CD33^{\Delta E2}$ iPSdMiG supports a CD33-specific effect of the CD33 agonistic antibody clones 1c7/1 as well as P67.6 and excludes a potential effect of Fc-binding receptors.

The CD33-specific antibody P67.6 binds an epitope in the variable domain of CD33, which contains the sialic acid-binding domain (Pérez-Oliva *et al*., 2011). The agonistic effect of P67.6 suggests either a direct activation of CD33 through stimulation of the sialic acid-binding domain or an activation via crosslinking of two or more receptors. The latter effect is known from several other proteins including TREM2 (Humphrey *et al*., 2006; Lindstrom & Einarson, 1979; Takahashi *et al*., 2005). In contrast, CD33 antibody clone 1c7/1 binds an epitope in the constant C2-region of CD33 distant from the sialic acid-binding domain, which supports the receptor crosslinking hypothesis. In line with this hypothesis, the monovalent P67.6 F(ab) did not activate CD33. Antibody-mediated receptor crosslinking depends on multimerization of the receptors and is achieved via binding of the two F(ab) fragments of a single antibody to two receptors. Thereby, several receptors are brought in close proximity, which initiates receptor signaling via intracellular domains or adaptor proteins. Papain-mediated cleavage of the antibody results – in contrast to pepsin-mediated cleavage – in two monovalent F(ab) and one Fc fragment per antibody (Coulter & Harris, 1983; Mariant *et al*., 1991). Thus, F(ab) antibodies can only bind but not crosslink receptors as they are not able to bring receptors in close proximity to each other and to stabilize interactions of the intracellular domains (Kaye & Janeway, 1984). However, CD33-specific antibody clone WM53, a full-length antibody with a similar epitope as P67.6 (Pérez-Oliva *et al*., 2011), was not capable of activating CD33. This questions the crosslinking hypothesis as WM53 should in theory be able to crosslink CD33. However, it is possible that WM53 stabilizes CD33-DAP12 cell surface expression and interferes with receptor endocytosis, which might be important for DAP12 signaling and is already known for ITIM signaling of CD33 (Walter *et al*., 2008). On the other hand, CD33$^{\Delta E2}$-DAP12 reporter cells were not activated by CD33-specific antibody 1c7/1, although 1c7/1 is able to bind to CD33$^{\Delta E2}$. Hence, the sialic acid-binding domain also might play a crucial role in CD33 activation. As CD33-specific antibody WM53 binds an epitope in the variable domain, which contains the sialic acid-binding domain, it might block a conformational change within the region of the sialic acid-binding domain, which might be required to initiate CD33 signaling.

Taken together, the CD33 reporter cell line identified two CD33-specific antibodies, which were able to activate CD33M in the CD33 reporter cell line and in iPSdMiG. Thus, the developed CD33 reporter cell line is a well-functioning tool to study CD33 activation, whose results could also be translated to native CD33M-expressing cells

such as iPSC-derived microglia. Furthermore, CD33 activation might be dependent on receptor crosslinking and the expression of the sialic acid-binding domain, which need to be followed further up in details.

4.3 Loss of CD33 signaling results in inflammation

Genome-wide association studies identified CD33 as one of several genetic risk factors to develop late-onset AD (Hollingworth *et al*., 2011; Lambert *et al*., 2013; Naj *et al*., 2011). Recent studies reported that the more common allele for CD33 in the Caucasian population for the SNP rs3865444(C/C) showed increased CD33 surface expression and an increased number of $CD33^{+}$ microglia in human brains. In addition, the C/C allele for rs3865444 positively correlated with the Aβ plaque load in the brains of AD patients (Bradshaw *et al*., 2013; Griciuc *et al*., 2013). In contrast, the less common allele for CD33 in the Caucasian population for the SNP rs3865444(A/A) was found to reduce the risk for developing AD with an overall odds ratio of 0.89 (Hollingworth *et al*., 2011; Lambert *et al*., 2013; Naj *et al*., 2011). Further, the A/A allele for rs3865444 is co-inherited with a polymorphism in rs12459419 (T/T allele), which mediates splicing of exon 2 of CD33 ($CD33^{\Delta E2}$) (Malik *et al*., 2013). Recent studies showed that the T/T allele for rs12459419 – resulting in expression of $CD33^{\Delta E2}$ – is associated with decreased CD33 surface expression. $CD33^{\Delta E2}$ is not transported to the plasma membrane but rather found intracellularly in peroxisomes of human primary monocytes and neutrophils with rs3865444(A/A) and rs12459419(T/T) alleles (Malik *et al*., 2013; Siddiqui *et al*., 2017). Moreover, exon 2 of CD33 encodes for a major part of the sialic acid-binding domain. Thus, exon-2 deleted CD33 ($CD33^{\Delta E2}$) lacks a functional sialic acid-binding domain. Expression of $CD33^{\Delta E2}$ in human blood neutrophils and monocytes was hypothesized to result in increased phagocytic capacity similar to a complete knockout of *CD33* (Malik *et al*., 2013; Siddiqui *et al*., 2017). Therefore, it is speculated that $CD33^{\Delta E2}$ is not capable of classical sialic acid-driven CD33 ITIM signaling but rather is comparable to $CD33^{-/-}$ cells, i.e., a gene knockout.

In line with recent findings, $CD33^{\Delta E2}$-expressing iPSdMiG showed diminished CD33 surface expression comparable to $CD33^{-/-}$ iPSdMiG but clearly increased mRNA transcripts of $CD33^{\Delta E2}$ and no gene transcription of CD33M (Malik *et al*., 2013; Siddiqui *et al*., 2017). Remarkably, WT iPSdMiG exhibited a slight increase in $CD33^{\Delta E2}$ mRNA

levels compared to CD33$^{-/-}$, which might indicate a low percentage of exon 2 splicing is occurring in WT iPSdMiG. *INPP5D/SHIP1* and *TYROBP/DAP12* mRNA levels were increased in CD33$^{-/-}$ and with a very small magnitude in CD33$^{\Delta E2}$ iPSdMiG, too. However, the biological relevance of this small increase in CD33$^{\Delta E2}$ iPSdMiG remains questionable. Variants of both, the inositol phosphatase INPP5D/SHIP1 and the ITAM-containing TYROBP are associated with an increased risk to develop AD (Lambert *et al*., 2013) but they have opposing signaling functions. SHIP1 is associated with ITIM signaling. Following activation, SHIP1 dephosphorylates downstream targets, such as PIP_3, and thereby acts as a negative regulator of proliferation and survival (An *et al*., 2005; Damen *et al*., 1996; Isnardi *et al*., 2006; Manno *et al*., 2016). But SHIP1 is also known to bind ITAMs of FcεRI and CD3 to exerts its regulatory effects (Osborne *et al*., 1996). Of most interest for AD research might be that SHIP1 was shown to dephosphorylate the ITAM of TYROBP (Peng *et al*., 2010). Thus, an increased *INPP5D/SHIP1* gene transcription could be a compensatory mechanism to cope with loss of CD33. On the other hand, increased *TYROBP* mRNA levels point to the opposite direction. The ITAM-bearing adaptor molecule TYROBP is associated with pro-inflammatory and pro-survival signaling initiated by, e.g., TREM2, CR3, or FcγRI (McVicar *et al*., 1998; Parsa *et al*., 2008; Peng *et al*., 2010; Wu *et al*., 2000).

Furthermore, transcription and expression levels of microglial receptors CD14 and FcγRI and mRNA levels of *TREM2* were upregulated in CD33$^{-/-}$ iPSdMiG. These receptors are known to exert pro-inflammatory signaling either in a TLR/MyD88-dependent (CD14) or ITAM-dependent (FcγRI and TREM2) way (Jiang *et al*., 2005; Linnartz & Neumann, 2013). This increase in gene transcription and protein expression was only observed for *CD14* mRNA levels in CD33$^{\Delta E2}$ iPSdMiG. In addition, CD45 and SIRPα levels were increased in CD33$^{-/-}$ but not CD33$^{\Delta E2}$ iPSdMiG. Both, CD45 and SIRPα are able to counteract microglial activation. Crosslinking of CD45, a protein tyrosine phosphatase family member, was shown to decrease p44/42 MAPK-dependent TNFα and NO secretion following Aβ treatment of murine primary microglia (Tan *et al*., 2000). SIRPα is an ITIM-containing microglial receptor and recognizes CD47, an anti-phagocytic signal (Oldenborg *et al*., 2000; Olsson *et al*., 2007). Depletion of SIRPα by RNA interference in murine peritoneal macrophages promoted phagocytosis of red blood cells (Okazawa *et al*., 2005). Thus, upregulation of genes and proteins belonging to the pro-inflammatory pathway, such as TYROBP,

CD14, and FcγRI, is opposed to upregulation of genes and proteins belonging to the anti-inflammatory pathway, such as INPP5D/SHIP1, CD45, and SIRPα in $CD33^{-/-}$ iPSdMiG. Therefore, a genetic compensation response to loss of CD33 is inconclusive in $CD33^{-/-}$ iPSdMiG but not observed in $CD33^{\Delta E2}$ iPSdMiG. Of note, all iPSdMiG were highly positive for the measured microglial markers indicating a pure harvested microglia population.

Increased transcription and expression of ITIM and ITAM-associated molecules might alter downstream signaling events. Human CD33 signals via its intracellular ITIM and ITIM-like domains to modulate activatory ITAM signaling, like many other SIGLECs (Paul *et al*., 2000; Taylor *et al*., 1999). The ITIM-ITAM signaling axis is tightly regulated. Activation of ITIM signaling by, e.g., *trans*-binding of SIGLECs to sialic acids of another host cell counteracts activatory ITAM signaling to prevent collateral damage to host cells (Claude *et al*., 2013; Linnartz & Neumann, 2013). However, it is still a matter of debate whether such short receptors as CD33 – with only two extracellular immunoglobulin domains – frequently bind *trans*-targets on other cells (L. Zhao, 2019). In addition, healthy microglia perform contact inhibition (Askew *et al*., 2017; Nimmerjahn *et al*., 2005), which further limits *trans* interaction within these monoculture assays. CD33 can bind in *cis* to sialylated proteins or lipids on the same cells, as well, which increases the activation threshold of the cell (Doody *et al*., 1995). Loss of CD33 surface expression led to a mild imbalance in this system with slightly increased phosphorylation of SYK in $CD33^{-/-}$ and $CD33^{\Delta E2}$ iPSdMiG. However, stimulation of the ITAM signaling pathway by crosslinking antibodies for TREM2 and FcγRI increased this imbalance in $CD33^{-/-}$ but not $CD33^{\Delta E2}$ iPSdMiG with a more pronounced elevation of phosphorylated SYK compared to WT iPSdMiG. SYK phosphorylation tended to be increased in $CD33^{\Delta E2}$ iPSdMiG following ITAM pathway activation as well but with a similar ratio than in the untreated condition. In $CD33^{-/-}$ iPSdMiG, however, TREM2 and FcγRI stimulation resulted in an exacerbated activation of the ITAM signaling pathway compared to stimulated WT and $CD33^{\Delta E2}$ iPSdMiG. This could be either due to increased receptor expression or due to missing counterregulatory signaling such as CD33 activation by *cis*-interaction. The higher protein expression of FcγRI measured by flow cytometry and the higher gene transcript levels of *FCGR1A* and *TREM2*, which might also result in higher protein levels, could cause the higher SYK phosphorylation as more protein can be activated by the antibody. In addition, TREM2 stimulation seemed to induce higher SYK

phosphorylation levels in all iPSdMiG lines compared to FcγRI stimulation. Yet, FcγRI-treated samples were stored at -80 °C while TREM2-treated samples were processed immediately. This technical difference clearly influenced the pSYK/tSYK ratio as it showed an overall strong reduction. Thus, the difference seen between the two stimulations is most likely a technical artifact.

SYK signaling is able to induce the release of inflammatory cytokines (Dennehy *et al*., 2008; Parsa *et al*., 2008). In addition, antibody-mediated blocking of CD33 signaling or *CD33*-targeting siRNA treatment were shown to increase the production of TNFα, IL-1β, and CXCL8 in human monocytes (Lajaunias *et al*., 2005). Likewise, knockout of *CD33* but also expression of $CD33^{\Delta E2}$ in iPSdMiG resulted in increased mRNA levels of *TNF*, *IL1B*, *IL6*, *CXCL8*, and *IL10* suggesting an increased cellular activation of $CD33^{-/-}$ and $CD33^{\Delta E2}$-expressing iPSdMiG. Interestingly, the increase of *IL6* and *IL10* gene transcripts was much higher in $CD33^{-/-}$ compared to $CD33^{\Delta E2}$ iPSdMiG indicating a stronger cellular activation of $CD33^{-/-}$ iPSdMiG. Elevation of *TNF* and *IL1B* gene transcripts hint towards a pro-inflammatory cellular activation after knockout of *CD33* but also expression of $CD33^{\Delta E2}$ in iPSdMiG. Further, triggers, such as TNFα and IL-1β, are known to increase CXCL8 production in microglia (Ehrlich *et al*., 1998). Consequently, *CXCL8* upregulation is in line with elevation of *TNF* and *IL1B*. In addition, increased CXCL8 levels were found in AD brain tissue lysates, where it might contribute to inhibition of Aβ-induced neuronal apoptosis and increase neuronal BDNF production (Ashutosh *et al*., 2011). Thus, upregulation of CXCL8 might be beneficial in AD. IL-6 is known to be involved in auto-immune and inflammatory processes in many diseases (Kristiansen & Mandrup-Poulsen, 2005; Nishimoto, 2006; Swardfager *et al*., 2010). Upregulation of *IL6* supports the hypothesis of a pro-inflammatory microglial phenotype upon deletion of *CD33* or expression of $CD33^{\Delta E2}$ in iPSdMiG. On the other hand, IL-10 maintains homeostasis by antagonizing the NF-κB pathway, which results in downregulation of, e.g., TLR-triggered pro-inflammatory cytokine release (de Waal Malefyt *et al*., 1991; Rennick *et al*., 1992). IL-10, secreted by macrophages and microglia, mainly results in autocrine signaling to regulate the immune response upon pathogen encountering (Giambartolomei *et al*., 2002). Thus, increased *IL10* mRNA levels might point towards an attempt to antagonize the pro-inflammatory cellular activation and could be the reason for lower levels of *TNF* and *IL1B*. Nevertheless, the cytokine and chemokine upregulation must be interpreted

cautiously as they only show mRNA levels, which might not necessarily translate into protein levels as well as protein secretion levels.

The ITIM-ITAM signaling axis is known to regulate microglial key competences, such as phagocytosis or radical production (Kawabori *et al*., 2015; Shahraz *et al*., 2015; Y. Wang & Neumann, 2010). An increase in SYK phosphorylation and cytokine mRNA levels could indicate increased cellular activation in $CD33^{-/-}$ and to lesser extend in $CD33^{\Delta E2}$ iPSdMiG. However, in a disease context, this activation can be either beneficial or detrimental. Increased CD33 surface expression was previously correlated with increased Aβ burden and decreased phagocytic uptake (Bradshaw *et al*., 2013; Griciuc *et al*., 2013), while expression of $CD33^{\Delta E2}$ in human myeloid cells is hypothesized to increase phagocytic capacity (Siddiqui *et al*., 2017). In line with these recent findings, both, $CD33^{-/-}$ and $CD33^{\Delta E2}$ iPSdMiG exhibited increased phagocytosis of pHrodo-labeled *S. aureus* BioParticles as well as aggregated $A\beta_{1-42}$ compared to WT iPSdMiG – a potential sign of beneficial microglial activation. Thus, targeting CD33 signaling or expression could be an option to increase Aβ uptake in AD. The production of ROS, which comes along with the phagocytic uptake of, e.g., bacteria, as phagocytosis-associated oxidative burst is an important competence of microglia and a hallmark of a potent pro-inflammatory immune response. However, the oxidative burst is undirect – i.e., it does not discriminate between self and non-self cells. To protect neighboring host cells, such as neurons or other glia cells, from collateral damage, ROS production is a tightly controlled mechanism. TYROBP signaling is known to activate the nicotinamide adenine dinucleotide phosphate (NADPH) oxidase (NOX) 2 to produce ROS (Graham *et al*., 2007). TYROBP gene transcripts and SYK phosphorylation levels were elevated in $CD33^{-/-}$ iPSdMiG, which could be an indication for increased TYROBP signaling. However, $CD33^{-/-}$ iPSdMiG did not exhibit constitutive increased ROS production compared to WT and $CD33^{\Delta E2}$ iPSdMiG. Stimulation with *S. aureus* BioParticles increased ROS production in all genotypes with a higher magnitude in $CD33^{-/-}$ iPSdMiG. Thus, knockout of *CD33* but not expression of $CD33^{\Delta E2}$ in iPSdMiG resulted in increased phagocytosis-associated oxidative burst. In line, murine Siglec-E and human SIGLEC11 – both ITIM-containing receptors – were shown to inhibit the phagocytosis-associated oxidative burst (Claude *et al*., 2013; Shahraz *et al*., 2015; Y. Wang & Neumann, 2010). Interestingly, $CD33^{\Delta E2}$ iPSdMiG showed a slightly lower, yet insignificant, oxidative burst following *S. aureus* BioParticles treatment than WT iPSdMiG. However, the oxidative burst was

significantly lower in CD33$^{\Delta E2}$ than in CD33$^{-/-}$ iPSdMiG suggesting a modulation of ROS production by CD33$^{\Delta E2}$ similar to full-length CD33 but independent of plasma membrane signaling. The decreased oxidative burst in CD33$^{\Delta E2}$ iPSdMiG and the peroxisomal location of CD33$^{\Delta E2}$ might infer a role in peroxisomal proliferation and ROS metabolism.

ROS production was determined by DHE fluorescence intensity. In principle, DHE can discriminate between superoxide and other oxidative agents. Superoxide oxidizes DHE to 2-hydroxyethidium whereas DHE is oxidized by other agents to form ethidium with only slightly different spectra. Discrimination of these two species using fluorescence microscopy or flow cytometry and defined filter sets is often impossible (Fernandes *et al*., 2007; Q. Wang & Zou, 2017). Therefore, the type of ROS measured in iPSdMiG using DHE remained inconclusive.

In summary, deletion of *CD33* results in inflammatory activation of human iPSC-derived microglia characterized by increased ITAM pathway activation, cytokine transcription, phagocytosis, and phagocytosis-associated oxidative burst. In contrast, expression of CD33$^{\Delta E2}$ in iPSdMiG only represents a partial loss of CD33 signaling with less pronounced increase in cytokine transcription, increased ITAM pathway activation, and phagocytosis but not phagocytosis-associated oxidative burst.

4.4 Implications for Alzheimer's disease

The detrimental processes underlying the development of Alzheimer's disease are likely to start decades before the diagnosis (Rajan *et al*., 2015). It is hypothesized that in this presymptomatic stage microglia fail to clear off accumulating Aβ in a phase of microglial dysregulation where microglia are activated but unable to properly phagocytose Aβ (Heneka *et al*., 2015). Once Aβ plaques and NFTs have formed and neurons have started to die, microglia become even more activated exacerbating neurodegeneration. Microglia-mediated inflammation is a double-edged sword: It is necessary to maintain homeostasis and clear Aβ deposits, cellular debris as well as apoptotic cells. Yet, it can also lead to the release of ROS, which causes collateral damage to neurons and increases tau pathology (Lovell *et al*., 2004; Su *et al*., 2010). To cure AD, two fundamental prerequisites are needed: an effective treatment and a reliable biomarker to detect disease onset before irreversible damage is done. In particular, the long time span between disease onset and diagnosis makes it difficult

to find reliable biomarkers (Humpel, 2011; Rajan *et al*., 2015). Current studies describe a combination of amyloid positron emission tomography (PET) imaging and cerebrospinal fluid (CSF) levels of Aβ (Aβ42 or Aβ42/Aβ40) as well as TAU (phosphorylated and total TAU) as most effective for disease prediction. Thereby, in earlier stages of the disease Aβ levels in the CSF drop indicating sequestration due to plaque formation in the brain. However, these biomarker assays still lack high precision and stability (Forlenza *et al*., 2015; Jack *et al*., 2018; Palmqvist *et al*., 2016; Strozyk *et al*., 2003; Tapiola *et al*., 2009). Further, as Aβ plaque formation in the brain is the direct cause of decreased CSF Aβ levels it is a matter of debate whether this biomarker can predict the disease sufficiently early to successful intervene. Thus, there is a need for new biomarkers. Recently, molecules monitoring glial activation such as soluble TREM2 or YKL-40 drew attention as potential biomarkers in the CSF, yet, with inconclusive ability to predict the development of cognitive impairment (Craig-Schapiro *et al*., 2010; Heslegrave *et al*., 2016; Knapskog *et al*., 2020). However, even if a reliable and consistent biomarker for early presymptomatic diagnosis existed, there is no effective treatment to cure AD so far.

To date, pharmaceutical companies test antibodies in clinical trials targeting Aβ aggregates and plaques to increase their uptake by microglia (summarized in Mullard, 2019). Yet, most of them fail because they lack efficacy, which can have several reasons. The bioavailability of peripheral-administered antibodies in the brain is very low due to their restricted ability to pass the blood-brain barrier (St-Amour *et al*., 2013). In addition, the antibody might not effectively enhance the microglial dysregulated phagocytic capacities, or the disease progress is irreversible. Furthermore, the Fc receptor-mediated uptake of the Aβ plaque-antibody complexes can also have adverse effects as ITAM-mediated Fc-binding receptor signaling produces radicals, such as ROS, which can lead to damage and death of neighboring cells, including neurons (Lovell *et al*., 2004; Su *et al*., 2010; Ulvestad *et al*., 1994). Thus, new strategies to target AD are currently investigated. The most relevant strategies – except for directly targeting Aβ or TAU – are targeting microglia. GWAS identified many microglial protein variants to impact AD development including CD33 (Hollingworth *et al*., 2011; Lambert *et al*., 2009; Naj *et al*., 2011).

Expression of full-length CD33 but not exon 2-deleted $CD33^{\Delta E2}$ might promote a dysregulated microglia phenotype by dampening cellular activation and impairing microglial phagocytosis (Bradshaw *et al*., 2013; Griciuc *et al*., 2013). Two major

differences between expression of full-length CD33 and CD33$^{\Delta E2}$ need to be considered: the loss of the sialic acid-binding domain, and the change of location of CD33$^{\Delta E2}$, which is found in peroxisomes (Hernández-Caselles *et al*., 2006; Siddiqui *et al*., 2017). Upon ligand binding CD33 undergoes endocytosis. This process is concomitant with CD33 signaling as it was shown that ITIM tyrosine phosphorylation favors receptor endocytosis (Walter *et al*., 2008). Thus, endocytosis of CD33 might be a prerequisite for classical CD33-mediated ITIM signaling. CD33$^{\Delta E2}$ lacks the sialic acid binding domain and is scarcely present on the cell surface. Hence, receptor endocytosis and classical CD33-mediated ITIM signaling might not be possible in CD33$^{\Delta E2}$-expressing microglia resulting in increased cellular activation. However, cellular activation of CD33$^{\Delta E2}$-expressing iPSdMiG was slightly dampened compared to a full *CD33* knockout. Further, CD33$^{\Delta E2}$-expressing iPSdMiG did not exhibit increased phagocytosis-associated oxidative burst compared to CD33$^{-/-}$ iPSdMiG suggesting a, to date, unknown mode of action of CD33$^{\Delta E2}$. Recent studies found that CD33-related SIGLECs 5 and 14 can be efficiently activated by the lipids cardiolipin and 5-palmitic acid-hydroxy stearic acid. Thereby, the lipid recognition site is independent from the sialic acid-binding domain (Suematsu *et al*., 2019). A possible activation of CD33$^{\Delta E2}$ through lipids could explain the dampened activatory phenotype of CD33$^{\Delta E2}$-expressing iPSdMiG without increased oxidative burst compared to CD33$^{-/-}$ iPSdMiG. These differences in microglial activation could be the key to the protective role of CD33$^{\Delta E2}$ in AD.

Microglial activation is, in principle, a necessity to clear Aβ plaques. On the other hand, chronic microglial activation results in chronic neuroinflammation and exacerbation of AD (Edison *et al*., 2008; Heneka *et al*., 2015). Evidence of missing activation of diffuse Aβ plaque-associated microglia in early stages of AD indicate an aberrant microglial phenotype (Sasaki *et al*., 1997). Moreover, polymorphisms of CD33 and TREM2 result in decreased Aβ uptake, which could be a consequence of decreased microglial activation (Bradshaw *et al*., 2013; Griciuc *et al*., 2013; Yeh *et al*., 2016). Some studies claim that dystrophic or senescent rather than reactive microglia are associated with AD pathology (D. M. Angelova & Brown, 2019; Caldeira *et al*., 2017; Wolfgang J. Streit *et al*., 2009). Thus, microglial activation, which was observed in both, CD33$^{-/-}$ and CD33$^{\Delta E2}$-expressing iPSdMiG, might be beneficial to clear forming Aβ plaques in the early presymptomatic stages of AD. In addition to the increased phagocytic capacity observed in CD33$^{-/-}$ and CD33$^{\Delta E2}$-expressing iPSdMiG, increased levels of

phosphorylated SYK could indicate a pro-survival and proliferative microglial phenotype (Linnartz & Neumann, 2013; Mocsai *et al*., 2006; Wakselman *et al*., 2008). This possibly counteracts a senescent or dystrophic microglial phenotype and prevents early plaque formation and thus disease onset. Furthermore, Aβ plaques often contain sialic acid residues (Salminen & Kaarniranta, 2009; Szumanska *et al*., 1987), which might directly dampen their phagocytic uptake orchestrated by full-length CD33-sialic acid interactions. Thus, therapeutic intervention in CD33 signaling might be beneficial in AD.

Yet, an intervention, which equals a knockout of *CD33* might not be preferable as complete ablation of *CD33* also increased the potentially neurotoxic phagocytosis-associated oxidative burst. On the other hand, ROS can desialylate glycans (Eguchi *et al*., 2005). Therefore, an increased oxidative burst – as observed in $CD33^{-/-}$ iPSdMiG – could lead to desialylation of engaged Aβ plaques. Desialylated targets are not able to dampen the microglial response by interaction with SIGLECs, which would eventually result in increased phagocytic uptake of desialylated Aβ plaques. However, the mode of action of ROS is undirected, i.e., it acts on Aβ plaques and neighboring neurons equally, which can lead to neuronal loss. To what extend the increased oxidative burst in $CD33^{-/-}$ iPSdMiG results in collateral damage of neighboring neurons remains to be investigated. Certainly, a partial loss of CD33 signaling – as seen in iPSdMiG expressing AD-protective $CD33^{\Delta E2}$ – which promotes microglial activation and phagocytosis without increasing the associated oxidative burst, might be less neurotoxic, and thus, beneficial in AD.

To achieve a partial loss of CD33 signaling, a blocking antibody for full-length CD33 or a small molecule blocking CD33 signaling could be promising treatment options. A small molecule antagonist might be preferable as the bioavailability of peripheral-administered antibodies in the brain is very low (St-Amour *et al*., 2013). With a similar hypothesis, TREM2 – with opposite signaling function – was targeted in recent studies. Here, a TREM2-specific antibody was used to stabilize TREM2 on the cell surface and protect it from cleavage, thereby increasing TREM2-induced ITAM signaling (Schlepckow *et al*., 2020). However, high antibody doses (up to 100 mg/kg bodyweight) were administered intravenously in mice to reach concentration in the range of the EC_{50} in the brain. The high concentration administered questions this strategy and might be the major disadvantage of targeting microglial receptors, such as TREM2 or CD33, via peripheral-administered antibodies. It remains to be

investigated how these high antibody concentrations – used by, e.g., Schlepckow *et al*., 2020 – affect peripheral immune cells expressing the target protein or by binding to Fc-binding receptors, and whether this strategy leads to collateral damage of cells including neurons due to enhanced cellular activation and release of ROS. To minimize the risk of adverse off-target effects, a small molecule modulating CD33 signaling, which might be even able to cross the blood-brain barrier, would be preferable over a CD33 blocking antibody.

Another possibility to modulate CD33 signaling to result in beneficial microglial activation is to modulate expression of $CD33^{\Delta E2}$ in microglia by either depletion of full-length CD33 or increasing splicing efficiency of exon 2 in CD33. A recent report showed that the splicing regulators serine and arginine rich splicing factor (SRSF) 1 and polypyrimidine tract binding protein (PTBP) 1 increased exon 2 inclusion in the mature CD33 mRNA (van Bergeijk *et al*., 2019). Blocking SRSF1 and PTBP1 from binding to the CD33 locus could be an alternative to increase splicing of exon 2 and result in increased expression of $CD33^{\Delta E2}$ in microglia.

Taken together, full-length CD33 exerts an anti-inflammatory effect in microglia, hampering uptake of Aβ in critical disease stages, which is not seen for $CD33^{\Delta E2}$. A modulation of CD33 signaling might be beneficial, however, it can result in the production of ROS, thereby possibly exacerbating the disease. A modulation to favor expression of $CD33^{\Delta E2}$ seems to be a safer approach. However, further research needs to be performed to follow up this concept in detail.

5 Summary

CD33 is expressed on immune cells of myeloid origin, such as macrophages and microglia. Upon activation, CD33 recruits and activates protein tyrosine phosphatases, which results in attenuation of the activatory signaling pathway. Recently, polymorphisms in the *CD33* gene were linked to late-onset Alzheimer's disease (AD). However, the exact function of CD33 in AD remains to be discovered.

In the present thesis, the transcriptome of human induced pluripotent stem cell-derived microglia (iPSdMiG) was compared to human primary microglia in a first step. The *in silico* RNA sequencing analysis showed that the transcriptome of iPSdMiG closely resembled that of human primary microglia. Furthermore, a CD33 reporter cell line was generated to identify possible modulators of CD33 signaling. The reporter cell lines expressed a fusion protein consisting of the extracellular domain of either human full-length CD33M or exon 2-deleted $CD33^{\Delta E2}$ linked to the transmembrane and intracellular domains of the DNAX-Activation Protein 12 (DAP12). CD33 activation was observed in CD33M, but not in $CD33^{\Delta E2}$-expressing reporter cells by the CD33 antibody clone P67.6 and partially by clone 1c7/1. Both antibodies were confirmed to activate CD33 by antagonizing TREM2-induced phosphorylation of SYK in iPSdMiG. Moreover, the impact of CD33 signaling on microglial homeostasis was analyzed using wild type and isogenic *CD33* knockout ($CD33^{-/-}$) as well as $CD33^{\Delta E2}$-expressing iPSdMiG. $CD33^{-/-}$ and $CD33^{\Delta E2}$-expressing iPSdMiG showed increased mRNA levels of inflammatory cytokines and chemokines. Increased gene transcript levels and surface expression of several microglial receptors was observed in $CD33^{-/-}$ but not $CD33^{\Delta E2}$-expressing iPSdMiG. Further, $CD33^{-/-}$ and $CD33^{\Delta E2}$-expressing iPSdMiG showed an increase in SYK phosphorylation and phagocytosis of amyloid $\beta_{1\text{-}42}$ as well as bacterial particles. The phagocytosis-associated oxidative burst was only increased in $CD33^{-/-}$ but not $CD33^{\Delta E2}$-expressing iPSdMiG.

In summary, both, deletion of *CD33* and expression of $CD33^{\Delta E2}$ resulted in increased microglial activation in human iPSdMiG, which might be beneficial in respect to AD. However, $CD33^{-/-}$ but not $CD33^{\Delta E2}$ led to a presumable neurotoxic increased oxidative burst in iPSdMiG.

6 References

Abud, E. M., Ramirez, R. N., Martinez, E. S., Healy, L. M., Nguyen, C. H. H., Newman, S. A., Yeromin, A. V., Scarfone, V. M., Marsh, S. E., Fimbres, C., Caraway, C. A., Fote, G. M., Madany, A. M., Agrawal, A., Kayed, R., Gylys, K. H., Cahalan, M. D., Cummings, B. J., Antel, J. P., … Blurton-Jones, M. (2017). iPSC-Derived Human Microglia-like Cells to Study Neurological Diseases. *Neuron*, *94*(2), 278-293.e9. https://doi.org/10.1016/j.neuron.2017.03.042

Aizenstein, H. J., Nebes, R. D., Saxton, J. A., Price, J. C., Mathis, C. A., Tsopelas, N. D., Ziolko, S. K., James, J. A., Snitz, B. E., Houck, P. R., Bi, W., Cohen, A. D., Lopresti, B. J., DeKosky, S. T., Halligan, E. M., & Klunk, W. E. (2008). Frequent amyloid deposition without significant cognitive impairment among the elderly. *Arch Neurol*, *65*(11), 1509–1517. https://doi.org/10.1001/archneur.65.11.1509

Alias, E., Dharmapatni, A. S., Holding, A. C., Atkins, G. J., Findlay, D. M., Howie, D. W., Crotti, T. N., & Haynes, D. R. (2012). Polyethylene particles stimulate expression of ITAM-related molecules in peri-implant tissues and when stimulating osteoclastogenesis in vitro. *Acta Biomater*, *8*(8), 3104–3112. https://doi.org/10.1016/j.actbio.2012.04.037

Allen, N. J., & Lyons, D. A. (2018). System Formation and Function. *Science*, *185*(October), 181–185.

Alliot, F., Godin, I., & Pessac, B. (1999). Microglia derive from progenitors, originating from the yolk sac, and which proliferate in the brain. *Developmental Brain Research*, *117*(2), 145–152. https://doi.org/10.1016/S0165-3806(99)00113-3

Almende, B. V, Thieurmel, B., & Titouan, R. (2019). *visNetwork: Network Visualization using "vis.js" Library* (2.0.9).

Alzheimer, A. (1907). Über eine eigenartige Erkrankung der Hirnrinde. *Allgemeine Zeitschrift Für Psychiatrie Und Psychisch-Gerichtliche Medizin*, *64*.

An, H., Xu, H., Zhang, M., Zhou, J., Feng, T., Qian, C., Qi, R., & Cao, X. (2005). Src homology 2 domain-containing inositol-5-phosphatase 1 (SHIP1) negatively regulates TLR4-mediated LPS response primarily through a phosphatase activity- and PI-3K-independent mechanism. *Blood*, *105*(12), 4685–4692. https://doi.org/10.1182/blood-2005-01-0191

Angata, T., Margulies, E. H., Green, E. D., & Varki, A. (2004). Large-scale sequencing of the CD33-related Siglec gene cluster in five mammalian species reveals rapid evolution by multiple mechanisms. *Proc Natl Acad Sci U S A*, *101*(36), 13251–13256. https://doi.org/10.1073/pnas.0404833101

Angata, T., & Varki, A. (2002). Chemical diversity in the sialic acids and related alpha-keto acids: an evolutionary perspective. *Chem Rev*, *102*(2), 439–469. https://www.ncbi.nlm.nih.gov/pubmed/11841250

Angelova, D. M., & Brown, D. R. (2019). Microglia and the aging brain: are senescent microglia the key to neurodegeneration? *Journal of Neurochemistry*, *151*(6), 676–688. https://doi.org/10.1111/jnc.14860

Angelova, P. R., & Abramov, A. Y. (2018). Role of mitochondrial ROS in the brain: from physiology to neurodegeneration. *FEBS Letters*, *592*(5), 692–702. https://doi.org/10.1002/1873-3468.12964

Ansari, M. A., & Scheff, S. W. (2010). Oxidative stress in the progression of alzheimer disease in the frontal cortex. *Journal of Neuropathology and Experimental Neurology*, *69*(2), 155–167. https://doi.org/10.1097/NEN.0b013e3181cb5af4

Asea, A., Rehli, M., Kabingu, E., Boch, J. A., Baré, O., Auron, P. E., Stevenson, M. A., & Calderwood, S. K. (2002). Novel signal transduction pathway utilized by extracellular HSP70. Role of toll-like receptor (TLR) 2 and TLR4. *Journal of Biological Chemistry*, *277*(17), 15028–15034. https://doi.org/10.1074/jbc.M200497200

Ashutosh, Kou, W., Cotter, R., Borgmann, K., Wu, L., Persidsky, R., Sakhuja, N., & Ghorpade, A. (2011). CXCL8 protects human neurons from amyloid-β-induced neurotoxicity: relevance to Alzheimer's disease. *Biochem Biophys Res Commun*, *412*(4), 565–571. https://doi.org/10.1016/j.bbrc.2011.07.127

Askew, K., Li, K., Olmos-Alonso, A., Garcia-Moreno, F., Liang, Y., Richardson, P., Tipton, T., Chapman, M. A., Riecken, K., Beccari, S., Sierra, A., Molnár, Z., Cragg, M. S., Garaschuk, O., Perry, V. H., & Gomez-Nicola, D. (2017). Coupled Proliferation and Apoptosis Maintain the Rapid Turnover of Microglia in the Adult Brain. *Cell Reports*, *18*(2), 391–405. https://doi.org/10.1016/j.celrep.2016.12.041

Avril, T., Floyd, H., Lopez, F., Vivier, E., & Crocker, P. R. (2004). The Membrane-Proximal Immunoreceptor Tyrosine-Based Inhibitory Motif Is Critical for the Inhibitory Signaling Mediated by Siglecs-7 and -9, CD33-Related Siglecs Expressed on Human Monocytes and NK Cells. *The Journal of Immunology*, *173*(11), 6841–6849. https://doi.org/10.4049/jimmunol.173.11.6841

Avril, T., Wagner, E. R., Willison, H. J., & Crocker, P. R. (2006). Sialic acid-binding immunoglobulin-like lectin 7 mediates selective recognition of sialylated glycans expressed on Campylobacter jejuni lipooligosaccharides. *Infection and Immunity*, *74*(7), 4133–4141. https://doi.org/10.1128/IAI.02094-05

Azevedo, F. A. C., Carvalho, L. R. B., Grinberg, L. T., Farfel, J. M., Ferretti, R. E. L., Leite, R. E. P., Filho, W. J., Lent, R., & Herculano-Houzel, S. (2009). Equal numbers of neuronal and nonneuronal cells make the human brain an isometrically scaled-up primate brain. *Journal of Comparative Neurology*, *513*(5), 532–541. https://doi.org/10.1002/cne.21974

Beamer, E., Gölöncsér, F., Horváth, G., Beko, K., Otrokocsi, L., Koványi, B., & Sperlágh, B. (2016). Purinergic mechanisms in neuroinflammation: An update from molecules to behavior. *Neuropharmacology*, *104*, 94–104. https://doi.org/10.1016/j.neuropharm.2015.09.019

Bellenguez, C., Kucukali, F., Jansen, I., Andrade, V., Morenau-Grau, S., Amin, N., Grenier-Boley, B., Kleideman, L., Holsman, P., Garcia, P., Campos Martin, R., Naj, A., Qiong, Y., Bis, J. C., Damotte, V., Vander Lee, S., Boland, A., Costa, M., Chapuis, J., … Lambert, J.-C. (2020). Large meta-analysis of genome-wide association studies expands knowledge of the genetic etiology of Alzheimer disease and highlights potential translational opportunities. *MedRxiv*, *30*, 2020.10.01.20200659. http://medrxiv.org/content/early/2020/10/03/2020.10.01.20200659.abstract

Bennett, F. C., Bennett, M. L., Yaqoob, F., Mulinyawe, S. B., Grant, G. A., Hayden Gephart, M., Plowey, E. D., & Barres, B. A. (2018). A Combination of Ontogeny and CNS Environment Establishes Microglial Identity. *Neuron*, *98*(6), 1170-1183.e8. https://doi.org/10.1016/j.neuron.2018.05.014

Bhattacherjee, A., Rodrigues, E., Jung, J., Luzentales-Simpson, M., Enterina, J. R., Galleguillos, D., St. Laurent, C. D., Nakhaei-Nejad, M., Fuchsberger, F. F., Streith, L., Wang, Q., Kawasaki, N., Duan, S., Bains, A., Paulson, J. C., Rademacher, C., Giuliani, F., Sipione, S., Macauley, M. S., … Macauley, M. S. (2019). Repression of phagocytosis by human CD33 is not conserved with mouse CD33. *Commun Biol*, *2*(1), 1–13. https://doi.org/10.1038/s42003-019-0698-6

Bochkov, Y. A., & Palmenberg, A. C. (2006). Translational efficiency of EMCV IRES in bicistronic vectors is dependent upon IRES sequence and gene location. *BioTechniques*, *41*(3), 283–292. https://doi.org/10.2144/000112243

Bornhöfft, K. F., Goldammer, T., Rebl, A., & Galuska, S. P. (2018). Siglecs: A journey through the evolution of sialic acid-binding immunoglobulin-type lectins. *Developmental and Comparative Immunology*, *86*, 219–231. https://doi.org/10.1016/j.dci.2018.05.008

Bradshaw, E. M., Chibnik, L. B., Keenan, B. T., Ottoboni, L., Raj, T., Tang, A., Rosenkrantz, L. L., Imboywa, S., Lee, M., Von Korff, A., Morris, M. C., Evans, D. A., Johnson, K., Sperling, R. A., Schneider, J. A., Bennett, D. A., & De Jager, P. L. (2013). CD33 Alzheimer's disease locus: altered monocyte function and amyloid biology. *Nat Neurosci*, *16*(7), 848–850. https://doi.org/10.1038/nn.3435

Brinkman-Van Der Linden, E. C., & Varki, A. (2000). New aspects of siglec binding specificities, including the significance of fucosylation and of the sialyl-Tn epitope. *Journal of Biological Chemistry*, *275*(12), 8625–8632. https://doi.org/10.1074/jbc.275.12.8625

Brosig, A., Kuhrt, H., Wiedemann, P., Kohen, L., Bringmann, A., & Hollborn, M. (2015). Gene expression regulation in retinal pigment epithelial cells induced by viral RNA and viral/bacterial DNA. *Mol Vis*, *21*, 1000–1016. http://dx.doi.org/

Burnstock, G. (1990). Overview. Purinergic mechanisms. *Ann N Y Acad Sci*, *603*, 1–17; discussion 18. https://www.ncbi.nlm.nih.gov/pubmed/1981306

Butovsky, O., Jedrychowski, M. P., Moore, C. S., Cialic, R., Lanser, A. J., Gabriely, G., Koeglsperger, T., Dake, B., Wu, P. M., Doykan, C. E., Fanek, Z., Liu, L., Chen, Z., Rothstein, J. D., Ransohoff, R. M., Gygi, S. P., Antel, J. P., & Weiner, H. L. (2014). Identification of a unique TGF-β-dependent molecular and functional signature in microglia. *Nature Neuroscience*, *17*(1), 131–143. https://doi.org/10.1038/nn.3599

Cai, H., Wang, Y., McCarthy, D., Wen, H., Borchelt, D. R., Price, D. L., & Wong, P. C. (2001). BACE1 is the major β-secretase for generation of Aβ peptides by neurons. *Nature Neuroscience*, *4*(3), 233–234. https://doi.org/10.1038/85064

Cait, J., Hughes, M. R., Zeglinski, M. R., Chan, A. W., Osterhof, S., Wilder Scott, R., Hernaez, D. C., Cait, A., Wayne Vogl, A., Bernatchez, P., Michael Underhill, T., Granville, D. J., Murphy, T. H., Roskelley, C. D., & McNagny, K. M. (2019). Podocalyxin is required for maintaining blood–brain barrier function during acute inflammation. *Proceedings of the National Academy of Sciences of the United States of America*, *116*(10), 4518–4527. https://doi.org/10.1073/pnas.1814766116

Caldeira, C., Cunha, C., Vaz, A. R., Falcão, A. S., Barateiro, A., Seixas, E., Fernandes, A., & Brites, D. (2017). Key aging-associated alterations in primary microglia response to beta-amyloid stimulation. *Frontiers in Aging Neuroscience*, *9*(August), 1–23. https://doi.org/10.3389/fnagi.2017.00277

Cao, H., & Crocker, P. R. (2011). Evolution of CD33-related siglecs: regulating host immune functions and escaping pathogen exploitation? *Immunology*, *132*(1), 18–26. https://doi.org/10.1111/j.1365-2567.2010.03368.x

Carlin, A. F., Lewis, A. L., Varki, A., & Nizet, V. (2007). Group B streptococcal capsular sialic acids interact with siglecs (immunoglobulin-like lectins) on human leukocytes. *Journal of Bacteriology*, *189*(4), 1231–1237. https://doi.org/10.1128/JB.01155-06

Carlson, M. (2019). *org.Hs.eg.db: Genome wide annotation for Human* (3.8.2).

Chambers, C., Smith, F., Williams, C., Marcos, S., Liu, Z. H., Hayter, P., Ciaramella, G., Keighley, W., Gribbon, P., & Sewing, A. (2003). Measuring intracellular calcium fluxes in high throughput mode. *Combinatorial Chemistry & High Throughput Screening*, *6*(4), 355–362. https://doi.org/doi: 10.2174/138620703106298446

Chan, G., White, C. C., Winn, P. A., Cimpean, M., Replogle, J. M., Glick, L. R., Cuerdon, N. E., Ryan, K. J., Johnson, K. A., Schneider, J. A., Bennett, D. A., Chibnik, L. B., Sperling, R. A., Bradshaw, E. M., & De Jager, P. L. (2015). CD33 modulates TREM2: convergence of Alzheimer loci. *Nat Neurosci*, *18*(11), 1556–1558. https://doi.org/10.1038/nn.4126

Chanput, W., Mes, J. J., & Wichers, H. J. (2014). THP-1 cell line: An in vitro cell model for immune modulation approach. *International Immunopharmacology*, *23*(1), 37–45. https://doi.org/10.1016/j.intimp.2014.08.002

Chen, T. W., Wardill, T. J., Sun, Y., Pulver, S. R., Renninger, S. L., Baohan, A., Schreiter, E. R., Kerr, R. A., Orger, M. B., Jayaraman, V., Looger, L. L., Svoboda, K., & Kim, D. S. (2013). Ultrasensitive fluorescent proteins for imaging neuronal activity. *Nature*, *499*(7458), 295–300. https://doi.org/10.1038/nature12354

Chen, X., & Varki, A. (2010). Advances in the biology and chemistry of sialic acids. *ACS Chemical Biology*, *5*(2), 163–176. https://doi.org/10.1021/cb900266r

Chou, H. H., Hayakawa, T., Diaz, S., Krings, M., Indriati, E., Leakey, M., Paabo, S., Satta, Y., Takahata, N., & Varki, A. (2002). Inactivation of CMP-N-acetylneuraminic acid hydroxylase occurred prior to brain expansion during human evolution. *Proc Natl Acad Sci U S A*, *99*(18), 11736–11741. https://doi.org/10.1073/pnas.182257399

Cirrito, J. R., Yamada, K. A., Finn, M. B., Sloviter, R. S., Bales, K. R., May, P. C., Schoepp, D. D., Paul, S. M., Mennerick, S., & Holtzman, D. M. (2005). Synaptic activity regulates interstitial fluid amyloid-β levels in vivo. *Neuron*, *48*(6), 913–922. https://doi.org/10.1016/j.neuron.2005.10.028

Claude, J., Linnartz-Gerlach, B., Kudin, A. P., Kunz, W. S., & Neumann, H. (2013). Microglial CD33-related Siglec-E inhibits neurotoxicity by preventing the phagocytosis-associated oxidative burst. *J Neurosci*, *33*(46), 18270–18276. https://doi.org/10.1523/jneurosci.2211-13.2013

Cleveland, D. W., Hwo, S. Y., & Kirschner, M. W. (1977). Purification of tau, a microtubule-associated protein that induces assembly of microtubules from purified tubulin. *Journal of Molecular Biology*, *116*(2), 207–225. https://doi.org/10.1016/0022-2836(77)90213-3

Cohen, M., Matcovitch, O., David, E., Barnett-Itzhaki, Z., Keren-Shaul, H., Blecher-Gonen, R., Jaitin, D. A., Sica, A., Amit, I., & Schwartz, M. (2014). Chronic exposure to TGF β1 regulates myeloid cell inflammatory response in an IRF 7-dependent manner . *The EMBO Journal*, *33*(24), 2906–2921. https://doi.org/10.15252/embj.201489293

Coulter, A., & Harris, R. (1983). Simplified preparation of rabbit fab fragments. *Journal of Immunological Methods*, *59*(2), 199–203. https://doi.org/10.1016/0022-1759(83)90031-5

Craig-Schapiro, R., Perrin, R. J., Roe, C. M., Xiong, C., Carter, D., Cairns, N. J., Mintun, M. A., Peskind, E. R., Li, G., Galasko, D. R., Clark, C. M., Quinn, J. F., D'Angelo, G., Malone, J. P., Townsend, R. R., Morris, J. C., Fagan, A. M., & Holtzman, D. M. (2010). YKL-40: A novel prognostic fluid biomarker for preclinical Alzheimer's disease. *Biological Psychiatry*, *68*(10), 903–912. https://doi.org/10.1016/j.biopsych.2010.08.025

Crocker, P. R., & Gordon, S. (1986). Properties and distribution of a lectin-like hemagglutinin differentially expressed by murine stromal tissue macrophages. *Journal of Experimental Medicine*, *164*.

Crocker, P. R., & Gordon, S. (1989). Mouse macrophage hemagglutinin (sheep erythrocyte receptor) with specificity for sialylated glycoconjugates characterized by a monoclonal antibody. *Journal of Experimental Medicine*, *169*.

Crocker, P. R., Paulson, J. C., & Varki, A. (2007). Siglecs and their roles in the immune system. *Nat Rev Immunol*, *7*(4), 255–266. https://doi.org/10.1038/nri2056

Daigneault, M., Preston, J. A., Marriott, H. M., Whyte, M. K. B., & Dockrell, D. H. (2010). The identification of markers of macrophage differentiation in PMA-stimulated THP-1 cells and monocyte-derived macrophages. *PLoS ONE*, *5*(1). https://doi.org/10.1371/journal.pone.0008668

Dalziel, H. H., & Westfall, D. P. (1994). Receptors for adenine nucleotides and nucleosides: subclassification, distribution, and molecular characterization. *Pharmacol Rev*, *46*(4), 449–466. https://www.ncbi.nlm.nih.gov/pubmed/7899473

Damen, J. E., Liu, L., Rosten, P., Humphries, R. K., Jefferson, A. B., Majerus, P. W., & Krystal, G. (1996). The 145-kDa protein induced to associate with She by multiple cytokines is an inositol tetraphosphate and phosphatidylinositol 3,4,5-trisphosphate 5-phosphatase. *Proceedings of the National Academy of Sciences of the United States of America*, *93*(4), 1689–1693. https://doi.org/10.1073/pnas.93.4.1689

Damle, N. K., & Frost, P. (2003). Antibody-targeted chemotherapy with immunoconjugates of calicheamicin. *Current Opinion in Pharmacology*, *3*(4), 386–390. https://doi.org/10.1016/S1471-4892(03)00083-3

Davalos, D., Grutzendler, J., Yang, G., Kim, J. V., Zuo, Y., Jung, S., Littman, D. R., Dustin, M. L., & Gan, W. B. (2005). ATP mediates rapid microglial response to local brain injury in vivo. *Nature Neuroscience*, *8*(6), 752–758. https://doi.org/10.1038/nn1472

de Waal Malefyt, R., Abrams, J., Bennett, B., Figdor, C. G., & de Vries, J. E. (1991). Interleukin 10(IL-10) inhibits cytokine synthesis by human monocytes: an autoregulatory role of IL-10 produced by monocytes. *J Exp Med*, *174*(5), 1209–1220. https://www.ncbi.nlm.nih.gov/pubmed/1940799

Dennehy, K. M., Ferwerda, G., Faro-Trindade, I., Pyz, E., Willment, J. A., Taylor, P. R., Kerrigan, A., Tsoni, S. V., Gordon, S., Meyer-Wentrup, F., Adema, G. J., Kullberg, B. J., Schweighoffer, E., Tybulewicz, V., Mora-Montes, H. M., Gow, N. A. R., Williams, D. L., Netea, M. G., & Brown, G. D. (2008). Syk kinase is required for collaborative cytokine production induced through Dectin-1 and Toll-like receptors. *European Journal of Immunology*, *38*(2), 500–506. https://doi.org/10.1002/eji.200737741

Dobin, A., Davis, C. A., Schlesinger, F., Drenkow, J., Zaleski, C., Jha, S., Batut, P., Chaisson, M., & Gingeras, T. R. (2013). STAR: ultrafast universal RNA-seq aligner. *Bioinformatics*, *29*(1), 15–21. https://doi.org/10.1093/bioinformatics/bts635

Doody, G. M., Justement, L. B., Delibrias, C. C., Matthews, R. J., Lin, J., Thomas, M. L., & Fearon, D. T. (1995). A role in B cell activation for CD22 and the protein tyrosine phosphatase SHP. *Science*, *269*(5221), 242–244. https://doi.org/10.1126/science.7618087

Durafourt, B. A., Moore, C. S., Zammit, D. A., Johnson, T. A., Zaguia, F., Guiot, M. C., Bar-Or, A., & Antel, J. P. (2012). Comparison of polarization properties of human adult microglia and blood-derived macrophages. *Glia*, *60*(5), 717–727. https://doi.org/10.1002/glia.22298

Edison, P., Archer, H. A., Gerhard, A., Hinz, R., Pavese, N., Turkheimer, F. E., Hammers, A., Tai, Y. F., Fox, N., Kennedy, A., Rossor, M., & Brooks, D. J. (2008). Microglia, amyloid, and cognition in Alzheimer's disease: An [11C](R)PK11195-PET and [11C]PIB-PET study. *Neurobiol Dis*, *32*(3), 412–419. https://doi.org/10.1016/j.nbd.2008.08.001

Eguchi, H., Ikeda, Y., Ookawara, T., Koyota, S., Fujiwara, N., Honke, K., Wang, P. G., Taniguchi, N., & Suzuki, K. (2005). Modification of oligosaccharides by reactive oxygen species decreases sialyl lewis x-mediated cell adhesion. *Glycobiology*, *15*(11), 1094–1101. https://doi.org/10.1093/glycob/cwj003

Ehrlich, L. C., Hu, S., Sheng, W. S., Sutton, R. L., Rockswold, G. L., Peterson, P. K., & Chao, C. C. (1998). Cytokine regulation of human microglial cell IL-8 production. *Journal of Immunology (Baltimore, Md. : 1950)*, *160*(4), 1944–1948. http://www.ncbi.nlm.nih.gov/pubmed/9469457

Esparza, T. J., Zhao, H., Cirrito, J. R., Cairns, N. J., Bateman, R. J., Holtzman, D. M., & Brody, D. L. (2013). Amyloid-β oligomerization in Alzheimer dementia versus high-pathology controls. *Ann Neurol*, *73*(1), 104–119. https://doi.org/10.1002/ana.23748

Esquerda-Canals, G., Montoliu-Gaya, L., Güell-Bosch, J., & Villegas, S. (2017). Mouse Models of Alzheimer's Disease. *Journal of Alzheimer's Disease*, *57*(4), 1171–1183. https://doi.org/10.3233/JAD-170045

Ewels, P., Magnusson, M., Lundin, S., & Käller, M. (2016). MultiQC: Summarize analysis results for multiple tools and samples in a single report. *Bioinformatics*, *32*(19), 3047–3048. https://doi.org/10.1093/bioinformatics/btw354

Feldman, E. J., Brandwein, J., Stone, R., Kalaycio, M., Moore, J., Julie O'Connor, N. W., Roboz, G. J., Miller, C., Chopra, R., Jurcic, J. C., Brown, R., Ehmann, W. C., Schulman, P., Frankel, S. R., De Angela, D., & Scheinberg, D. (2005). Phase III randomized multicenter study of a humanized anti-CD33 monoclonal antibody, lintuzumab, in combination with chemotherapy, versus chemotherapy alone in patients with refractory or first-relapsed acute myeloid leukemia. *Journal of Clinical Oncology*, *23*(18), 4110–4116. https://doi.org/10.1200/JCO.2005.09.133

Fernandes, D. C., Wosniak, J., Pescatore, L. A., Bertoline, M. A., Liberman, M., Laurindo, F. R. M., & Santos, C. X. C. (2007). Analysis of DHE-derived oxidation products by HPLC in the assessment of superoxide production and NADPH oxidase activity in vascular systems. *American Journal of Physiology - Cell Physiology*, *292*(1), 413–422. https://doi.org/10.1152/ajpcell.00188.2006

Forlenza, O. V., Radanovic, M., Talib, L. L., Aprahamian, I., Diniz, B. S., Zetterberg, H., & Gattaz, W. F. (2015). Cerebrospinal fluid biomarkers in Alzheimer's disease: Diagnostic accuracy and prediction of dementia. *Alzheimer's and Dementia: Diagnosis, Assessment and Disease Monitoring*, *1*(4), 455–463. https://doi.org/10.1016/j.dadm.2015.09.003

Freeman, S. D., Kelm, S., Barber, E. K., & Crocker, P. R. (1995). Characterization of CD33 as a new member of the sialoadhesin family of cellular interaction molecules. *Blood*, *85*(8), 2005–2012. http://dx.doi.org/

Friker, L. L., Scheiblich, H., Hochheiser, I. V., Brinkschulte, R., Riedel, D., Latz, E., Geyer, M., & Heneka, M. T. (2020). β-Amyloid Clustering around ASC Fibrils Boosts Its Toxicity in Microglia. *Cell Reports*, *30*(11), 3743-3754.e6. https://doi.org/10.1016/j.celrep.2020.02.025

Fujikura, M., Iwahara, N., Hisahara, S., Kawamata, J., Matsumura, A., Yokokawa, K., Saito, T., Manabe, T., Matsushita, T., Suzuki, S., & Shimohama, S. (2019). CD14 and Toll-Like Receptor 4 Promote Fibrillar Aβ 42 Uptake by Microglia Through A Clathrin-Mediated Pathway. *Journal of Alzheimer's Disease*, *68*(1), 323–337. https://doi.org/10.3233/JAD-180904

Fujimoto, T., Anderson, K., Jacobsen, S. E. W., Nishikawa, S. I., & Nerlov, C. (2007). Cdk6 blocks myeloid differentiation by interfering with Runx1 DNA binding and Runx1-C/EBPα interaction. *EMBO Journal*, *26*(9), 2361–2370. https://doi.org/10.1038/sj.emboj.7601675

Galatro, T. F., Holtman, I. R., Lerario, A. M., Vainchtein, I. D., Brouwer, N., Sola, P. R., Veras, M. M., Pereira, T. F., Leite, R. E. P., Möller, T., Wes, P. D., Sogayar, M. C., Laman, J. D., Dunnen, W. den, Pasqualucci, C. A., Oba-Shinjo, S. M., Boddeke, E. W. G. M., Marie, S. K. N., & Eggen, B. J. L. (2017). Transcriptomic analysis of purified human cortical microglia reveals age-associated changes. *Nature Neuroscience*, *20*(8), 1162. https://doi.org/doi:10.1038/nn.4597

Gautier, E. L., Shay, T., Miller, J., Greter, M., Jakubzick, C., Ivanov, S., Helft, J., Chow, A., Elpek, K. G., Gordonov, S., Mazloom, A. R., Ma'Ayan, A., Chua, W. J., Hansen, T. H., Turley, S. J., Merad, M., Randolph, G. J., Best, A. J., Knell, J., … Benoist, C. (2012). Gene-expression profiles and transcriptional regulatory pathways that underlie the identity and diversity of mouse tissue macrophages. *Nature Immunology*, *13*(11), 1118–1128. https://doi.org/10.1038/ni.2419

Gervaix, A., West, D., Leoni, L. M., Richman, D. D., Wong-Staal, F., & Corbeil, J. (1997). A new reporter cell line to monitor HIV infection and drug susceptibility in vitro. *Proceedings of the National Academy of Sciences of the United States of America*, *94*(9), 4653–4658. https://doi.org/10.1073/pnas.94.9.4653

Giambartolomei, G. H., Dennis, V. A., Lasater, B. L., Murthy, P. K., & Philipp, M. T. (2002). Autocrine and exocrine regulation of interleukin-10 production in THP-1 cells stimulated with Borrelia burgdorferi lipoproteins. *Infect Immun*, *70*(4), 1881–1888. https://www.ncbi.nlm.nih.gov/pubmed/11895951

Giles, F., Estey, E., & O'Brien, S. (2003). Gemtuzumab Ozogamicin in the Treatment of Acute Myeloid Leukemia. *Cancer*, *98*(10), 2095–2104. https://doi.org/10.1002/cncr.11791

Ginhoux, F., Greter, M., Leboeuf, M., Nandi, S., See, P., Gokhan, S., Mehler, M. F., Conway, S. J., Ng, L. G., Stanley, E. R., Samokhvalov, I. M., & Merad, M. (2010). Fate Mapping Analysis Reveals That Adult Microglia Derive from Primitive Macrophages. *Science*, *701*(November), 841–845.

Götz, J., Bodea, L. G., & Goedert, M. (2018). Rodent models for Alzheimer disease. *Nature Reviews Neuroscience*, *19*(10), 583–598. https://doi.org/10.1038/s41583-018-0054-8

Götz, J., Chen, F., Van Dorpe, J., & Nitsch, R. M. (2001). Formation of neurofibrillary tangles in P301L tau transgenic mice induced by Aβ42 fibrils. *Science*, *293*(5534), 1491–1495. https://doi.org/10.1126/science.1062097

Götz, J., Halliday, G., & Nisbet, R. M. (2019). Molecular Pathogenesis of the Tauopathies. *Annual Review of Pathology: Mechanisms of Disease*, *14*, 239–261. https://doi.org/10.1146/annurev-pathmechdis-012418-012936

Graham, D. B., Stephenson, L. M., Lam, S. K., Brim, K., Lee, H. M., Bautista, J., Gilfillan, S., Akilesh, S., Fujikawa, K., & Swat, W. (2007). An ITAM-signaling pathway controls cross-presentation of particulate but not soluble antigens in dendritic cells. *J Exp Med*, *204*(12), 2889–2897. https://doi.org/10.1084/jem.20071283

Griciuc, A., Serrano-Pozo, A., Parrado, A. R., Lesinski, A. N., Asselin, C. N., Mullin, K., Hooli, B., Choi, S. H., Hyman, B. T., & Tanzi, R. E. (2013). Alzheimer's disease risk gene CD33 inhibits microglial uptake of amyloid beta. *Neuron*, *78*(4), 631–643. https://doi.org/10.1016/j.neuron.2013.04.014

Guerreiro, R., Wojtas, A., Bras, J., Carrasquillo, M., Rogaeva, E., Majounie, E., Cruchaga, C., Sassi, C., Kauwe, J. S., Younkin, S., Hazrati, L., Collinge, J., Pocock, J., Lashley, T., Williams, J., Lambert, J. C., Amouyel, P., Goate, A., Rademakers, R., … Group, A. G. A. (2013). TREM2 variants in Alzheimer's disease. *N Engl J Med*, *368*(2), 117–127. https://doi.org/10.1056/NEJMoa1211851

Guillemin, G. J., & Brew, B. J. (2016). *Pericytes : a Review of Function and Identification*. *75*(3), 388–397. https://doi.org/10.1189/jlb.0303114.1

Haenseler, W., Sansom, S. N., Buchrieser, J., Newey, S. E., Moore, C. S., Nicholls, F. J., Chintawar, S., Schnell, C., Antel, J. P., Allen, N. D., Cader, M. Z., Wade-Martins, R., James, W. S., & Cowley, S. A. (2017). A Highly Efficient Human Pluripotent Stem Cell Microglia Model Displays a Neuronal-Co-culture-Specific Expression Profile and Inflammatory Response. *Stem Cell Reports*, *8*(6), 1727–1742. https://doi.org/10.1016/j.stemcr.2017.05.017

Hanisch, U. K. (2002). Microglia as a source and target of cytokines. *Glia*, *40*(2), 140–155. https://doi.org/10.1002/glia.10161

Hart, G. W., & Copeland, R. J. (2010). Glycomics hits the big time. *Cell*, *143*(5), 672–676. https://doi.org/10.1016/j.cell.2010.11.008

Heinz, S., Benner, C., Spann, N., Bertolino, E., Lin, Y. C., Laslo, P., Cheng, J. X., Murre, C., Singh, H., & Glass, C. K. (2010). Simple Combinations of Lineage-Determining Transcription Factors Prime cis-Regulatory Elements Required for Macrophage and B Cell Identities. *Molecular Cell*, *38*(4), 576–589. https://doi.org/10.1016/j.molcel.2010.05.004

Heneka, M. T., Carson, M. J., Khoury, J. El, Landreth, G. E., Brosseron, F., Feinstein, D. L., Jacobs, A. H., Wyss-Coray, T., Vitorica, J., Ransohoff, R. M., Herrup, K., Frautschy, S. A., Finsen, B., Brown, G. C., Verkhratsky, A., Yamanaka, K., Koistinaho, J., Latz, E., Halle, A., … Kummer, M. P. (2015). Neuroinflammation in Alzheimer's disease. *The Lancet Neurology*, *14*(4), 388–405. https://doi.org/10.1016/S1474-4422(15)70016-5

Herculano-Houzel, S. (2014). The glia/neuron ratio: How it varies uniformly across brain structures and species and what that means for brain physiology and evolution. *Glia*, *62*(9), 1377–1391. https://doi.org/10.1002/glia.22683

Hernández-Caselles, T., Martínez-Esparza, M., Pérez-Oliva, A. B., Quintanilla-Cecconi, A. M., García-Alonso, A., Alvarez-López, D. M. R., & García-Peñarrubia, P. (2006). A study of CD33 (SIGLEC-3) antigen expression and function on activated human T and NK cells: two isoforms of CD33 are generated by alternative splicing. *Journal of Leukocyte Biology*, *79*(1), 46–58. https://doi.org/10.1189/jlb.0205096

Heslegrave, A., Heywood, W., Paterson, R., Magdalinou, N., Svensson, J., Johansson, P., Öhrfelt, A., Blennow, K., Hardy, J., Schott, J., Mills, K., & Zetterberg, H. (2016). Increased cerebrospinal fluid soluble TREM2 concentration in Alzheimer's disease. *Mol Neurodegener*, *11*, 3. https://doi.org/10.1186/s13024-016-0071-x

Heurtier, V., Owens, N., Gonzalez, I., Mueller, F., Proux, C., Mornico, D., Clerc, P., Dubois, A., & Navarro, P. (2019). The molecular logic of Nanog-induced self-renewal in mouse embryonic stem cells. *Nature Communications*, *10*(1). https://doi.org/10.1038/s41467-019-09041-z

Hickman, S., Izzy, S., Sen, P., Morsett, L., & El Khoury, J. (2018). Microglia in neurodegeneration. *Nature Neuroscience*, *21*(10), 1359–1369. https://doi.org/10.1038/s41593-018-0242-x

Hinderlich, S., Weidemann, W., Yardeni, T., Horstkorte, R., & Huizing, M. (2015). UDP-GlcNAc 2-Epimerase/ManNAc Kinase (GNE): A Master Regulator of Sialic Acid Synthesis. *Top Curr Chem*, *366*, 97–137. https://doi.org/10.1007/128_2013_464

Hollingworth, P., Harold, D., Sims, R., Gerrish, A., Lambert, J. C., Carrasquillo, M. M., Abraham, R., Hamshere, M. L., Pahwa, J. S., Moskvina, V., Dowzell, K., Jones, N., Stretton, A., Thomas, C., Richards, A., Ivanov, D., Widdowson, C., Chapman, J., Lovestone, S., … others. (2011). Common variants at ABCA7, MS4A6A/MS4A4E, EPHA1, CD33 and CD2AP are associated with Alzheimer's disease. *Nat Genet*, *43*(5), 429–435. https://doi.org/10.1038/ng.803

Huang, Z.-Y., Hunter, S., Kim, M.-K., Indik, Z. K., & Schreiber, A. D. (2003). The effect of phosphatases SHP-1 and SHIP-1 on signaling by the ITIM- and ITAM-containing Fcγ receptors FcγRIIB and FcγRIIA. *Journal of Leukocyte Biology*, *73*(6), 823–829. https://doi.org/10.1189/jlb.0902454

Humpel, C. (2011). Identifying and validating biomarkers for Alzheimer's disease. *Trends in Biotechnology*, *29*(1), 26–32. https://doi.org/10.1016/j.tibtech.2010.09.007

Humphrey, M. B., Daws, M. R., Spusta, S. C., Niemi, E. C., Torchia, J. A., Lanier, L. L., Seaman, W. E., & Nakamura, M. C. (2006). TREM2, a DAP12-associated receptor, regulates osteoclast differentiation and function. *Journal of Bone and Mineral Research*, *21*(2), 237–245. https://doi.org/10.1359/JBMR.051016

Irie, A., Koyamat, S., Kozutsumi, Y., Kawasaki, T., & Suzuki, A. (1998). The molecular basis for the absence of N-glycolylneuraminic acid in humans. *Journal of Biological Chemistry*, *273*(25), 15866–15871. https://doi.org/10.1074/jbc.273.25.15866

Isnardi, I., Bruhns, P., Bismuth, G., Fridman, W. H., & Daëron, M. (2006). The SH2 domain-containing inositol 5-phosphatase SHIP1 is recruited to the intracytoplasmic domain of human FcγRIIB and is mandatory for negative regulation of B cell activation. *Immunology Letters*, *104*(1–2), 156–165. https://doi.org/10.1016/j.imlet.2005.11.027

Jack, C. R., Bennett, D. A., Blennow, K., Carrillo, M. C., Dunn, B., Haeberlein, S. B., Holtzman, D. M., Jagust, W., Jessen, F., Karlawish, J., Liu, E., Molinuevo, J. L., Montine, T., Phelps, C., Rankin, K. P., Rowe, C. C., Scheltens, P., Siemers, E., Snyder, H. M., … Silverberg, N. (2018). NIA-AA Research Framework: Toward a biological definition of Alzheimer's disease. *Alzheimer's and Dementia*, *14*(4), 535–562. https://doi.org/10.1016/j.jalz.2018.02.018

Jäkel, S., & Dimou, L. (2017). Glial cells and their function in the adult brain: A journey through the history of their ablation. *Frontiers in Cellular Neuroscience*, *11*(February), 1–17. https://doi.org/10.3389/fncel.2017.00024

Januszyk, M., Rennert, R., Sorkin, M., Maan, Z., Wong, L., Whittam, A., Whitmore, A., Duscher, D., & Gurtner, G. (2015). Evaluating the Effect of Cell Culture on Gene Expression in Primary Tissue Samples Using Microfluidic-Based Single Cell Transcriptional Analysis. *Microarrays*, *4*(4), 540–550. https://doi.org/10.3390/microarrays4040540

Jia, H., Rochefort, N. L., Chen, X., & Konnerth, A. (2011). In vivo two-photon imaging of sensory-evoked dendritic calcium signals in cortical neurons. *Nat Protoc*, *6*(1), 28–35. https://doi.org/10.1038/nprot.2010.169

Jiang, Z., Georgel, P., Du, X., Shamel, L., Sovath, S., Mudd, S., Huber, M., Kalis, C., Keck, S., Galanos, C., Freudenberg, M., & Beutler, B. (2005). CD14 is required for MyD88-independent LPS signaling. *Nature Immunology*, *6*(6), 565–570. https://doi.org/10.1038/ni1207

Jin, Y., Nie, D., Li, J., Du, X., Lu, Y., Li, Y., Liu, C., Zhou, J., & Pan, J. (2017). Gas6/AXL signaling regulates self-renewal of chronic myelogenous leukemia stem cells by stabilizing β-catenin. *Clinical Cancer Research*, *23*(11), 2842–2855. https://doi.org/10.1158/1078-0432.CCR-16-1298

Jones, C., Virji, M., & Crocker, P. R. (2003). Recognition of sialylated meningococcal lipopolysaccharide by siglecs expressed on myeloid cells leads to enhanced bacterial uptake. *Molecular Microbiology*, *49*(5), 1213–1225. https://doi.org/10.1046/j.1365-2958.2003.03634.x

Jonsson, T., Stefansson, H., Steinberg, S., Jonsdottir, I., Jonsson, P. V, Snaedal, J., Bjornsson, S., Huttenlocher, J., Levey, A. I., Lah, J. J., Rujescu, D., Hampel, H., Giegling, I., Andreassen, O. A., Engedal, K., Ulstein, I., Djurovic, S., Ibrahim-Verbaas, C., Hofman, A., … Stefansson, K. (2013). Variant of TREM2 associated with the risk of Alzheimer's disease. *N Engl J Med*, *368*(2), 107–116. https://doi.org/10.1056/NEJMoa1211103

Jung, Y., Decker, A. M., Wang, J., Lee, E., Kana, L. A., Yumoto, K., Cackowski, F. C., Rhee, J., Carmeliet, P., Buttitta, L., Morgan, T. M., & Taichman, R. S. (2016). Endogenous GAS6 and Mer receptor signaling regulate prostate cancer stem cells in bone marrow. *Oncotarget*, *7*(18), 25698–25711. https://doi.org/10.18632/oncotarget.8365

Kageshita, T., Hirai, S., Kimura, T., Hanai, N., Ohta, S., & Ono, T. (1995). Association between Sialyl Lewisa Expression and Tumor Progression in Melanoma. *Cancer Research*, *55*(8), 1748–1751. https://doi.org/10.1016/0923-1811(95)93868-2

Kametani, F., & Hasegawa, M. (2018). Reconsideration of amyloid hypothesis and tau hypothesis in Alzheimer's disease. *Frontiers in Neuroscience*, *12*(JAN). https://doi.org/10.3389/fnins.2018.00025

Karantzali, E., Lekakis, V., Ioannou, M., Hadjimichael, C., Papamatheakis, J., & Kretsovali, A. (2011). Sall1 regulates embryonic stem cell differentiation in association with Nanog. *Journal of Biological Chemistry*, *286*(2), 1037–1045. https://doi.org/10.1074/jbc.M110.170050

Kawabori, M., Kacimi, R., Kauppinen, T., Calosing, C., Kim, J. Y., Hsieh, C. L., Nakamura, M. C., & Yenari, M. A. (2015). Triggering receptor expressed on myeloid cells 2 (TREM2) deficiency attenuates phagocytic activities of microglia and exacerbates ischemic damage in experimental stroke. *Journal of Neuroscience*, *35*(8), 3384–3396. https://doi.org/10.1523/JNEUROSCI.2620-14.2015

Kaye, J., & Janeway, C. A. (1984). *The Fab fragment of a directly activating monoclonal antibody that precipitates a disulfide-linked heterodimer from a helper T cell clone blocks activation by either allogeneic Ia or antigen and self-Ia. 159*.

Keenan, A. B., Torre, D., Lachmann, A., Leong, A. K., Wojciechowicz, M. L., Utti, V., Jagodnik, K. M., Kropiwnicki, E., Wang, Z., & Ma'ayan, A. (2019). ChEA3: transcription factor enrichment analysis by orthogonal omics integration. *Nucleic Acids Research*, *47*(W1), W212–W224. https://doi.org/10.1093/nar/gkz446

Kierdorf, K., Erny, D., Goldmann, T., Sander, V., Schulz, C., Perdiguero, E. G., Wieghofer, P., Heinrich, A., Riemke, P., Hölscher, C., Müller, D. N., Luckow, B., Brocker, T., Debowski, K., Fritz, G., Opdenakker, G., Diefenbach, A., Biber, K., Heikenwalder, M., … Prinz, M. (2013). Microglia emerge from erythromyeloid precursors via Pu.1-and Irf8-dependent pathways. *Nature Neuroscience*, *16*(3), 273–280. https://doi.org/10.1038/nn.3318

Kim, J. H., Lee, S. R., Li, L. H., Park, H. J., Park, J. H., Lee, K. Y., Kim, M. K., Shin, B. A., & Choi, S. Y. (2011). High cleavage efficiency of a 2A peptide derived from porcine teschovirus-1 in human cell lines, zebrafish and mice. *PLoS ONE*, *6*(4), 1–8. https://doi.org/10.1371/journal.pone.0018556

Klein, M., Obermaier, B., Angele, B., Pfister, H. W., Wagner, H., Koedel, U., & Kirschning, C. J. (2008). Innate immunity to pneumococcal infection of the central nervous system depends on toll-like receptor (TLR) 2 and TLR4. *Journal of Infectious Diseases*, *198*(7), 1028–1036. https://doi.org/10.1086/591626

Knapskog, A. B., Henjum, K., Idland, A. V., Eldholm, R. S., Persson, K., Saltvedt, I., Watne, L. O., Engedal, K., & Nilsson, L. N. G. (2020). Cerebrospinal fluid sTREM2 in Alzheimer's disease: comparisons between clinical presentation and AT classification. *Scientific Reports*, *10*(1), 1–10. https://doi.org/10.1038/s41598-020-72878-8

Kobayashi, M., Konishi, H., Sayo, A., Takai, T., & Kiyama, H. (2016). TREM2/DAP12 signal elicits proinflammatory response in microglia and exacerbates neuropathic pain. *Journal of Neuroscience*, *36*(43), 11138–11150. https://doi.org/10.1523/JNEUROSCI.1238-16.2016

Kober, D. L., Alexander-Brett, J. M., Karch, C. M., Cruchaga, C., Colonna, M., Holtzman, M. J., & Brett, T. J. (2016). Neurodegenerative disease mutations in TREM2 reveal a functional surface and distinct loss-of-function mechanisms. *ELife*, *5*(DECEMBER2016), 1–24. https://doi.org/10.7554/eLife.20391

Koedam, E. L. G. E., Lauffer, V., Van Der Vlies, A. E., Van Der Flier, W. M., Scheltens, P., & Pijnenburg, Y. A. L. (2010). Early-versus late-onset Alzheimer's disease: More than age alone. *Journal of Alzheimer's Disease*, *19*(4), 1401–1408. https://doi.org/10.3233/JAD-2010-1337

Kolde, R. (2019). *pheatmap: Pretty Heatmaps* (1.0.12).

Krakauer, M., Sorensen, P., Khademi, M., Olsson, T., & Sellebjerg, F. (2008). Increased IL-10 mRNA and IL-23 mRNA expression in multiple sclerosis: interferon-beta treatment increases IL-10 mRNA expression while reducing IL-23 mRNA expression. *Mult Scler*, *14*(5), 622–630. https://doi.org/10.1177/1352458507087136

Kristiansen, O. P., & Mandrup-Poulsen, T. (2005). Interleukin-6 and Diabetes: The Good, the Bad, or the Indifferent? *Diabetes*, *54 Suppl 2*. https://doi.org/10.2337/diabetes.54.suppl_2.s114

Kuhn, P. H., Wang, H., Dislich, B., Colombo, A., Zeitschel, U., Ellwart, J. W., Kremmer, E., Roßner, S., & Lichtenthaler, S. F. (2010). ADAM10 is the physiologically relevant, constitutive α-secretase of the amyloid precursor protein in primary neurons. *EMBO Journal*, *29*(17), 3020–3032. https://doi.org/10.1038/emboj.2010.167

Lajaunias, F., Dayer, J. M., & Chizzolini, C. (2005). Constitutive repressor activity of CD33 on human monocytes requires sialic acid recognition and phosphoinositide 3-kinase-mediated intracellular signaling. *Eur J Immunol*, *35*(1), 243–251. https://doi.org/10.1002/eji.200425273

Lambert, J. C., Heath, S., Even, G., Campion, D., Sleegers, K., Hiltunen, M., Combarros, O., Zelenika, D., Bullido, M. J., Tavernier, B., Letenneur, L., Bettens, K., Berr, C., Pasquier, F., Fievet, N., Barberger-Gateau, P., Engelborghs, S., De Deyn, P., Mateo, I., … Amouyel, P. (2009). Genome-wide association study identifies variants at CLU and CR1 associated with Alzheimer's disease. *Nat Genet*, *41*(10), 1094–1099. https://doi.org/10.1038/ng.439

Lambert, J. C., Ibrahim-Verbaas, C. A., Harold, D., Naj, A. C., Sims, R., Bellenguez, C., DeStafano, A. L., Bis, J. C., Beecham, G. W., Grenier-Boley, B., Russo, G., Thorton-Wells, T. A., Jones, N., Smith, A. V, Chouraki, V., Thomas, C., Ikram, M. A., Zelenika, D., Vardarajan, B. N., … others. (2013). Meta-analysis of 74,046 individuals identifies 11 new susceptibility loci for Alzheimer's disease. *Nat Genet*, *45*(12), 1452–1458. https://doi.org/10.1038/ng.2802

Langfelder, P., & Horvath, S. (2008). WGCNA: An R package for weighted correlation network analysis. *BMC Bioinformatics*, *9*. https://doi.org/10.1186/1471-2105-9-559

Lawson, L. J., Perry, V. H., Dri, P., & Gordon, S. (1990). Heterogeneity in the distribution and morphology of microglia in the normal adult mouse brain. *Neuroscience*, *39*(1), 151–170. https://doi.org/10.1016/0306-4522(90)90229-W

Lawson, L. J., Perry, V. H., & Gordon, S. (1992). Turnover of resident microglia in the normal adult mouse brain. *Neuroscience*, *48*(2), 405–415. https://doi.org/10.1016/0306-4522(92)90500-2

Lewis, J., Dickson, D. W., Lin, W. L., Chisholm, L., Corral, A., Jones, G., Yen, S. H., Sahara, N., Skipper, L., Yager, D., Eckman, C., Hardy, J., Hutton, M., & McGowan, E. (2001). Enhanced neurofibrillary degeneration in transgenic mice expressing mutant tau and APP. *Science*, *293*(5534), 1487–1491. https://doi.org/10.1126/science.1058189

Liao, Y., Smyth, G. K., & Shi, W. (2014). featureCounts: an efficient general purpose program for assigning sequence reads to genomic features. *Bioinformatics*, *30*(7), 923–930. https://doi.org/10.1093/bioinformatics/btt656

Lindstrom, J., & Einarson, B. (1979). Antigenic modulation and receptor loss in experimental autoimmune myasthenia gravis. *Muscle & Nerve*, *2*(3), 173–179. https://doi.org/10.1002/mus.880020304

Linenberger, M. L. (2005). CD33-directed therapy with gemtuzumab ozogamicin in acute myeloid leukemia: Progress in understanding cytotoxicity and potential mechanisms of drug resistance. *Leukemia*, *19*(2), 176–182. https://doi.org/10.1038/sj.leu.2403598

Linnartz, B., & Neumann, H. (2013). Microglial activatory (immunoreceptor tyrosine-based activation motif)- and inhibitory (immunoreceptor tyrosine-based inhibition motif)-signaling receptors for recognition of the neuronal glycocalyx. *Glia*, *61*(1), 37–46. https://doi.org/10.1002/glia.22359

Linnartz, B., Wang, Y., & Neumann, H. (2010). Microglial immunoreceptor tyrosine-based activation and inhibition motif signaling in neuroinflammation. *Int J Alzheimers Dis*, *2010*. https://doi.org/10.4061/2010/587463

Liu, Y., Chen, G.-Y., & Zheng, P. (2010). *CD24-Siglec G/10 discriminates danger- from pathogen-associated molecular patterns*. *30*(12), 557–561. https://doi.org/10.1016/j.it.2009.09.006.CD24-Siglec

Lock, K., Zhang, J., Lu, J., Lee, S. H., & Crocker, P. R. (2004). Expression of CD33-related siglecs on human mononuclear phagocytes, monocyte-derived dendritic cells and plasmacytoid dendritic cells. *Immunobiology*, *209*(1–2), 199–207. https://doi.org/10.1016/j.imbio.2004.04.007

Long, E. M., Millen, B., Kubes, P., & Robbins, S. M. (2009). Lipoteichoic acid induces unique inflammatory responses when compared to other toll-like receptor 2 ligands. *PLoS ONE*, *4*(5). https://doi.org/10.1371/journal.pone.0005601

Love, M. I., Huber, W., & Anders, S. (2014). Moderated estimation of fold change and dispersion for RNA-seq data with DESeq2. *Genome Biol*, *15*(12), 550. https://doi.org/10.1186/s13059-014-0550-8

Lovell, M. A., Xiong, S., Xie, C., Davies, P., & Markesbery, W. R. (2004). Induction of hyperphosphorylated tau in primary rat cortical neuron cultures mediated by oxidative stress and glycogen synthase kinase-3. *Journal of Alzheimer's Disease*, *6*(6), 659–671. https://doi.org/10.3233/jad-2004-6610

Malik, M., Simpson, J. F., Parikh, I., Wilfred, B. R., Fardo, D. W., Nelson, P. T., & Estus, S. (2013). CD33 Alzheimer's risk-altering polymorphism, CD33 expression, and exon 2 splicing. *J Neurosci*, *33*(33), 13320–13325. https://doi.org/10.1523/JNEUROSCI.1224-13.2013

Malvandi, A. M., Mehrzad, J., & Saleh-moghaddam, M. (2013). Biologically relevant doses of mixed aflatoxins B and G up-regulate MyD88, TLR2, TLR4 and CD14 transcripts in human PBMCs. *Immunopharmacol Immunotoxicol*, *35*(4), 528–532. https://doi.org/10.3109/08923973.2013.803572

Mancuso, R., Van Den Daele, J., Fattorelli, N., Wolfs, L., Balusu, S., Burton, O., Liston, A., Sierksma, A., Fourne, Y., Poovathingal, S., Arranz-Mendiguren, A., Sala Frigerio, C., Claes, C., Serneels, L., Theys, T., Perry, V. H., Verfaillie, C., Fiers, M., & De Strooper, B. (2019). Stem-cell-derived human microglia transplanted in mouse brain to study human disease. *Nature Neuroscience*, *22*(12), 2111–2116. https://doi.org/10.1038/s41593-019-0525-x

Manno, B., Oellerich, T., Schnyder, T., Corso, J., Losing, M., Neumann, K., Urlaub, H., Batista, F. D., Engelke, M., & Wienands, J. (2016). The Dok-3/Grb2 adaptor module promotes inducible association of the lipid phosphatase SHIP with the BCR in a coreceptor-independent manner. *Eur J Immunol*, *46*(11), 2520–2530. https://doi.org/10.1002/eji.201646431

Mariant, M., Camagna, M., Tarditi, L., & Seccamani, E. (1991). A new enzymatic method to obtain high-yield F(ab)2 suitable for clinical use from mouse IgGl. *Molecular Immunology*, *28*(1–2), 69–77. https://doi.org/10.1016/0161-5890(91)90088-2

Martinez, F. O., & Gordon, S. (2014). The M1 and M2 paradigm of macrophage activation: Time for reassessment. *F1000Prime Reports*, *6*(March), 1–13. https://doi.org/10.12703/P6-13

Masuda, T., Iwamoto, S., Mikuriya, S., Tozaki-Saitoh, H., Tamura, T., Tsuda, M., & Inoue, K. (2015). Transcription factor IRF1 is responsible for IRF8-mediated IL-1β expression in reactive microglia. *Journal of Pharmacological Sciences*, *128*(4), 216–220. https://doi.org/10.1016/j.jphs.2015.08.002

Mathews, M., Wißfeld, J., Shahraz, A., Semkova, V., Neumann, H., & Brüstle, O. (n.d.). *Up-scaled production of human iPSC-derived microglia in a developmentally informed paradigm using novel macrocarrier system*.

McVicar, D. W., Taylor, L. S., Gosselin, P., Willette-Brown, J., Mikhael, A. I., Geahlen, R. L., Nakamura, M. C., Linnemeyer, P., Seaman, W. E., Anderson, S. K., Ortaldo, J. R., & Mason, L. H. (1998). DAP12-mediated signal transduction in natural killer cells. A dominant role for the Syk protein-tyrosine kinase. *J Biol Chem*, *273*(49), 32934–32942. https://www.ncbi.nlm.nih.gov/pubmed/9830044

Meilinger, D., Fellinger, K., Bultmann, S., Rothbauer, U., Bonapace, I. M., Klinkert, W. E., Spada, F., & Leonhardt, H. (2009). Np95 interacts with de novo DNA methyltransferases, Dnmt3a and Dnmt3b, and mediates epigenetic silencing of the viral CMV promoter in embryonic stem cells. *EMBO Rep*, *10*(11), 1259–1264. https://doi.org/10.1038/embor.2009.201

Merriam, A. E., Aronson, M. K., Gaston, P., Wey, S. -L, & Katz, I. (1988). The Psychiatric Symptoms of Alzheimer's Disease. *Journal of the American Geriatrics Society*, *36*(1), 7–22. https://doi.org/10.1111/j.1532-5415.1988.tb03427.x

Michelucci, A., Heurtaux, T., Grandbarbe, L., Morga, E., & Heuschling, P. (2009). Characterization of the microglial phenotype under specific pro-inflammatory and anti-inflammatory conditions: Effects of oligomeric and fibrillar amyloid-β. *Journal of Neuroimmunology*, *210*(1–2), 3–12. https://doi.org/10.1016/j.jneuroim.2009.02.003

Mizuguchi, H., Xu, Z., Ishii-Watabe, A., Uchida, E., & Hayakawa, T. (2000). IRES-Dependent Second Gene Expression Is Significantly Lower Than Cap-Dependent First Gene Expression in a Bicistronic Vector. *Molecular Therapy*, *1*(4), 376–382. https://doi.org/10.1006/mthe.2000.0050

Mocsai, A., Abram, C. L., Jakus, Z., Hu, Y., Lanier, L. L., & Lowell, C. A. (2006). Integrin signaling in neutrophils and macrophages uses adaptors containing immunoreceptor tyrosine-based activation motifs. *Nat Immunol*, *7*(12), 1326–1333. https://doi.org/10.1038/ni1407

Morrison, H. W., & Filosa, J. A. (2013). A quantitative spatiotemporal analysis of microglia morphology during ischemic stroke and reperfusion. *Journal of Neuroinflammation*, *10*, 1–20. https://doi.org/10.1186/1742-2094-10-4

Mossad, O. (2016). *N-Glycolylneuraminic acid disrupts the cellular homeostasis in THP1- monocyte derived macrophages*.

Muffat, J., Li, Y., Yuan, B., Mitalipova, M., Omer, A., Corcoran, S., Bakiasi, G., Tsai, L. H., Aubourg, P., Ransohoff, R. M., & Jaenisch, R. (2016). Efficient derivation of microglia-like cells from human pluripotent stem cells. *Nature Medicine*, *22*(11), 1358–1367. https://doi.org/10.1038/nm.4189

Mullard, A. (2019). Anti-amyloid failures stack up as Alzheimer antibody flops. *Nature Reviews Drug Discovery*. https://doi.org/10.1038/d41573-019-00064-1

Mullen, A. C., & Wrana, J. L. (2017). TGF-β family signaling in embryonic and somatic stem-cell renewal and differentiation. *Cold Spring Harbor Perspectives in Biology*, *9*(7). https://doi.org/10.1101/cshperspect.a022186

Naj, A. C., Jun, G., Beecham, G. W., Wang, L. S., Vardarajan, B. N., Buros, J., Gallins, P. J., Buxbaum, J. D., Jarvik, G. P., Crane, P. K., Larson, E. B., Bird, T. D., Boeve, B. F., Graff-Radford, N. R., De Jager, P. L., Evans, D., Schneider, J. A., Carrasquillo, M. M., Ertekin-Taner, N., … others. (2011). Common variants at MS4A4/MS4A6E, CD2AP, CD33 and EPHA1 are associated with late-onset Alzheimer's disease. *Nat Genet*, *43*(5), 436–441. https://doi.org/10.1038/ng.801

Nimmerjahn, A., Kirchhoff, F., & Helmchen, F. (2005). Resting microglial cells are highly dynamic surveillants of brain parenchyma in vivo. *Science*, *308*(5726), 1314–1318. https://doi.org/10.1126/science.1110647

Nishimoto, N. (2006). Interleukin-6 in Rheumatoid Arthritis. *Current Opinion in Rheumatology*, *18*(3). https://doi.org/10.1097/01.bor.0000218949.19860.d1

Nunan, J., & Small, D. H. (2000). Regulation of APP cleavage by a-, b- and g-secretases. *FEBS Lett*, *483*(1), 6–10.

Okazawa, H., Motegi, S., Ohyama, N., Ohnishi, H., Tomizawa, T., Kaneko, Y., Oldenborg, P.-A., Ishikawa, O., & Matozaki, T. (2005). Negative Regulation of Phagocytosis in Macrophages by the CD47-SHPS-1 System. *The Journal of Immunology*, *174*(4), 2004–2011. https://doi.org/10.4049/jimmunol.174.4.2004

Okuda, T., Nishimura, M., Nakao, M., & Fujita, Y. (2001). RUNX1/AML1: A central player in hematopoiesis. *International Journal of Hematology*, *74*(3), 252–257. https://doi.org/10.1007/BF02982057

Oldenborg, P. A., Zheleznyak, A., Fang, Y. F., Lagenaur, C. F., Gresham, H. D., & Lindberg, F. P. (2000). Role of CD47 as a marker of self on red blood cells. *Science*, *288*(5473), 2051–2054. https://doi.org/10.1126/science.288.5473.2051

Olson, J. K., Girvin, A. M., & Miller, S. D. (2001). Direct Activation of Innate and Antigen-Presenting Functions of Microglia following Infection with Theiler's Virus. *Journal of Virology*, *75*(20), 9780–9789. https://doi.org/10.1128/jvi.75.20.9780-9789.2001

Olsson, M., Nilsson, A., & Oldenborg, P. A. (2007). Dose-dependent inhibitory effect of CD47 in macrophage uptake of IgG-opsonized murine erythrocytes. *Biochemical and Biophysical Research Communications*, *352*(1), 193–197. https://doi.org/10.1016/j.bbrc.2006.11.002

Osaki, M., Oshimura, M., & Ito, H. (2004). PI3K-Akt pathway: Its functions and alterations in human cancer. *Apoptosis*, *9*(6), 667–676. https://doi.org/10.1023/B:APPT.0000045801.15585.dd

Osborne, M. A., Zenner, G., Lubinus, M., Zhang, X., Songyang, Z., Cantley, L. C., Majerus, P., Burn, P., & Kochan, J. P. (1996). The inositol 5'-phosphatase SHIP binds to immunoreceptor signaling motifs and responds to high affinity IgE receptor aggregation. *Journal of Biological Chemistry*, *271*(46), 29271–29278. https://doi.org/10.1074/jbc.271.46.29271

Ousman, S. S., Wang, J., & Campbell, I. L. (2005). Differential Regulation of Interferon Regulatory Factor (IRF)-7 and IRF-9 Gene Expression in the Central Nervous System during Viral Infection. *Journal of Virology*, *79*(12), 7514–7527. https://doi.org/10.1128/jvi.79.12.7514-7527.2005

Padler-Karavani, V., Hurtado-Ziola, N., Chang, Y. C., Sonnenburg, J. L., Ronaghy, A., Yu, H., Verhagen, A., Nizet, V., Chen, X., Varki, N. M., Varki, A., & Angata, T. (2014). Rapid evolution of binding specificities and expression patterns of inhibitory CD33-related Siglecs in primates. *FASEB J*, *28*(3), 1280–1293. https://doi.org/10.1096/fj.13-241497

Palmqvist, S., Mattsson, N., & Hansson, O. (2016). Cerebrospinal fluid analysis detects cerebral amyloid-β accumulation earlier than positron emission tomography. *Brain*, *139*(4), 1226–1236. https://doi.org/10.1093/brain/aww015

Paolicelli, R. C., Bolasco, G., Pagani, F., Maggi, L., Scianni, M., Panzanelli, P., Giustetto, M., Ferreira, T. A., Guiducci, E., Dumas, L., Ragozzino, D., & Gross, C. T. (2011). Synaptic pruning by microglia is necessary for normal brain development. *Science*, *333*(6048), 1456–1458. https://doi.org/10.1126/science.1202529

Park, J., Min, J. S., Kim, B., Chae, U. Bin, Yun, J. W., Choi, M. S., Kong, I. K., Chang, K. T., & Lee, D. S. (2015). Mitochondrial ROS govern the LPS-induced pro-inflammatory response in microglia cells by regulating MAPK and NF-κB pathways. *Neuroscience Letters*, *584*, 191–196. https://doi.org/10.1016/j.neulet.2014.10.016

Parsa, K. V. L., Butchar, J. P., Rajaram, M. V. S., Cremer, T. J., & Tridandapani, S. (2008). The tyrosine kinase Syk promotes phagocytosis of Francisella through the activation of Erk. *Mol Immunol*, *45*(10), 3012–3021. https://doi.org/10.1016/j.molimm.2008.01.011

Pastor, D. M., Poritz, L. S., Olson, T. L., Kline, C. L., Harris, L. R., Koltun, W. A., Chinchilli, V. M., & Irby, R. B. (2010). Primary cell lines: False representation or model system? A comparison of four human colorectal tumors and their coordinately established cell lines. *International Journal of Clinical and Experimental Medicine*, *3*(1), 69–83.

Patt, L. M., & Grimes, W. J. (1974). Cell surface glycolipid and glycoprotein glycosyltransferases of normal and transformed cells. *Journal of Biological Chemistry*, *249*(13), 4157–4165. https://doi.org/10.1016/S0021-9258(19)42497-6

Paul, S. P., Taylor, L. S., Stansbury, E. K., & McVicar, D. W. (2000). Myeloid specific human CD33 is an inhibitory receptor with differential ITIM function in recruiting the phosphatases SHP-1 and SHP-2. *Blood*, *96*(2), 483–490. https://www.ncbi.nlm.nih.gov/pubmed/10887109

Peng, Q., Malhotra, S., Torchia, J. A., Kerr, W. G., Coggeshall, K. M., & Humphrey, M. B. (2010). TREM2- and DAP12-dependent activation of PI3K requires DAP10 and is inhibited by SHIP1. *Sci Signal*, *3*(122), ra38. https://doi.org/10.1126/scisignal.2000500

Pérez-Oliva, A. B., Martínez-Esparza, M., Vicente-Fernández, J. J., Corral-San Miguel, R., García-Peñarrubia, P., & Hernández-Caselles, T. (2011). Epitope mapping, expression and post-translational modifications of two isoforms of CD33 (CD33M and CD33m) on lymphoid and myeloid human cells. *Glycobiology*, *21*(6), 757–770. https://doi.org/10.1093/glycob/cwq220

Petersdorf, S. H., Kopecky, K. J., Slovak, M., Willman, C., Nevill, T., Brandwein, J., Larson, R. A., Erba, H. P., Stiff, P. J., Stuart, R. K., Walter, R. B., Tallman, M. S., Stenke, L., & Appelbaum, F. R. (2013). A phase 3 study of gemtuzumab ozogamicin during induction and postconsolidation therapy in younger patients with acute myeloid leukemia. *Blood*, *121*(24), 4854–4860. https://doi.org/10.1182/blood-2013-01-466706

Pubill, D., Dayanithi, G., Siatka, C., Andrés, M., Dufour, M. N., Guillon, G., & Mendre, C. (2001). ATP induces intracellular calcium increases and actin cytoskeleton disaggregation via P2x receptors. *Cell Calcium*, *29*(5), 299–309. https://doi.org/10.1054/ceca.2000.0194

R Core Team. (2020). *R: A language and environment for statistical computing* (4.0.3). R Foundation for Statistical Computing, Vienna, Austria.

Rajan, K. B., Wilson, R. S., Weuve, J., Barnes, L. L., & Evans, D. A. (2015). Cognitive impairment 18 years before clinical diagnosis of Alzheimer disease dementia. *Neurology*, *85*(10), 898–904. https://doi.org/10.1212/WNL.0000000000001774

Rasmussen, M. A., Holst, B., Tumer, Z., Johnsen, M. G., Zhou, S., Stummann, T. C., Hyttel, P., & Clausen, C. (2014). Transient p53 suppression increases reprogramming of human fibroblasts without affecting apoptosis and DNA damage. *Stem Cell Reports*, *3*(3), 404–413. https://doi.org/10.1016/j.stemcr.2014.07.006

Ravandi, F. (2011). Gemtuzumab Ozogamicin: One Size Does Not Fit All—The Case for Personalized Therapy. *Journal of Clinical Oncology*, *29*(5), 349–351. https://doi.org/10.1200/JCO.2010.32.9086

Reed-Geaghan, E. G., Savage, J. C., Hise, A. G., & Landreth, G. E. (2009). CD14 and toll-like receptors 2 and 4 are required for fibrillar Aβ-stimulated microglial activation. *J Neurosci*, *29*(38), 11982–11992. https://doi.org/10.1523/JNEUROSCI.3158-09.2009

Rennick, D., Berg, D., & Holland, G. (1992). Interleukin 10: an overview. *Prog Growth Factor Res*, *4*(3), 207–227. https://www.ncbi.nlm.nih.gov/pubmed/1307489

Rentz, D. M., Locascio, J. J., Becker, J. A., Moran, E. K., Eng, E., Buckner, R. L., Sperling, R. A., & Johnson, K. A. (2010). Cognition, reserve, and amyloid deposition in normal aging. *Ann Neurol*, *67*(3), 353–364. https://doi.org/10.1002/ana.21904

Richards, B., Karpilow, J., Dunn, C., Zharkikh, L., Maxfield, A., Kamb, A., & Teng, D. H. F. (1999). Creation of a stable human reporter cell line suitable for FACS-based, transdominant genetic selection. *Somatic Cell and Molecular Genetics*, *25*(4), 191–205. https://doi.org/10.1023/A:1019206625658

Río-Hortega, P. (1919). El “Tercer Elemento” de los Centros Nerviosos I-IV. *Boletín de La Sociedad Española de Biología*, 67–82, 91–103, 108–121, 154–171.

Risso, D., Ngai, J., Speed, T. P., & Dudoit, S. (2014). Normalization of RNA-seq data using factor analysis of control genes or samples. *Nature Biotechnology*, *32*(9), 896–902. https://doi.org/10.1038/nbt.2931

Rossi, A., Kontarakis, Z., Gerri, C., Nolte, H., Hölper, S., Krüger, M., & Stainier, D. Y. R. (2015). Genetic compensation induced by deleterious mutations but not gene knockdowns. *Nature*, *524*(7564), 230–233. https://doi.org/10.1038/nature14580

Roy, S., Guler, R., Parihar, S. P., Schmeier, S., Kaczkowski, B., Nishimura, H., Shin, J. W., Negishi, Y., Ozturk, M., Hurdayal, R., Kubosaki, A., Kimura, Y., de Hoon, M. J. L., Hayashizaki, Y., Brombacher, F., & Suzuki, H. (2015). Batf2/Irf1 Induces Inflammatory Responses in Classically Activated Macrophages, Lipopolysaccharides, and Mycobacterial Infection. *The Journal of Immunology*, *194*(12), 6035–6044. https://doi.org/10.4049/jimmunol.1402521

RStudio Team. (2020). *RStudio: Integrated Development Environment for R.* (1.3.1056). RStudio, PBC, Boston, MA.

Salminen, A., & Kaarniranta, K. (2009). Siglec receptors and hiding plaques in Alzheimer’s disease. *J Mol Med (Berl)*, *87*(7), 697–701. https://doi.org/10.1007/s00109-009-0472-1

Sasaki, A., Yamaguchi, H., Ogawa, A., Sugihara, S., & Nakazato, Y. (1997). Microglial activation in early stages of amyloid β protein deposition. *Acta Neuropathologica*, *94*(4), 316–322. https://doi.org/10.1007/s004010050713

Schauer, R. (1982). Chemistry, metabolism, and biological functions of sialic acids. *Adv Carbohydr Chem Biochem*, *40*, 131–234. https://www.ncbi.nlm.nih.gov/pubmed/6762816

Scheff, S. W., Ansari, M. A., & Mufson, E. J. (2016). Oxidative stress and hippocampal synaptic protein levels in elderly cognitively intact individuals with Alzheimer’s disease pathology. *Neurobiology of Aging*, *42*, 1–12. https://doi.org/10.1016/j.neurobiolaging.2016.02.030

Schetters, S. T. T., Gomez-Nicola, D., Garcia-Vallejo, J. J., & Van Kooyk, Y. (2018). Neuroinflammation: Microglia and T cells get ready to tango. *Frontiers in Immunology*, *8*(JAN). https://doi.org/10.3389/fimmu.2017.01905

Schlepckow, K., Monroe, K. M., Kleinberger, G., Cantuti-Castelvetri, L., Parhizkar, S., Xia, D., Willem, M., Werner, G., Pettkus, N., Brunner, B., Sülzen, A., Nuscher, B., Hampel, H., Xiang, X., Feederle, R., Tahirovic, S., Park, J. I., Prorok, R., Mahon, C., … Haass, C. (2020). Enhancing protective microglial activities with a dual function TREM 2 antibody to the stalk region. *EMBO Molecular Medicine*, *12*(4), 1–22. https://doi.org/10.15252/emmm.201911227

Schoenhofen, I. C., McNally, D. J., Brisson, J. R., & Logan, S. M. (2006). Elucidation of the CMP-pseudaminic acid pathway in Helicobacter pylori: Synthesis from UDP-N-acetylglucosamine by a single enzymatic reaction. *Glycobiology*, *16*(9), 8–14. https://doi.org/10.1093/glycob/cwl010

Schwarzkopf, M., Knobeloch, K. P., Rohde, E., Hinderlich, S., Wiechens, N., Lucka, L., Horak, I., Reutter, W., & Horstkorte, R. (2002). Sialylation is essential for early development in mice. *Proceedings of the National Academy of Sciences of the United States of America*, *99*(8), 5267–5270. https://doi.org/10.1073/pnas.072066199

Sergushichev, A., Korotkevich, G., & Sukhov, V. (2019). *Fast gene set enrichment analysis*. https://doi.org/10.1101/060012

Shahraz, A., Kopatz, J., Mathy, R., Kappler, J., Winter, D., Kapoor, S., Schutza, V., Scheper, T., Gieselmann, V., & Neumann, H. (2015). Anti-inflammatory activity of low molecular weight polysialic acid on human macrophages. *Sci Rep*, *5*, 16800. https://doi.org/10.1038/srep16800

Shea, Y. F., Chu, L. W., Chan, A. O. K., Ha, J., Li, Y., & Song, Y. Q. (2016). A systematic review of familial Alzheimer’s disease: Differences in presentation of clinical features among three mutated genes and potential ethnic differences. *Journal of the Formosan Medical Association*, *115*(2), 67–75. https://doi.org/10.1016/j.jfma.2015.08.004

Shichita, T., Hasegawa, E., Kimura, A., Morita, R., Sakaguchi, R., Takada, I., Sekiya, T., Ooboshi, H., Kitazono, T., Yanagawa, T., Ishii, T., Takahashi, H., Mori, S., Nishibori, M., Kuroda, K., Akira, S., Miyake, K., & Yoshimura, A. (2012). Peroxiredoxin family proteins are key initiators of post-ischemic inflammation in the brain. *Nature Medicine*, *18*(6), 911–917. https://doi.org/10.1038/nm.2749

Shieh, C. H., Heinrich, A., Serchov, T., van Calker, D., & Biber, K. (2014). P2X7-dependent, but differentially regulated release of IL-6, CCL2, and TNF-α in cultured mouse microglia. *Glia*, *62*(4), 592–607. https://doi.org/10.1002/glia.22628

Shukla, V., Mishra, S. K., & Pant, H. C. (2011). Oxidative stress in neurodegeneration. *Advances in Pharmacological Sciences*, *2011*. https://doi.org/10.1155/2011/572634

Siddiqui, S. S., Springer, S. A., Verhagen, A., Sundaramurthy, V., Alisson-Silva, F., Jiang, W., Ghosh, P., & Varki, A. (2017). The Alzheimer's disease-protective CD33 splice variant mediates adaptive loss of function via diversion to an intracellular pool. *J Biol Chem*, *292*(37), 15312–15320. https://doi.org/10.1074/jbc.M117.799346

Sierra, A., de Castro, F., del Río-Hortega, J., Rafael Iglesias-Rozas, J., Garrosa, M., & Kettenmann, H. (2016). The "Big-Bang" for modern glial biology: Translation and comments on Pío del Río-Hortega 1919 series of papers on microglia. *Glia*, *64*(11), 1801–1840. https://doi.org/10.1002/glia.23046

Smith, A. M., Gibbons, H. M., Oldfield, R. L., Bergin, P. M., Mee, E. W., Faull, R. L. M., & Dragunow, M. (2013). The transcription factor PU.1 is critical for viability and function of human brain microglia. *Glia*, *61*(6), 929–942. https://doi.org/10.1002/glia.22486

Solito, E., & Sastre, M. (2012). Microglia function in Alzheimer's disease. *Front Pharmacol*, *3*, 14. https://doi.org/10.3389/fphar.2012.00014

Sosna, J., Philipp, S., Iii, R. A., Reyes-ruiz, J. M., Baglietto-vargas, D., Laferla, F. M., & Glabe, C. G. (2018). *Early long-term administration of the CSF1R inhibitor PLX3397 ablates microglia and reduces accumulation of intraneuronal amyloid , neuritic plaque deposition and pre-fibrillar oligomers in 5XFAD mouse model of Alzheimer ' s disease*. 1–11.

Spangenberg, E., Severson, P. L., Hohsfield, L. A., Crapser, J., Zhang, J., Burton, E. A., Zhang, Y., Spevak, W., Lin, J., Phan, N. Y., Habets, G., Rymar, A., Tsang, G., Walters, J., Nespi, M., Singh, P., Broome, S., Ibrahim, P., Zhang, C., … Green, K. N. (2019). Sustained microglial depletion with CSF1R inhibitor impairs parenchymal plaque development in an Alzheimer's disease model. *Nature Communications*, *10*(1), 1–21. https://doi.org/10.1038/s41467-019-11674-z

Squarzoni, P., Oller, G., Hoeffel, G., Pont-Lezica, L., Rostaing, P., Low, D., Bessis, A., Ginhoux, F., & Garel, S. (2014). Microglia Modulate Wiring of the Embryonic Forebrain. *Cell Reports*, *8*(5), 1271–1279. https://doi.org/10.1016/j.celrep.2014.07.042

St-Amour, I., Paré, I., Alata, W., Coulombe, K., Ringuette-Goulet, C., Drouin-Ouellet, J., Vandal, M., Soulet, D., Bazin, R., & Calon, F. (2013). Brain bioavailability of human intravenous immunoglobulin and its transport through the murine blood-brain barrier. *Journal of Cerebral Blood Flow and Metabolism*, *33*(12), 1983–1992. https://doi.org/10.1038/jcbfm.2013.160

Stadhouders, R., Filion, G. J., & Graf, T. (2019). Transcription factors and 3D genome conformation in cell-fate decisions. *Nature*, *569*(7756), 345–354. https://doi.org/10.1038/s41586-019-1182-7

Stamenkovic, I., & Seed, B. (1990). The B-cell antigen CD22 mediates monocyte and erythrocyte adhesion. *Nature*, *345*(6270), 74–77. https://doi.org/10.1038/345074a0

Stevens, B., Allen, N. J., Vazquez, L. E., Howell, G. R., Christopherson, K. S., Nouri, N., Micheva, K. D., Mehalow, A. K., Huberman, A. D., Stafford, B., Sher, A., Litke, A. M. M., Lambris, J. D., Smith, S. J., John, S. W. M., & Barres, B. A. (2007). The Classical Complement Cascade Mediates CNS Synapse Elimination. *Cell*, *131*(6), 1164–1178. https://doi.org/10.1016/j.cell.2007.10.036

Stout, R. D., Jiang, C., Matta, B., Tietzel, I., Watkins, S. K., & Suttles, J. (2005). Macrophages Sequentially Change Their Functional Phenotype in Response to Changes in Microenvironmental Influences. *The Journal of Immunology*, *175*(1), 342–349. https://doi.org/10.4049/jimmunol.175.1.342

Streit, W J, Graeber, M. B., & Kreutzberg, G. W. (1988). Functional plasticity of microglia: a review. *Glia*, *1*(5), 301–307. https://doi.org/10.1002/glia.440010502

Streit, Wolfgang J., Braak, H., Xue, Q. S., & Bechmann, I. (2009). Dystrophic (senescent) rather than activated microglial cells are associated with tau pathology and likely precede neurodegeneration in Alzheimer's disease. *Acta Neuropathologica*, *118*(4), 475–485. https://doi.org/10.1007/s00401-009-0556-6

Strozyk, D., Blennow, K., White, L. R., & Launer, L. J. (2003). CSF Aß 42 levels correlate with amyloid-neuropathology in a population-based autopsy study. *Neurology*, *60*(4), 652–656. https://doi.org/10.1212/01.WNL.0000046581.81650.D0

Su, B., Wang, X., Lee, H. gon, Tabaton, M., Perry, G., Smith, M. A., & Zhu, X. (2010). Chronic oxidative stress causes increased tau phosphorylation in M17 neuroblastoma cells. *Neuroscience Letters*, *468*(3), 267–271. https://doi.org/10.1016/j.neulet.2009.11.010

Suematsu, R., Miyamoto, T., Saijo, S., Yamasaki, S., Tada, Y., Yoshida, H., & Miyake, Y. (2019). Identification of lipophilic ligands of Siglec5 and -14 that modulate innate immune responses. *Journal of Biological Chemistry*, *294*(45), 16776–16788. https://doi.org/10.1074/jbc.RA119.009835

Svennerholm, L. (1980). Structure and Biology of Cell Membrane Gangliosides. *Cholera and Related Diarrheas, 43rd Nobel Symposium, Stockholm*, 80–87. https://doi.org/10.1159/000403251

Swardfager, W., Lanctôt, K., Rothenburg, L., Wong, A., Cappell, J., & Herrmann, N. (2010). A Meta-Analysis of Cytokines in Alzheimer's Disease. *Biological Psychiatry*, *68*(10). https://doi.org/10.1016/j.biopsych.2010.06.012

Szumanska, G., Vorbrodt, A. W., Mandybur, T. I., & Wisniewski, H. M. (1987). Lectin histochemistry of plaques and tangles in Alzheimer's disease. *Acta Neuropathol*, *73*(1), 1–11. http://dx.doi.org/

Takahashi, K., Rochford, C. D. P., & Neumann, H. (2005). Clearance of apoptotic neurons without inflammation by microglial triggering receptor expressed on myeloid cells-2. *Journal of Experimental Medicine*, *201*(4), 647–657. https://doi.org/10.1084/jem.20041611

Takahashi, K., & Yamanaka, S. (2006). Induction of Pluripotent Stem Cells from Mouse Embryonic and Adult Fibroblast Cultures by Defined Factors. *Cell*, *126*(4), 663–676. https://doi.org/10.1016/j.cell.2006.07.024

Tan, J., Town, T., Mori, T., Wu, Y., Saxe, M., Crawford, F., & Mullan, M. (2000). CD45 opposes β-amyloid peptide-induced microglial activation via inhibition of p44/42 mitogen-activated protein kinase. *Journal of Neuroscience*, *20*(20), 7587–7594. https://doi.org/10.1523/jneurosci.20-20-07587.2000

Tanaka, T., Murakami, K., Bando, Y., & Yoshida, S. (2015). Interferon regulatory factor 7 participates in the M1-like microglial polarization switch. *Glia*, *63*(4), 595–610. https://doi.org/10.1002/glia.22770

Tapiola, T., Alafuzoff, I., Herukka, S. K., Parkkinen, L., Hartikainen, P., Soininen, H., & Pirttilä, T. (2009). Cerebrospinal fluid β-amyloid 42 and tau proteins as biomarkers of Alzheimer-type pathologic changes in the brain. *Archives of Neurology*, *66*(3), 382–389. https://doi.org/10.1001/archneurol.2008.596

Taylor, V. C., Buckley, C. D., Douglas, M., Cody, A. J., Simmons, D. L., & Freeman, S. D. (1999). The myeloid-specific sialic acid-binding receptor, CD33, associates with the protein-tyrosine phosphatases, SHP-1 and SHP-2. *J Biol Chem*, *274*(17), 11505–11512. https://www.ncbi.nlm.nih.gov/pubmed/10206955

Teschendorf, C., Warrington, K. H., Siemann, D. W., & Muzyczka, N. (2002). Comparison of the EF-1 alpha and the CMV promoter for engineering stable tumor cell lines using recombinant adeno-associated virus. *Anticancer Res*, *22*(6A), 3325–3330. https://www.ncbi.nlm.nih.gov/pubmed/12530082

Töpfer, K., Cartellieri, M., Michen, S., Wiedemuth, R., Muller, N., Lindemann, D., Bachmann, M., Fussel, M., Schackert, G., & Temme, A. (2015). DAP12-based activating chimeric antigen receptor for NK cell tumor immunotherapy. *J Immunol*, *194*(7), 3201–3212. https://doi.org/10.4049/jimmunol.1400330

Toyota, Y., Ikeda, M., Shinagawa, S., Matsumoto, T., Matsumoto, N., Hokoishi, K., Fukuhara, R., Ishikawa, T., Mori, T., Adachi, H., Komori, K., & Tanabe, H. (2007). Comparison of behavioral and psychological symptoms in early-onset and late-onset Alzheimer's disease. *International Journal of Geriatric Psychiatry*, *22*(9), 896–901. https://doi.org/10.1002/gps.1760

Tsuchiya, S., Yamabe, M., Yamaguchi, Y., Kobayashi, Y., Konno, T., & Tada, K. (1980). Establishment and characterization of a human acute monocytic leukemia cell line (THP-1). *International Journal of Cancer*, *26*(2), 171–176. https://doi.org/10.1002/ijc.2910260208

Ulvestad, E., Williams, K., Matre, R., Nyland, H., Olivier, A., & Antel, J. (1994). Fc Receptors for IgG on Cultured Human Microglia Mediate Cytotoxicity and Phagocytosis of Antibody-coated Targets. *Journal of Neuropathology & Experimental Neurology*, *53*(1), 27–36. https://academic.oup.com/jnen/article-abstract/53/1/27/2610254?redirectedFrom=fulltext

van Bergeijk, P., Seneviratne, U., Aparicio-Prat, E., Stanton, R., & Hasson, S. A. (2019). SRSF1 and PTBP1 Are trans-Acting Factors That Suppress the Formation of a CD33 Splicing Isoform Linked to Alzheimer's Disease Risk Petra. *Molecular and Cellular Biology*, *39*(18).

Varki, A. (2011a). Evolutionary forces shaping the Golgi glycosylation machinery: why cell surface glycans are universal to living cells. *Cold Spring Harb Perspect Biol*, *3*(6). https://doi.org/10.1101/cshperspect.a005462

Varki, A. (2011b). Since there are PAMPs and DAMPs, there must be SAMPs? Glycan "self-associated molecular patterns" dampen innate immunity, but pathogens can mimic them. *Glycobiology*, *21*(9), 1121–1124. https://doi.org/10.1093/glycob/cwr087

Varki, A. (2020). PAMPs, DAMPs and SAMPs: Host Glycans are Self-Associated Molecular Patterns, but subject to Microbial Molecular Mimicry. *The FASEB Journal*, *34*(S1), 1. https://doi.org/https://doi.org/10.1096/fasebj.2020.34.s1.00178

Varki, A., & Gagneux, P. (2012). Multifarious roles of sialic acids in immunity. *Ann N Y Acad Sci*, *1253*, 16–36. https://doi.org/10.1111/j.1749-6632.2012.06517.x

Varki, N. M., & Varki, A. (2007). Diversity in cell surface sialic acid presentations: implications for biology and disease. *Lab Invest*, *87*(9), 851–857. https://doi.org/10.1038/labinvest.3700656

Wakselman, S., Béchade, C., Roumier, A., Bernard, D., Triller, A., & Bessis, A. (2008). Developmental neuronal death in hippocampus requires the microglial CD11b integrin and DAP12 immunoreceptor. *Journal of Neuroscience*, *28*(32), 8138–8143. https://doi.org/10.1523/JNEUROSCI.1006-08.2008

Walsh, D. M., Klyubin, I., Fadeeva, J. V., Cullen, W. K., Anwyl, R., Wolfe, M. S., Rowan, M. J., & Selkoe, D. J. (2002). Naturally secreted oligomers of amyloid β protein potently inhibit hippocampal long-term potentiation in vivo. *Nature*, *416*(6880), 535–539. https://doi.org/10.1038/416535a

Walter, R. B., Raden, B. W., Kamikura, D. M., Cooper, J. A., & Bernstein, I. D. (2005). Influence of CD33 expression levels and ITIM-dependent internalization on gemtuzumab ozogamicin-induced cytotoxicity. *Blood*, *105*(3), 1295–1302. https://doi.org/10.1182/blood-2004-07-2784

Walter, R. B., Raden, B. W., Zeng, R., Hausermann, P., Bernstein, I. D., & Cooper, J. A. (2008). ITIM-dependent endocytosis of CD33-related Siglecs: role of intracellular domain, tyrosine phosphorylation, and the tyrosine phosphatases, Shp1 and Shp2. *J Leukoc Biol*, *83*(1), 200–211. https://doi.org/10.1189/jlb.0607388

Wang, B., & Brand-Miller, J. (2003). The role and potential of sialic acid in human nutrition. *European Journal of Clinical Nutrition*, *57*(11), 1351–1369. https://doi.org/10.1038/sj.ejcn.1601704

Wang, G. Q., Suzutani, T., Yamamoto, Y., Fukui, Y., Nozawa, N., Schmid, D. S., Kurane, I., & Inoue, N. (2006). Generation of a reporter cell line for detection of infectious varicella-zoster virus and its application to antiviral studies. *Antimicrobial Agents and Chemotherapy*, *50*(9), 3142–3145. https://doi.org/10.1128/AAC.00342-06

Wang, J. Z., & Liu, F. (2008). Microtubule-associated protein tau in development, degeneration and protection of neurons. *Progress in Neurobiology*, *85*(2), 148–175. https://doi.org/10.1016/j.pneurobio.2008.03.002

Wang, Q., & Zou, M. H. (2017). Measurement of Reactive Oxygen Species (ROS) and Mitochondrial ROS in AMPK Knockout Mice Blood Vessels Qilong. *Physiology & Behavior*, *176*(3), 139–148. https://doi.org/10.1007/978-1-4939-7598-3

Wang, Y., & Neumann, H. (2010). Alleviation of neurotoxicity by microglial human Siglec-11. *J Neurosci*, *30*(9), 3482–3488. https://doi.org/10.1523/jneurosci.3940-09.2010

Warren, L., & Felsenfeld, H. (1962). The biosynthesis of sialic acids. *The Journal of Biological Chemistry*, *237*(5), 1421–1431. https://doi.org/10.1016/S0021-9258(19)83718-3

Weisman, G. A., Woods, L. T., Erb, L., & Seye, C. I. (2012). P2Y Receptors in the Mammalian Nervous System: Pharmacology, Ligands and Therapeutic Potential. In *CNS & Neurological Disorders - Drug Targets* (Vol. 11, Issue 6). https://doi.org/10.2174/187152712803581047

WHO. (2020). *WHO Dementia Report*. 21.09.2020. https://www.who.int/en/news-room/fact-sheets/detail/dementia

Wickham, H. (2016). *ggplot2: Elegant Graphics for Data Analysis*. Springer-Verlag New York.

Wißfeld, J., Mathews, M., Mossad, O., Picardi, P., Cinti, A., Redaelli, L., Pradier, L., Brüstle, O., & Neumann, H. (n.d.). Reporter cell assay for human CD33 validated by specific antibodies and human iPSC-derived microglia. *Scientific Reports*.

Wißfeld, J., Nozaki, I., Mathews, M., Raschka, T., Ebeling, C., Hornung, V., Brüstle, O., & Neumann, H. (2021). Deletion of Alzheimer's disease-associated CD33 results in an inflammatory human microglia phenotype. *GLIA*. https://doi.org/10.1002/glia.23968

Wu, J., Cherwinski, H., Spies, T., Phillips, J. H., & Lanier, L. L. (2000). DAP10 and DAP12 form distinct, but functionally cooperative, receptor complexes in natural killer cells. *J Exp Med*, *192*(7), 1059–1068. https://www.ncbi.nlm.nih.gov/pubmed/11015446

Yeh, F. L., Wang, Y., Tom, I., Gonzalez, L. C., & Sheng, M. (2016). TREM2 Binds to Apolipoproteins, Including APOE and CLU/APOJ, and Thereby Facilitates Uptake of Amyloid-Beta by Microglia. *Neuron*, *91*(2), 328–340. https://doi.org/10.1016/j.neuron.2016.06.015

Yu, G., & He, Q. Y. (2016). ReactomePA: an R/Bioconductor package for reactome pathway analysis and visualization. *Mol Biosyst*, *12*(2), 477–479. https://doi.org/10.1039/c5mb00663e

Yu, G., Wang, L. G., Han, Y., & He, Q. Y. (2012). clusterProfiler: an R package for comparing biological themes among gene clusters. *Omics*, *16*(5), 284–287. https://doi.org/10.1089/omi.2011.0118

Zhang, S., & Cui, W. (2014). Sox2, a key factor in the regulation of pluripotency and neural differentiation. *World Journal of Stem Cells*, *6*(3), 305. https://doi.org/10.4252/wjsc.v6.i3.305

Zhao, L. (2019). CD33 in Alzheimer's disease - Biology, pathogenesis, and therapeutics: A mini-review. *Gerontology*, *65*(4), 323–331. https://doi.org/10.1159/000492596

Zhao, Y., Wu, X., Li, X., Jiang, L. L., Gui, X., Liu, Y., Sun, Y., Zhu, B., Piña-Crespo, J. C., Zhang, M., Zhang, N., Chen, X., Bu, G., An, Z., Huang, T. Y., & Xu, H. (2018). TREM2 Is a Receptor for β-Amyloid that Mediates Microglial Function. *Neuron*, *97*(5), 1023-1031.e7. https://doi.org/10.1016/j.neuron.2018.01.031

Zhu, A., Ibrahim, J. G., & Love, M. I. (2019). Heavy-tailed prior distributions for sequence count data: removing the noise and preserving large differences. *Bioinformatics*, *35*(12), 2084–2092. https://doi.org/10.1093/bioinformatics/bty895

Appendix

Table 2: Top 10 enriched pathways of the modules identified by WGCNA using the ReactomePA database.

Module	Rank	Pathway	Gene Ratio	FDR-adjusted *p* value
green	1	The citric acid (TCA) cycle and respiratory electron transport	0.09	1.61E-11
	2	Respiratory electron transport, ATP synthesis by chemiosmotic coupling, and heat production by uncoupling proteins.	0.06	5.39E-09
	3	Respiratory electron transport	0.05	3.28E-07
	4	Protein localization	0.05	2.08E-03
	5	ER to Golgi Anterograde Transport	0.05	2.48E-03
	6	Class I peroxisomal membrane protein import	0.02	2.63E-03
	7	Pyruvate metabolism and Citric Acid (TCA) cycle	0.03	3.68E-03
	8	Asparagine N-linked glycosylation	0.07	1.09E-02
	9	Metabolism	0.28	1.61E-02
	10	Transport to the Golgi and subsequent modification	0.05	1.61E-02
turquoise	1	Neuronal System	0.06	1.01E-21
	2	Transmission across Chemical Synapses	0.04	5.70E-11
	3	Protein-protein interactions at synapses	0.02	5.96E-08
	4	Signal Transduction	0.26	2.12E-06
	5	Neurexins and neuroligins	0.01	2.24E-06
	6	Neurotransmitter receptors and postsynaptic signal transmission	0.03	2.87E-06
	7	Muscle contraction	0.03	3.03E-05
	8	Cardiac conduction	0.02	3.72E-05
	9	Potassium Channels	0.01	7.79E-05
	10	Platelet homeostasis	0.01	9.53E-05
red	1	Translation	0.10	3.74E-04
	2	L13a-mediated translational silencing of Ceruloplasmin expression	0.05	3.74E-04
	3	GTP hydrolysis and joining of the 60S ribosomal subunit	0.05	3.74E-04
	4	Eukaryotic Translation Initiation	0.05	4.95E-04
	5	Cap-dependent Translation Initiation	0.05	4.95E-04
	6	Formation of a pool of free 40S subunits	0.05	1.45E-03

Module	Rank	Pathway	Gene Ratio	FDR-adjusted *p* value
	7	Eukaryotic Translation Elongation	0.04	2.31E-03
	8	Peptide chain elongation	0.04	7.35E-03
	9	Selenocysteine synthesis	0.04	9.88E-03
	10	Nonsense-Mediated Decay (NMD)	0.04	1.32E-02
yellow	1	Respiratory electron transport, ATP synthesis by chemiosmotic coupling, and heat production by uncoupling proteins.	0.04	8.49E-03
	2	Degradation of DVL	0.03	8.49E-03
	3	Metabolism of polyamines	0.03	8.49E-03
	4	Respiratory electron transport	0.04	8.49E-03
	5	Degradation of GLI1 by the proteasome	0.03	8.49E-03
	6	Degradation of GLI2 by the proteasome	0.03	8.49E-03
	7	GLI3 is processed to GLI3R by the proteasome	0.03	8.49E-03
	8	Cross-presentation of soluble exogenous antigens (endosomes)	0.02	8.49E-03
	9	Autodegradation of Cdh1 by Cdh1:APC/C	0.03	1.51E-02
	10	Oxygen-dependent proline hydroxylation of Hypoxia-inducible Factor Alpha	0.03	1.51E-02
blue	1	Immune System	0.33	8.23E-12
	2	Innate Immune System	0.19	4.13E-11
	3	Neutrophil degranulation	0.11	7.86E-09
	4	Immunoregulatory interactions between a Lymphoid and a non-Lymphoid cell	0.03	6.51E-04
	5	Platelet activation, signaling and aggregation	0.05	1.79E-03
	6	Toll-like Receptor Cascades	0.04	2.80E-03
	7	DAP12 interactions	0.01	1.33E-02
	8	Signaling by Interleukins	0.08	1.33E-02
	9	Hemostasis	0.09	1.33E-02
	10	NR1H3 & NR1H2 regulate gene expression linked to cholesterol transport and efflux	0.01	1.90E-02
brown	1	Translation	0.14	7.68E-33
	2	SRP-dependent cotranslational protein targeting to membrane	0.08	1.27E-26
	3	Metabolism of RNA	0.20	1.27E-26
	4	Eukaryotic Translation Termination	0.07	2.91E-25
	5	Peptide chain elongation	0.07	2.73E-24
	6	Viral mRNA Translation	0.07	2.73E-24

Module	Rank	Pathway	Gene Ratio	FDR-adjusted *p* value
	7	rRNA processing	0.10	5.90E-24
	8	rRNA processing in the nucleus and cytosol	0.10	1.11E-23
	9	Eukaryotic Translation Elongation	0.07	1.13E-23
	10	Formation of a pool of free 40S subunits	0.07	1.25E-23
magenta	1	Peptide ligand-binding receptors	0.06	2.08E-02
	2	Transcriptional regulation by RUNX1	0.08	2.74E-02
	3	GPCR ligand binding	0.10	2.74E-02
	4	RUNX1 regulates transcription of genes involved in differentiation of HSCs	0.06	3.40E-02
	5	Class A/1 (Rhodopsin-like receptors)	0.08	3.51E-02
	6	Generic Transcription Pathway	0.23	6.01E-02
	7	Signaling by GPCR	0.14	8.99E-02
	8	Regulation of TP53 Activity through Association with Co-factors	0.02	1.50E-01
	9	GPCR downstream signalling	0.13	1.56E-01
	10	Transcriptional regulation of granulopoiesis	0.04	1.84E-01
pink	1	POU5F1 (OCT4), SOX2, NANOG activate genes related to proliferation	0.04	7.42E-08
	2	Transcriptional regulation of pluripotent stem cells	0.04	4.53E-07
	3	Assembly of collagen fibrils and other multimeric structures	0.05	1.74E-05
	4	Crosslinking of collagen fibrils	0.03	1.74E-05
	5	Collagen formation	0.06	1.27E-04
	6	Signaling by NODAL	0.03	1.27E-04
	7	Extracellular matrix organization	0.08	2.41E-02
	8	Amino acid transport across the plasma membrane	0.02	2.69E-02
	9	Cell surface interactions at the vascular wall	0.05	2.91E-02
	10	Collagen biosynthesis and modifying enzymes	0.03	6.96E-02
green-yellow	1	Formation of a pool of free 40S subunits	0.22	1.67E-12
	2	L13a-mediated translational silencing of Ceruloplasmin expression	0.22	1.67E-12
	3	SRP-dependent cotranslational protein targeting to membrane	0.22	1.67E-12
	4	GTP hydrolysis and joining of the 60S ribosomal subunit	0.22	1.67E-12
	5	Peptide chain elongation	0.20	1.67E-12

Module	Rank	Pathway	Gene Ratio	FDR-adjusted *p* value
	6	Viral mRNA Translation	0.20	1.67E-12
	7	Nonsense-Mediated Decay (NMD)	0.22	1.67E-12
	8	Nonsense Mediated Decay (NMD) enhanced by the Exon Junction Complex (EJC)	0.22	1.67E-12
	9	Eukaryotic Translation Elongation	0.20	1.67E-12
	10	Selenocysteine synthesis	0.20	1.67E-12
black	1	Respiratory electron transport, ATP synthesis by chemiosmotic coupling, and heat production by uncoupling proteins.	0.08	3.92E-05
	2	Respiratory electron transport	0.07	1.05E-04
	3	Dectin-2 family	0.04	5.95E-04
	4	The citric acid (TCA) cycle and respiratory electron transport	0.08	5.95E-04
	5	Defective GALNT3 causes familial hyperphosphatemic tumoral calcinosis (HFTC)	0.02	1.43E-02
	6	Defective GALNT12 causes colorectal cancer 1 (CRCS1)	0.02	1.43E-02
	7	Defective C1GALT1C1 causes Tn polyagglutination syndrome (TNPS)	0.02	1.61E-02
	8	Olfactory Signaling Pathway	0.04	1.82E-02
	9	Complex I biogenesis	0.04	3.48E-02
	10	Termination of O-glycan biosynthesis	0.02	4.15E-02
purple	1	Metabolism of RNA	0.25	4.53E-09
	2	rRNA processing in the nucleus and cytosol	0.11	3.55E-06
	3	Processing of Capped Intron-Containing Pre-mRNA	0.13	3.55E-06
	4	rRNA processing	0.11	4.68E-06
	5	mRNA Splicing	0.11	1.26E-05
	6	Major pathway of rRNA processing in the nucleolus and cytosol	0.10	2.81E-05
	7	mRNA Splicing - Major Pathway	0.10	2.99E-05
	8	rRNA modification in the nucleus and cytosol	0.06	3.95E-05
	9	Cohesin Loading onto Chromatin	0.03	7.97E-04
	10	Mitotic Telophase/Cytokines	0.03	2.35E-03

List of Publications

Publications

- Mathews M., **Wißfeld J.**, Shahraz A., Semkova V., Neuman H., Brüstle O. Up-scaled production of human iPSC-derived microglia in a developmentally informed paradigm using novel macrocarrier system. *In preparation*.
- **Wißfeld J.**, Mathews M., Mossad O., Picardi P., Cinti A., Redaelli L., Pradier L., Brüstle O., Neumann H. (2021) Reporter cell assay for human CD33 validated by specific antibodies and human iPSC-derived microglia. *Scientific Reports in revision*.
- **Wißfeld J.**, Nozaki I., Mathews M., Raschka T., Ebeling C., Hornung V., Brüstle O., Neumann H. (2021). Deletion of Alzheimer's Disease-associated CD33 Results in an Inflammatory Human Microglia Phenotype. *GLIA accepted and in press*.
- Shahraz A., **Wißfeld J.**, Ginolhac A., Mathews M., Sinkkonen L., Neumann H.. (2020). Phagocytosis-related NADPH oxidase 2 subunit gp91phox contributes to neurodegeneration after repeated systemic challenge with lipopolysaccharides. *GLIA*, 69(1), 137-150. https://doi.org/10.1002/glia.23890

Oral Presentations

- "*CD33 signaling*" – 5th PHAGO General Assembly Meeting, November 03, 2020, Teleconference Meeting
- "*CD33 signaling*" – 4th PHAGO General Assembly Meeting, October 29, 2019, London, UK
- "*CD33 reporter cell line*" – 3rd PHAGO General Assembly Meeting, October 22, 2018, Ludwigshafen, Germany

Conference Proceedings

- **Wißfeld J.**, Mathews-Arjendra M., Nozaki I., Raschka T., Ebeling C., Ebneth A., Brüstle O., Neumann H. "*Deletion of CD33 in Human iPSC-derived Microglia Results in a Proinflammatory Microglia Phenotype*" – ImmunoSensation^2 Cluster Science Days 2019, November 4-5, 2019, Bonn, Germany. Abstract no. 103
- **Wißfeld J.**, Mathews-Arjendra M., Brault E., van Outryve d'Ydewalle C., Picardi P., Redaelli L., Tarroni P., Ebneth A., Pradier L., Brüstle O., Neumann H. "*Microglial SIGLEC3/CD33 signaling*" – 4th PHAGO General Assembly Meeting, October 28-30, 2019, London, UK. Abstract no. 2
- **Wißfeld J.**, Mathews-Arjendra M., Nozaki I., Raschka T, Ebeling C., Ebneth A., Brüstle O., Neumann H. "*Increased phagocytosis and phagocytosis-associated oxidative burst after deletion of CD33 in human mononuclear phagocytes*" – ImmunoSensation Cluster Science Days 2018, November 5-6, 2018, Bonn, Germany. Abstract no. 86
- **Wißfeld J.**, Nozaki I., Mathews M., Brüstle O., Hornung V., Neumann H. "*Microglial SIGLEC3/CD33*" – 3rd PHAGO General Assembly Meeting, October 22-24, 2018, Ludwigshafen, Germany.
- **Wißfeld J.**, Nozaki I., Mathews M., Brüstle O., Hornung V., Neumann H. "*Increased phagocytosis and phagocytosis-associated oxidative burst after deletion of CD33 in human THP-1 macrophages*" – 2nd PHAGO General Assembly Meeting, October 25-27, 2017, Paris, France. Abstract no. 2

Acknowledgements

First, I would like to thank Prof. Dr. Harald Neumann for giving me the opportunity to perform my PhD in his team and guiding me through this fascinating project. Thank you for your continuous support of my project, for helpful discussions, and for your patience and motivation throughout the whole time.

I would also like to thank my second supervisor, Prof. Walter Witke for his positive involvement and insights into my PhD project. I am very grateful to Prof. Dr. Jochen Walter and Prof. Dr. Anton Bovier, for completing my doctoral committee as third and fourth members.

I would like to extend much gratitude towards Dr. Mona Mathews and the LIFE & BRAIN GmbH for all help and discussions regarding the iPSdMiG protocol. In addition, a special thanks goes to Dr. Mona Mathews, Dr. Jens Kopatz, Jonas Winkler, Dr. Michael Peitz, and Wen Jianbin for providing RNA sequencing data for my analysis, to Rita Jietou for excellent technical support and to Dr. Jonas Kaszian for his help regarding the calcium imaging analysis. Further, I would like to thank Laurent Pradier and Emmanuel Brault from Sanofi for generating and providing the P67.6 F(ab) antibody and endotoxin data of the CD33 antibodies.

Furthermore, I would like to express my deepest gratitude to Jonas Winkler, Dr. Mona Mathews, Dr. Christine Klaus, Dr. Anahita Shahraz, Annemarie Bungartz, Dr. Jens Kopatz, and Dr. Bettina Linnartz-Gerlach for fruitful discussions of ideas and theories. Thank you for all your time, your patience and your support within this time.

I am very grateful to the whole Institute of Reconstructive Neurobiology especially to the Neural Regeneration group for providing an excellent atmosphere inside and outside of the lab, for lively discussions and for your continuous support. I enjoyed every moment of my time as part of the group. I will always appreciate the memories and support from all of you!

Last but not the least, I would like to thank my parents, my brothers, my friends and especially my girlfriend Katrin for constantly supporting and believing in me. I am forever grateful for having you all in my life.